UNIVERSITÀ DEGLI STUDI DI MILANO

CORSO DI DOTTORATO

MEDICINA TRASLAZIONALE
Ciclo XXXVI

DIPARTIMENTO DI SCIENZE BIOMEDICHE PER LA SALUTE

TESI DI DOTTORATO DI RICERCA

DISSECTING THE ROLE OF ACID SPHINGOMYELINASE INHIBITION IN GAUCHER DISEASE AND GBA-DEPENDENT PARKINSON'S DISEASE *IN VITRO* MODELS

BIO/10

DOTTORANDA

Silvia BREVIARIO

TUTOR

Prof. Massimo AURELI

CO-TUTOR

Dott. Alessio Di Fonzo

COORDINATORE DEL DOTTORATO

Prof.ssa Chiarella SFORZA

A.A.
2022/2023

INDEX

1 ABSTRACT

GBA gene encodes for the lysosomal enzyme β-glucocerebrosidase (GCase), which is involved in the catabolism of glucosylceramide (GlcCer) into glucose and ceramide. Biallelic mutations in GBA gene result in the GCase loss of function, leading to the accumulation of GlcCer and causing Gaucher Disease (GD). GD is a lysosomal storage disorder that manifests in various forms, ranging from the severe neuropathic type II to the less severe non-neurological type I.
Interestingly, monoallelic mutations in GBA are now recognized as a major recessive genetic risk factor for Parkinson's Disease (PD), known as GBA-dependent PD. PD is a progressive neurodegenerative disorder characterized by the gradual loss of dopaminergic neurons and by the presence of aggregates of α-synuclein in the substancia nigra pars compacta of the brain.

Up to now, the molecular mechanism linking GCase deficiency to the onset of neurodegeneration is still unknown. This is largely due to the lack of suitable *in vitro* models that accurately replicate the complexities of the human pathology associated with these conditions.
To increase the complexity, it is important to consider that not all the individuals with GBA mutations develop PD. To understand this variability, the scientific community has explored the presence of other genetic variants in lysosomal enzymes that could influence the penetrance of GBA mutations.

Our collaborators at Humanitas university have analysed a panel of 50 lysosomal genes, involved in the onset of lysosomal storage disorders when mutated, in a cohort composed by *GBA* asymptomatic carriers and *GBA*-mutated PD patients. They found that *SMPD1* gene, coding for the enzyme acid sphingomyelinase (ASM), was more frequently mutated in controls than in GBA-PD, suggesting a possible protective effect of *SMPD1* mutation in *GBA* carriers.
In addition, a recent study has found that in a zebrafish GD model the inhibition of ASM, ameliorates the pathological phenotype and the survival, rescuing the mitochondrial chain function.

Based on these considerations, the aim of my PhD project was to investigate whether the inhibition of ASM could have a beneficial role in GBA-related pathologies exploiting 2D and 3D *in vitro* neuronal models.

To conduct this research, I generated two experimental models: a pharmacological one, using hiPSCs-derived dopaminergic neurons (hiPSCs-DANs), and a patient-derived one, using human midbrain organoids (hMOs).
For the pharmacological model, I treated DANs for 30 days with conduritol-B- epoxide (CBE), a specific inhibitor of GCase, to induce the GD-PD phenotype. This is an experimental model that we have already demonstrated to show GCase deficiency, neurodegeneration and GlcCer accumulation.
For the patient-derived one, I generate hMOs from iPSCs of a GD type I patient carrying the biallelic mutation N370S/F213I in GBA gene, who developed parkinsonism. I characterized this model and I demonstrated that

it recapitulates the pathological features observed in the 2D model, with the addition of α-synuclein aggregation.
These results point out that both dopaminergic neurons and organoids partially recapitulate the pathological phenotype observed *in vivo.* Thus, they constitute a good model for further investigations related to GD-PD pathology.

Furthermore, I treated both models with amitriptyline (AMI), a functional inhibitor of ASM, to verify the effect of ASM inhibition in GD-PD pathology.
I treated DANs 24h and 7 days before the collection at day 60 of differentiation. In hMOs instead the administration was longer, lasting 30 days and 70 days. Surprisingly, I found opposite results in the two models. Indeed, the acute (24h) and chronic (7 days) treatment with AMI has ameliorated the neurodegenerative phenotype in CBE-treated DANs, reducing GlcCer accumulation by increasing the non-lysosomal glucosylceramidase (NLGase) activity. Conversely, in hMOs the prolonged drug administration was detrimental for GD-PD organoids, increasing neurodegeneration and lysosomal impairment, without changes in GlcCer accumulation and promoting α-synuclein aggregation.

This study introduces two reliable *in vitro* models for studying GCase deficiency in neurons, providing valuable insights into GBA-related neurodegenerative disorders. However, midbrain organoids emerge as a preferable choice for these investigations since they closely mirror the physiological conditions of the brain.
And according to the results obtained, it become evident that ASM inhibition has a damaging effect on GBA-dependent Parkinson's disease *in vitro* models.

2 INTRODUCTION

2.1 Sphingolipids

2.1.1 Structure and chemical-physical properties

Sphingolipids (SLs) are a class of amphiphilic molecules that constitute cell membranes. They consist of a hydrophobic tail, called ceramide, embedded in the membrane lipid core and a hydrophilic polar head extending into the extracellular compartment. Ceramide, the common hydrophobic moiety in all SLs, is composed of a long-chain amino alcohol, the sphingosine, bound through an amidic linkage to a fatty acid chain, typically N-palmitoyl acid (C16) or stearic acid (C18) (**Figure 1**).

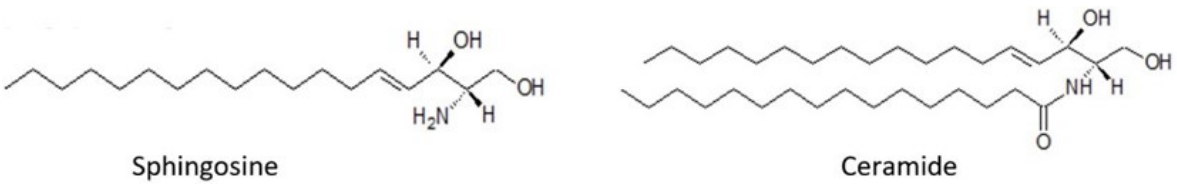

Figure 1. Chemical structure of sphingosine and ceramide

The amidic bond facilitates the formation of a dense network of hydrogen bonds between SLs and specific membrane proteins, leading to stable lateral interactions and self-segregation within the so-called "SL-enriched membrane domains" or "lipid rafts." These dynamic molecular assemblies, inclusive of cholesterol, serve as essential cellular signaling platforms, influencing ligand affinity, effector specificity, membrane sorting, receptor trafficking, and recycling.[1]

SLs play a dual role in organisms, contributing both structurally and functionally. Many cell surface interactions, communication with the extracellular matrix or to other cells, and signal transduction mechanisms depend on the modulation of SLs, designating them as bioactive molecules. These molecules play a role in inflammatory processes, cancer malignancies, and metastasis formations [2], impacting cell adhesion, proliferation, migration, growth, differentiation, and apoptosis.[3]

SLs are particularly enriched in the extracellular leaflet of the plasma membrane (PM), and they define the structure, integrity, and fluidity of the phospholipid (PL) bilayer. Abundantly expressed in the Central Nervous System (CNS), SLs participate in CNS development and homeostasis maintenance, however they are also implicated in inflammation and degenerative processes. Indeed, altered SL expression is reported in neurodegenerative disorders such as Alzheimer's Disease (AD) and Parkinson's Disease (PD), hypothesizing to be associated with the onset of pathological phenotypes. [4]

The hydrophobic tail, represented by ceramide, is common to all SLs despite potential variations in length of the carbon chain.
The hydrophilic head group, linked via a β-glycosidic linkage to the first hydroxy group of the ceramide backbone, defines different groups of SLs. The principal classes include phosphosphingolipids (PSL) and glycosphingolipids (GSL).

PSL are characterized by the presence of one or more phosphate groups in the hydrophilic moiety. This family includes sphingomyelin (SM) (**Figure 2a**), a prevalent PSL in most mammalian tissues, with a phosphocholine as a polar headgroup, and ceramide-1-phosphate (Cer1P), which plays a role in processes such as phagocytosis, stimulation of DNA synthesis, and inhibition of apoptosis.

In GSL the polar portion has a carbohydrate nature, ranging from monosaccharides in cerebrosides to polysaccharides in more complex GSL. GSLs are often categorized as neutral (cerebrosides and globosides) and acidic (gangliosides and sulfatides) based on their charge.

The simplest GSLs, called cerebrosides, are galactosylceramide (GalCer) (**Figure 2b**) and glucosylceramide (GlcCer) (**Figure 2c**), which are obtained from the β-linkage of galactose or glucose to ceramide. They are prevalently located at encephalic level and in the peripheral nervous tissue, with particular regards for myelin sheaths.

Cerebrosides act as metabolic precursors for more complex derivatives: GalCer is the precursor of sulfatides, while GlcCer can be modified by the addition of a molecule of galactose to form lactosylceramide (LacCer), an intermediate in the biosynthesis of Globo-, Isoglobo-, Lacto-, NeoLacto-or Ganglio-series. [3]

Globosides are SLs containing two or more sugar moieties among glucose, galactose, and N- acetyl-galactosamine.

Gangliosides, categorized as acidic GSLs, consist of an oligosaccharide chain composed of monosaccharide residues (ranging from 3 to 15-20) that binds through an α- glycosidic linkage one or more sialic acid residues, which confer a negative charge to gangliosides, enhancing their acidic properties. Predominantly located in the outer layer of the PM, gangliosides are especially concentrated in the ganglion cells of the central nervous system, particularly at nervous terminals. Anchored to the PM by a hydrophobic ceramide backbone, gangliosides extend their oligosaccharide moiety into the extracellular compartment. In this position, they serve as receptors, interacting with various membrane proteins to modulate recognition processes and

regulate crucial cell functions such as neurogenesis, synaptogenesis, and synaptic transmission. Among the ganglioside family, GM1 (**Figure 2d**), is the most represented species, constituting 10-20% of the total brain ganglioside content.[5] The simplest ganglioside, GM3 (**Figure 2e**), has been shown to play a role in the regulation of cell proliferation.

Sulfatides, acidic GSLs with a sulfuric group as a polar head, contribute to cell recognition, adhesion processes, protein trafficking, and cellular aggregation. They are esters of GalCer and sulfuric acid, which confers acidic properties and a highly negative charge at physiological pH. Notably, sulfatides are crucial constituents of the outer leaflet of the membrane in oligodendrocytes and Schwann cells, playing a fundamental role in myelin structuring and functioning. [6]

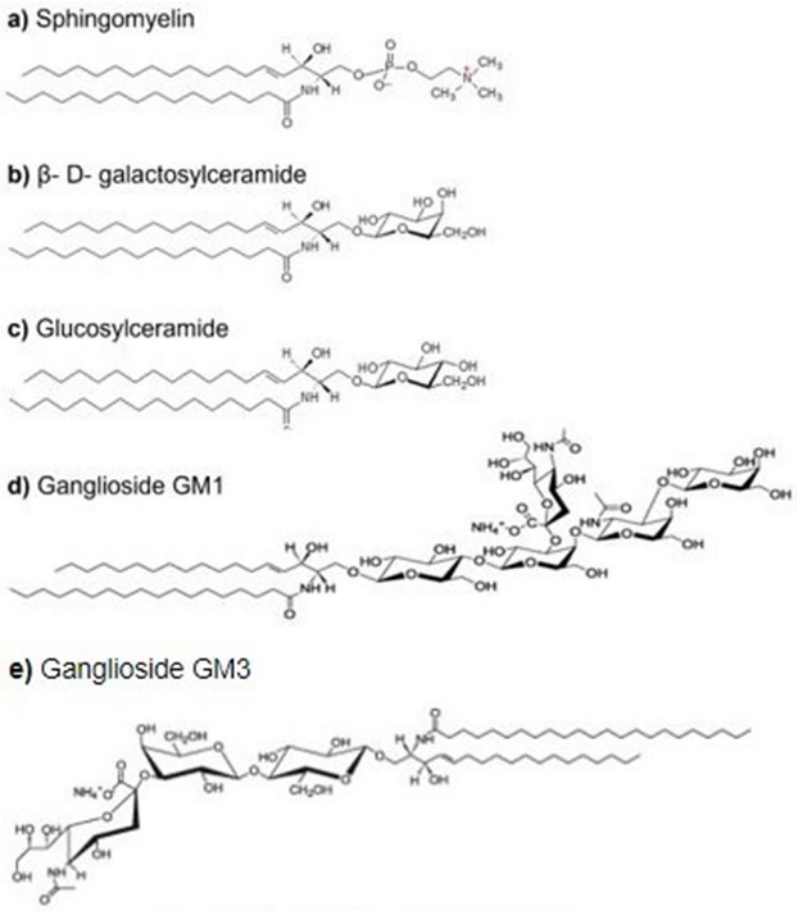

Figure 2. Chemical structure of the principal sphingolipids.
The first hydroxy group of the ceramide can be bound to a) a phosphocholine residue generating sphingomyelin; a monosaccharide molecule as for example galactose or glucose to give origin to either b) galactosylceramide or c) glucosylceramide; a longer oligosaccharide chain to which one or more sialic acid residues are attached forming gangliosides as the d) ganglioside GM1 and e) ganglioside GM3.

2.1.2 Sphingolipids metabolism

The metabolism of SLs involves intricate processes that are regulated by various intracellular and extracellular signaling pathways. These pathways regulate the enzymes responsible for SL biosynthesis, trafficking, and catabolism, influencing the PM GSLs' composition, which is characteristic of each cell type and varies based on developmental stage, cellular functions, and physiological/pathological conditions (**Figure 3**).

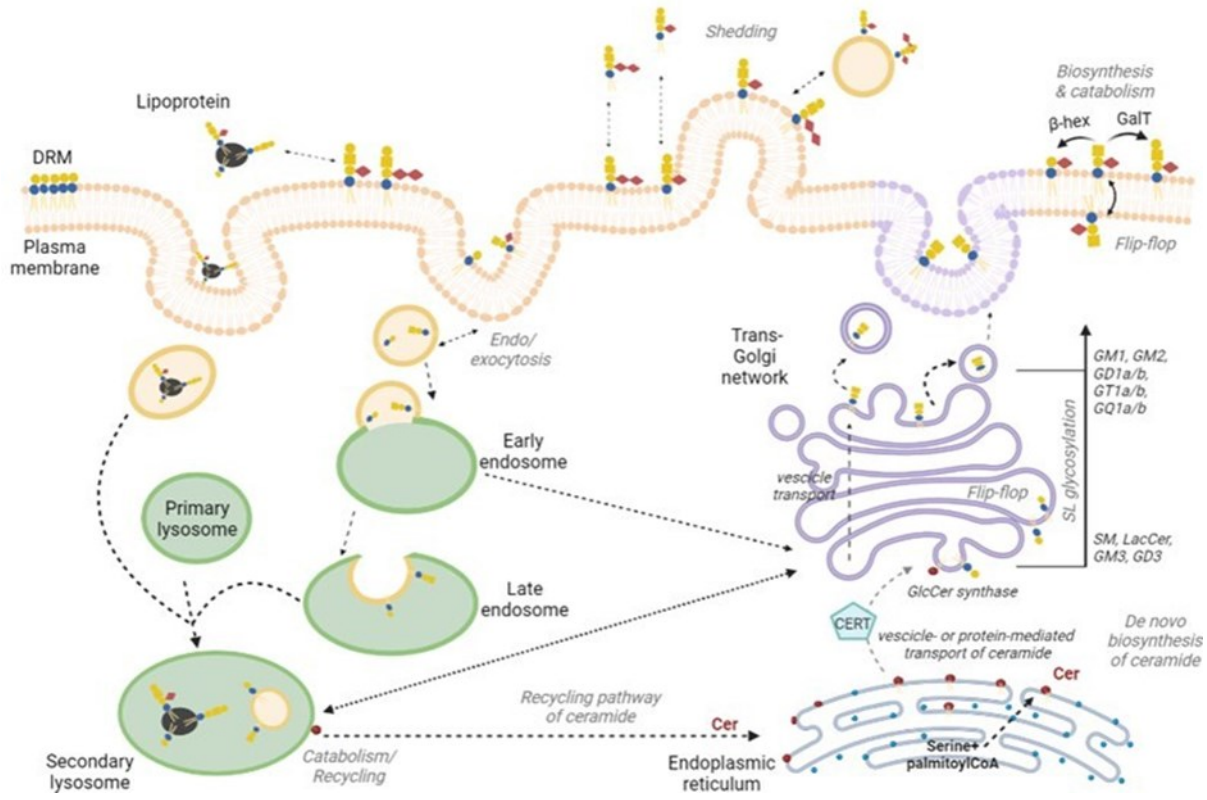

Figure 3. Schematic representation of the pathways involved in the SL metabolism (biosynthesis, trafficking, and catabolism) both at intracellular and at plasma membrane level (Cer= ceramide, SM= sphingomyelin; LacCer= lactosylceramide; GlcCer= glucosylceramide; β-hex= β-hexosaminidase; GalT= galactosyltransferase; DRM= detergent-resistant membrane portion)

2.1.2.1 Biosynthesis

Ceramide, constitutive in all SLs, is a crucial precursor for GSLs biosynthesis. The energetic cost of GSL biosynthesis is high for the cell, and besides de novo synthesis in the endoplasmic reticulum (ER), ceramide can also be derived from the sphingosine recycling pathway. In the metabolic salvage pathway, sphingosine obtained from complex SLs catabolism is directed from the lysosome to the ER, where it undergoes acylation.[7]

De novo biosynthesis of ceramide involves four steps (**Figure 4**), starting with the condensation of L-serine and palmitoyl-CoA in 3-keto-sphinganine, which is then reduced and subjected to addition of a fatty acid using acylic chains activated with Coenzyme A. The final desaturation step happens at the level of the endoplasmic reticulum.

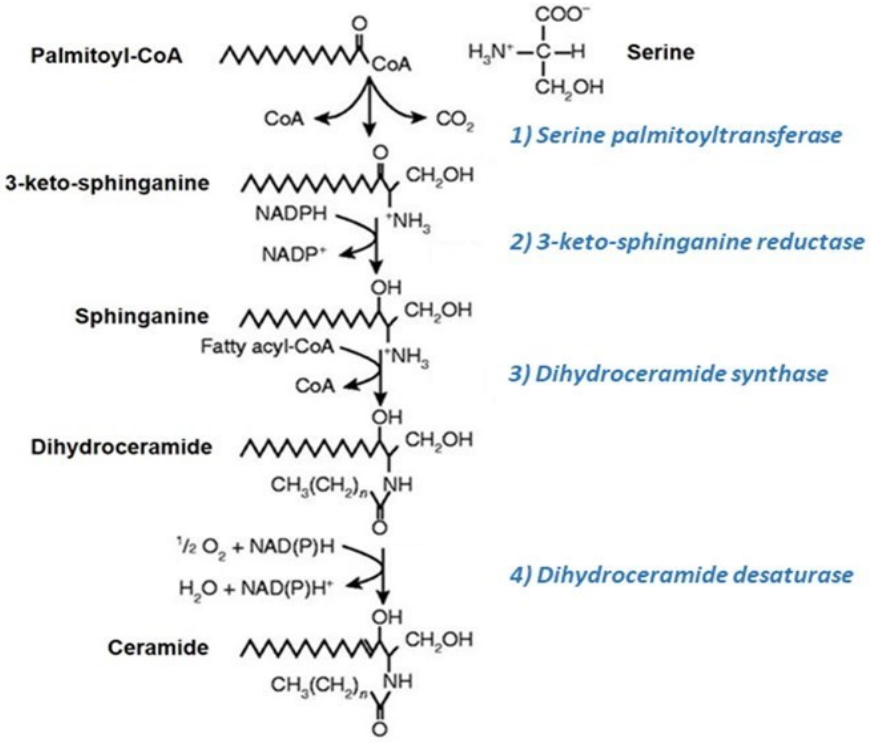

Figure 4. Pathway representing the de novo biosynthesis of ceramide starting from L-serine in the endoplasmic reticulum.

The newly synthesized ceramide is then transported to the Golgi apparatus or to PM through vesicular-dependent and independent mechanisms. In both sites, glycosyltransferases attach a hydrophilic head to the hydroxyl group located at C1 of ceramide[8], initiating complex SLs biosynthesis. Each SLs' class undergoes a typical biosynthetic process, which are summarized in **figure 5**.

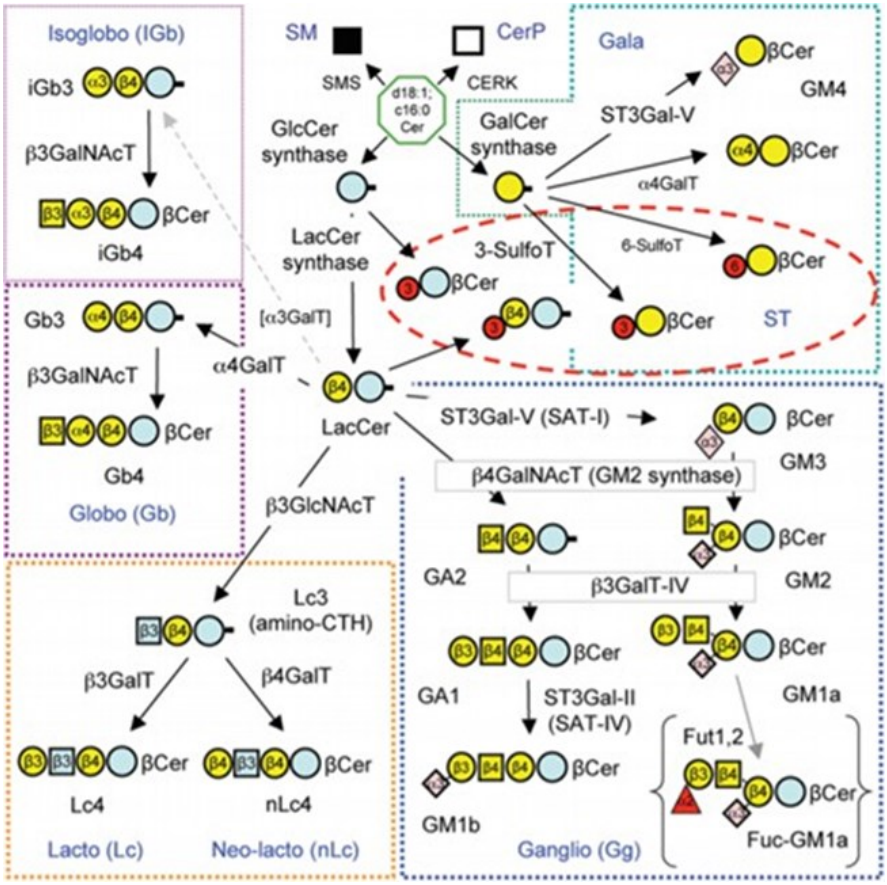

Figure 5. Biosynthesis of sphingolipids

Scheme representing the major headgroups addition in the Golgi apparatus during the biosynthesis of complex sphingolipids. Each section represents a GSL category. Green dashed area: ala-series; red dashed area: sulfatides; blu dashed area: gangliosides; yellow dashed area: lactosides and neolactosides; purple dashed area: globo and isoglobo series. Cer= ceramide; LacCer= alctosylceramide, GalCer= galactosylceramide; GlcCer= glucosylceramide; GalNAc= N-acetylgalactosamine; Fuc= fucosyl; T= transferase.

The biosynthesis of PSL Cer1P is mediated by a ceramide kinase (CERK) selective for ceramide with a minimum acyl chain of 12 carbons.

SM is produced at the level of PM and of the Golgi apparatus, by sphingomyelin synthase SMS2 and SMS1 respectively, that transfer the phosphocholine head group from a phosphatidylcholine to the ceramide and release diacylglycerol (DAG). SMS2 is also able to transfer phosphatidylethanolamine to ceramide, synthetizing PECer.

GSLs undergo synthesis through a stepwise process involving the consecutive addition of carbohydrate residues to the ceramide backbone or the growing saccharide chain. Specific membrane-bound glycosyltransferases transfer specific carbohydrates from a sugar nucleotide to a specific acceptor, resulting in the formation of the oligosaccharide chain.

The initial step occurs at the cis-Golgi network, where the synthesized ceramide is transported via vesicles.

Within the cytosolic leaflet, UDP-glucose ceramide glucosyltransferase catalyses the transfer of a glucose molecule from UDP to the hydroxyl group at C1, resulting in the formation of glucosylceramide. This GlcCer can either reach the PM or be translocated to the luminal side of the Golgi apparatus, where it undergoes further glycosylation by lactosylceramide synthase, leading to the production of LacCer, which represent a branching-off point for the formation of more complex GSLs. [9]

Gangliosides originate from LacCer and undergo synthesis within the Golgi apparatus lumen through the action of sialyl-transferases. This process involves the addition of sialic acids to a terminal galactose residue, forming an α-glycosidic bond. Following the sequential transfer of neutral sugars and sialic acids, facilitated by vesicle-mediated transport, gangliosides are subsequently incorporated into the outer leaflet of the PM (**Figure 6**).

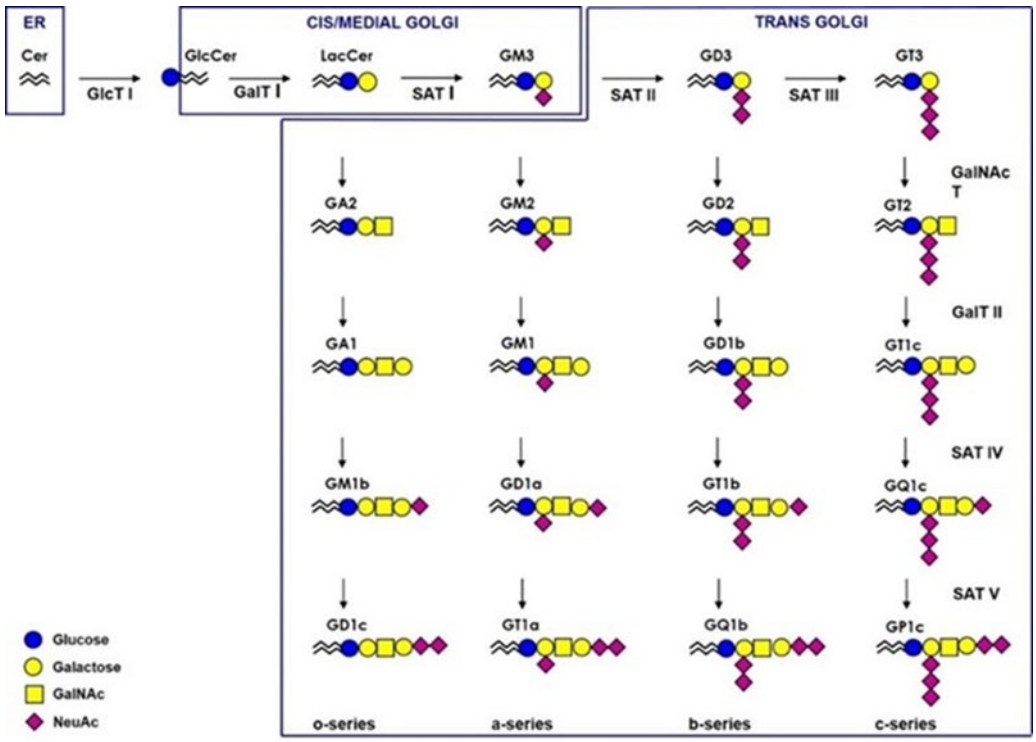

Figure 6. Schematic representation of the gangliosides series biosynthesis

2.1.2.2 Trafficking

SLs undergo extensive movements within the cell via vesicle- or protein-dependent pathways.[10] After the synthesis in the ER, SLs are subjected to several glycosylation steps necessary to form complex GSLs in the Golgi; once the synthesis is completed, lipids are transferred to the PM, where they can pass between membrane leaflets through spontaneous movement or thanks to the action of proteins called flippases.

2.1.2.3 Catabolism

Cell surface lipids exhibit a highly dynamic behaviour, constantly undergoing internalization through endocytosis and subsequent recycling to the PM. SL inserted in the PM are addressed to the lysosome through the endocytic pathway, where they are degraded by the sequential action of specific hydrolases.

Lysosomes and endosomes serve as the primary sites for the degradation of GSLs. These cytoplasmic organelles are spherical vacuoles enclosed by a lipid membrane with a diameter of 0.5 µm, containing enzymes involved in the catabolism of various macromolecules, originating from both intracellular damaged structures and those imported from the external environment. As a result, lysosomes are often referred to as the "digestive system" of the cell.

Portions of the PM containing GSLs designated to degradation are internalized through endocytosis, the vesicles pass through endosomes to reach and fuse with the lysosomes, becoming part of the intralysosomal membrane. Another distinctive feature of lysosomes is their acidic luminal pH (approximately 4.5-5), crucially maintained by ATP-dependent proton pumps (V-ATPases). This acidic environment is essential for the optimal functioning of the hydrolytic enzymes present in the lysosomal lumen. [11,12]

2.1.3 Sphingolipid hydrolases

Initially synthetized in the ER, lysosomal hydrolases are transferred to the Golgi apparatus, where they undergo a maturation process involving the addition of a mannose-6-phosphate (M6P) residue. At the trans-Golgi level, these enzymes are recognized by the M6P receptor (M6PR) and internalized into clathrin-coated vesicles. These vesicles, shedding their protein coats, emerge from the Trans-Golgi Network (TGN) and travel to the endosomal compartment (**Figure 7**).

Upon reaching the late endosome, the hydrolases detach from the M6PR. The M6PR then undergoes a retrograde journey via the vesicular pathway back to the TGN. In late endosomes hydrolases experience maturation induced by ATP-dependent proton pumps, leading to acidification with a pH range of 4-5. This acidic environment triggers the removal of the phosphate group from the mannose molecule and activates

the hydrolases. [11,12]

The majority of SL hydrolases are N-glycoproteins, identifiable within the endolysosomal compartment due to the exposure of Man6P residues. Both in the cytosol and on the PM exist Man6PR capable of capturing escaped glycohydrolases and directing them back to the lysosome.

An exception to this process is represented by β-glucocerebrosidase (GCase), which is transported to lysosomes in aM6P-independent manner, exploiting the lysosomal integral membrane protein (LIMP-2) for its transport. Notably, deficiencies in LIMP-2 can lead to the onset of the myoclonus-renal failure syndrome, sharing certain characteristics with Gaucher disease (GD).

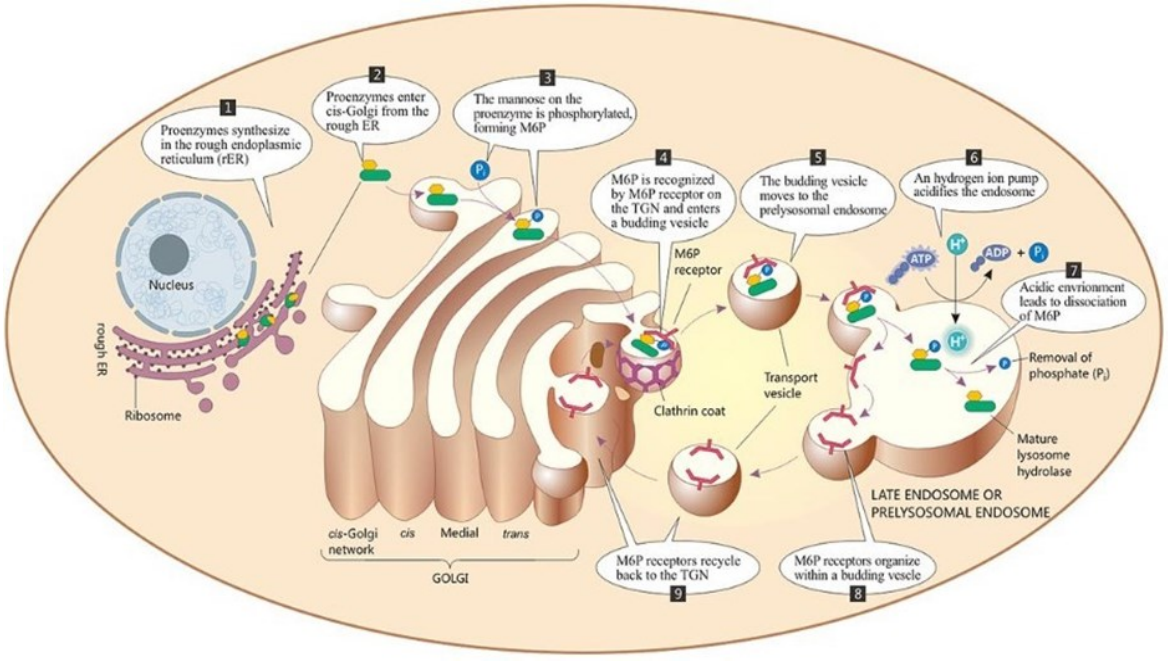

Figure 7. Schematic representation of the biosynthesis and transport of lysosomal enzymes

Glycohydrolases function by sequentially removing saccharide residues, starting from the non-reducing end of the oligosaccharide chain. However, they are unable to act on short-chain GSLs within the intralysosomal membrane. To overcome this limitation, the presence of activator proteins is crucial for proper GSL catabolism. Saposins (Sap A, B, C, and D) and GM2 Activator Protein[13] are examples of activator proteins that facilitate the presentation of the substrate to hydrolytic enzymes.

Upon the complete removal of the oligosaccharide chain, the resulting product is ceramide, which can be further hydrolyzed into sphingosine and a fatty acid. Sphingosine undergoes phosphorylation to form

sphingosine-1P or is converted back into ceramide in the ER, initiating the biosynthesis of new GSLs. Generally, all the molecules derived from this catabolic process can leave the lysosome and be recycled for biosynthetic purposes.

The key hydrolytic enzymes involved in this process include β-galactosidases, β-hexosaminidases, sialidases, α-mannosidases, β-mannosidases, β-glucocerebrosidases (GCase), and the non-lysosomal β-glucoceramidases (NLGase). Notably, NLGase predominantly operates at the PM level, distinguishing it from the others mentioned enzymes (**Figure 8**).

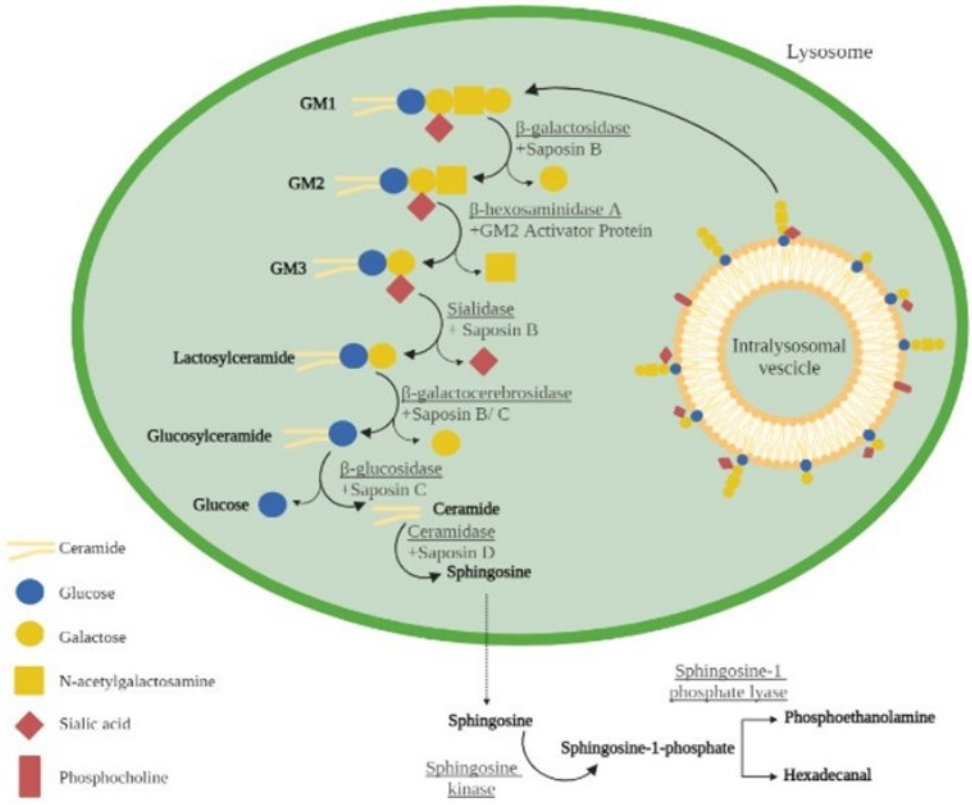

Figure 8. Schematic representation of the catabolism of complex glycosphingolipids.
The representation refers to the catabolism of ganglioside GM1 through the action of lysosomal glycohydrolases helped by their specific Saposins or Activator proteins.

2.1.3.1 β-galactosidases

There are two distinct forms of these enzymes implicated in the metabolism of lysosomal GSLs: β-galactocerebrosidase (β-gal, EC 3.2.1.23) participates in the catabolism of GalCer, LacCer, and galactosylsphingosine, while β-galactosidase removes galactose from glycoproteins and GM1 ganglioside

(**Figure 9**)[14]. The enzyme β-galactocerebrosidase, also known as β-galactosylceramidase (EC 3.2.1.46), primarily operates at the lysosomal level, but recent data suggest that its activity extends to the PM as well. Beyond their catabolic functions, these enzymes have been implicated in cellular senescence and neurodegeneration[15].

β-galactosidase activity serves not only as a marker for senescence but also as a potential marker for neuronal differentiation and apoptosis in human fibroblasts. On the cell surface, these enzymes likely play roles in cell-to-cell or cell-to-matrix interactions, influencing cell migration, differentiation, and axonal outgrowth [16].

2.1.3.2 β-hexosaminidases

The β-hexosaminidases (EC 3.3.1.52) are responsible for removing the N-acetylgalactosamine (GalNac) residue from the oligosaccharide chain of GM2 ganglioside, resulting in the production of GM3 (**Figure 8**). This enzyme exists in the same isoform associated with the PM or within the lysosome. During neuronal differentiation (**Figure 9**), these enzymes may actively participate in remodelling the outer layer of the PM, increasing their activity, and reaching their maximum when cells are at a fully differentiated state. [17]

Notably, PM-associated β-hexosaminidase activity tends to be higher in cells derived from patients with GD, especially in cases presenting the most severe form of the pathology with neuronopathic involvement. [18]

2.1.3.3 Mannosidases

Mannosidases constitute a group of enzymes involved in the hydrolysis of α- or β-linked mannose. There are two isoforms of α-mannosidases (EC 3.2.1.24) - the acid and basic α-mannosidases. These enzymes play a role in the lysosomal catabolism of N-linked glycoproteins by cleaving the mannosidic linkage from the non-reducing end of the saccharide chain[19] . On the other hand, β-mannosidases (EC 3.2.1.25) are responsible for hydrolyzing the β-mannosidic linkage found at the branching point of the pentasaccharide core of N-glycoproteins. [20]

2.1.3.4 β– glucosidases

β-glucosidases form a family of enzymes responsible for cleaving GlcCer into glucose and ceramide. This enzyme family is highly conserved across species, emphasizing their crucial functional roles. In eukaryotes, at least three different glucosidases mediate this reaction:

Lysosomal β-glucocerebrosidases (GCase, EC 3.2.1.45): Encoded by the GBA1 gene, GCase is sensitive to conduritol B epoxide (CBE) inhibition. It primarily operates in the lysosome but has also been reported to function at the PM level.

1. Non-lysosomal β-glucoceramidases (NLGase, EC 3.2.1.45): Encoded by the GBA2 gene, NLGase is

irreversibly inhibited by N-(5-adamantane-1-yl-methoxy-pentyl)-deoxynojirimycin (AMP-DNM) and is predominantly active at the PM level, ER, and endosomal vesicles. [21]

2. Cytosolic β-glucosidase (EC 3.2.1.21): Encoded by the GBA3 gene.

Although the pathology related to the loss of function of GBA3 is not fully understood, both emerging and past evidence suggest a direct involvement of GCase and NLGase in various diseases affecting the CNS. Specifically, loss-of-function mutations in NLGase have been linked to different forms of Ataxia.[22] Additionally, homozygous mutations in the GBA1 gene, encoding for GCase, have been associated with GD and GBA-related PD. [23]

GCase, a glycoprotein consisting of 495 amino acids, possesses four N-linked glycans, an 8-barrel structure, and a catalytic site containing two highly conserved carboxylic acid residues. [24] This enzyme exhibits activity not only within lysosomes but also at the PM (**Figure 9**), where it is involved in signaling cascades related to apoptosis and neuronal differentiation.[25] Despite its versatility across cellular compartments, GCase demonstrates optimal hydrolytic activity when associated with the lysosomal membrane. This preference is attributed to the enzyme's reliance on an acidic pH for optimal function and its promotion by negatively charged lipids and Saposin C. Notably, in contrast to the majority of lysosomal hydrolases, which are transported into lysosomes via M6PRs, GCase presents N-linked glycans that are directly recognized by the lysosomal membrane protein LIMP2 at the ER surface. This recognition facilitates the transport of GCase to lysosomes, contributing to its localization and function within these cellular organelles.

GCase deficiency causes GD, the most common lysosomal storage disorder, characterized by the accumulation of the un-catabolized substrate GlcCer in the lysosomes. Studies on human fibroblasts from GD patients revealed a substantial reduction in GCase activity at the PM compared to healthy subjects, confirming the dual localization of the GCase enzyme at both the cell surface and in lysosomes. [18]

The GBA2 gene, located on chromosome 9p13.3, encodes for the NLGase enzyme. This transmembrane protein is primarily associated with the PM, and to a lesser extent with the ER and endosomal vesicles. NLGase presents an intracellular N-terminal domain and an extracellular C-terminal domain[26] (**Figure 9**). This enzyme exhibits high expression levels in the brain, heart, skeletal muscle, and kidneys [27,28]. In humans, biallelic loss-of-function mutations of GBA2 result in the accumulation of GlcCer in lysosomes. This accumulation notably affects various organs, including liver, spleen, brain, and testis. Specifically, cerebellar spastic ataxia has been identified to correlate with GBA2 mutations, highlighting the neurological impact of these genetic alterations [22].

A hypothesized link exists between NLGase, neuronal differentiation, and neurodegeneration. In fibroblasts derived from GD patients, particularly those affected by the neuronopathic form with severe impacts on the

nervous system, a correlation was demonstrated. This correlation suggests that a reduction in GCase activity is associated with an increase in NLGase activity [18]. Such findings imply a potential interplay between these enzymes in the context of neurological conditions and may contribute to our understanding of the molecular mechanisms underlying neurodegenerative processes in GD.

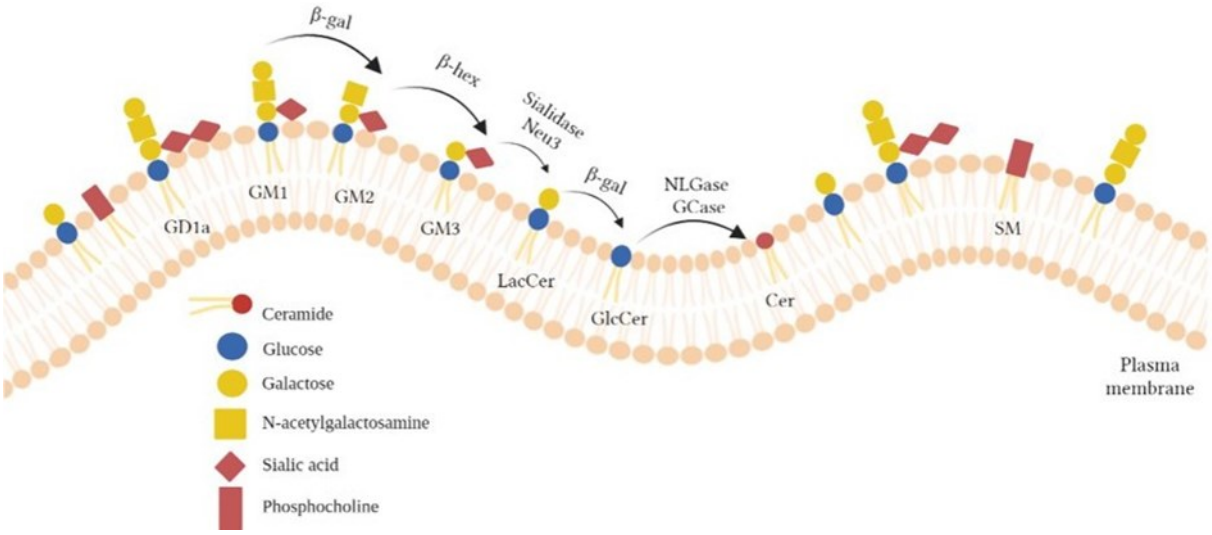

Figure 9. Catabolism of sphingolipids at PM level HexA= β-hexaminidase A; β-Gal= β-galactosidase; GCase= β-glucosidase; NLGase= β-glucosidase; SMase= sphingomyelinase; Neu3= sialidase 3; Cer= ceramide; GlcCer= glucosylceramide; LacCer= lactosylceramide; SM=sphingomyelin, GD1a, GM1, GM2, GM3 = gangliosides.

2.1.3.5 Acid sphingomyelinase

The acid sphingomyelinase (ASM, E.C. 3.1.4.12) lysosomal enzyme is responsible for the catabolism of SM into ceramide and phosphocholine.
It is encoded by sphingomyelin phosphodiesterase 1 gene (*SMPD1*) gene that consists of 6 exons and is located on chromosome 11p15.1-11p15.4.

The human ASM protein is initially synthesized as a 75 kDa pre-polypeptide consisting of 629 amino acids. This pre-polypeptide is then transformed into a 72 kDa precursor, undergoing extensive post-translational modifications during its transportation to the lysosome. Indeed, ASM exhibits optimal activity at a pH of 5.

Three types of human ASM transcripts have been identified: type 1, the primary ASM species, encodes an enzymatically active protein. Conversely, type 2 and type 3 transcripts do not produce functional enzymes due to alternative splicing, arising from a weak donor splice site in intron 3.

In humans, a genetic deficiency of ASM enzyme leads to Niemann–Pick disease types A and B, classified as lysosomal storage disorders. In particular, 185 *SMPD1* variants have been associated with this disease,

primarily manifesting as missense mutations (65.4%) or frameshift mutations (19%). [29]

Loss-of-function mutations in SMPD1 typically result in Niemann-Pick disease type A, a severe infantile neurovisceral form characterized by extensive hepatosplenomegaly and rapidly progressive neurological deterioration. Mutations that lead to the production of a partially active enzyme are associated with Niemann-Pick disease type B, which manifests as a primarily visceral condition allowing survival into adulthood. Some patients exhibit an intermediate phenotype, presenting neurological involvement and mental retardation. [30,31]

2.1.4 Sphingolipids in the Central Nervous System

Besides adipose tissue, the brain is the organ with the highest lipid content. The PM of neuronal cells exhibits a significant abundance of cholesterol and SLs, predominantly complex GSLs like gangliosides. These components play a crucial role in both embryonic development and neural differentiation.

Indeed, the development of the nervous system is characterized by a deep remodeling of PM SL composition in terms of expression level, complexity and distribution. Specifically, there is a notable increase in the overall content of GSLs in the brain as it develops. Simpler GSL species are replaced by more complex ones, indicating a crucial role of oligosaccharide chains in this process. During neuronal differentiation, there is a significant shift from globoside to ganglioside species, which is vital for proper brain function.

Gangliosides GD3 and GM3 are prominently expressed during the phase of neuronal stem cell proliferation[32] and their expression diminishes in the later stages of development. Gangliosides GM1, GD1a, GD1b, and GT1b characterize neurogenesis, axonal and dendritic arborization, as well as synaptogenesis phases[33]. Galactosylceramide (GalCer) and sulfatides become expressed in the later stages of development, playing a fundamental role in the myelination process, which is one of the final steps in oligodendrocyte differentiation[34]. (**Figure 10**).

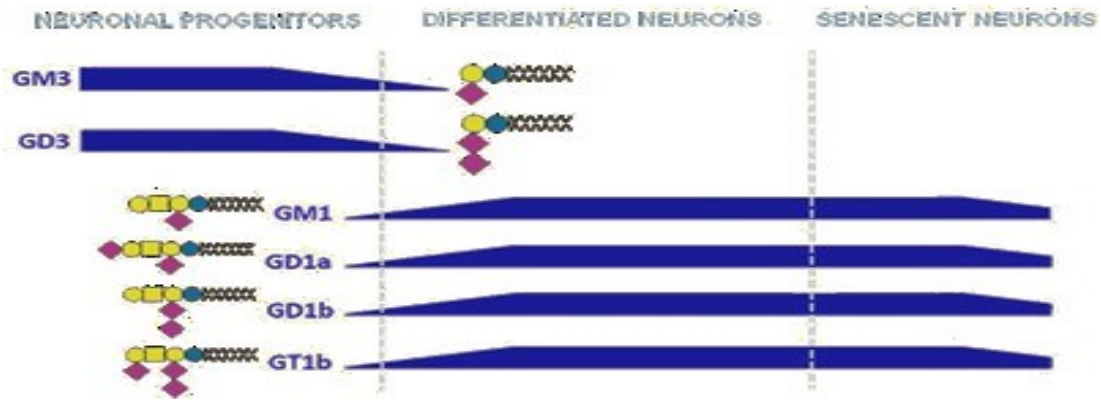

Figure 10. Modifications in neuron ganglioside pattern during neurodifferentiation

In humans, from the 6th month of gestational life, a rapid increase of ganglioside content begins, reaching its maximum peak at about 5 years of age. [35]
Coherently, during the nervous system development also the expression of the different glycosyltransferases and sialic-transferases changes.

In adulthood, each cerebral area experiences a distinct and gradual decline in ganglioside levels. Upon aging, there is an increase in the expression of simpler gangliosides like GM3, GD3, and GD1b, whereas more complex species such as GM1, GD1a, and GT1a show a decrease. Beyond the age of 20, the reduction extends to GalCer and SM, both essential components of myelin. These alterations in the SL pattern of the PM strongly influence neuronal functions. [5]

Various neurodegenerative diseases, such as PD, AD, and Huntington's disease, exhibit an accelerated decline in ganglioside level [36], along with a reduction in ganglioside expression when compared to individuals of the same age, particularly GM1 and GD1a [37]. In PD patients, for instance, there is a marked decrease in GM1 ganglioside expression observed in the substantia nigra (SN), the occipital cortex, and various peripheral tissues. Furthermore, in neuromelanin-containing neurons in the SN of PD subjects, there is a reported significant deficiency in the expression of genes involved in GM1 ganglioside synthesis, such as B3GALT4 and ST3GAL2. [38]

2.2 Lysosomal storage disorders

Lysosomal storage disorders (LSDs) include a range of pathological conditions characterized by inherited or acquired defects in the lysosomal catabolism of various molecules, including saccharides, glycogen, and peptides.

The consequence of lysosomal dysfunction is the accumulation of undigested material, leading to alterations in the shape and size of organelles and disturbances in the entire endo-lysosomal compartment. These disorders are categorized into different classes based on the nature of the accumulated compounds, including mucolipidoses, mucopolysaccharidoses, sphingolipidoses, oligosaccharidoses, neuronal ceroid lipofuscinoses, sialic acid disorders, and miscellaneous conditions[39].

From a phenotypical perspective, LSDs exhibit a broad variety of clinical manifestations that affect various organs. These manifestations span from cardiovascular issues and immunological manifestations to bone diseases and neurodegenerative phenotypes.
An example of lysosomal-associated neurodegeneration is present in the so-called *GBA*-related pathologies. These conditions are characterized by defects in lysosomal catabolism, which can lead to the onset of a neurodegenerative phenotype.

Indeed, the impaired activity of the endolysosomal compartment significantly impacts neuronal tissue. Neurons, being post-mitotic cells with limited regenerative capacity, are particularly susceptible to cellular stress and apoptosis. This vulnerability is enhanced by the combined effects of the accumulation of undegraded material [40] and dysregulated signalling. [41]

2.2.1 GBA-related pathologies

GBA is a gene located at 1q22, encoding the lysosomal enzyme β-glucocerebrosidase (GCase, IUBMB EC 3.2.1.45). GCase predominantly functions at the lysosomal level and is responsible for the catabolism of GlcCer into glucose and ceramide, achieved through hydrolytic cleavage of their β-glycosidic linkage. The GBA gene comprises 11 exons and features an untranslated pseudogene situated 16 kb downstream. Currently, more than 400 variants of this gene are recognized, the majority of which are missense mutations. However, there are also reported point mutations, frame-shift mutations, splicing mutations, and null alleles resulting from recombination with the homologous pseudogene sequence.

Alterations in the GBA gene are associated with various pathologies, including GD, PD, dementia with Lewy bodies, and REM sleep behaviour disorders [42,43].

Among the more than 300 loss-of-function variants reported for the GBA gene, the two most prevalent disease-causing mutations are L444P and N370S. These missense mutations are particularly diffused, as almost 85% of patients affected by GD and 95% of those with GBA-dependent PD present one of these mutations [44].

2.2.1.1 Gaucher Disease

GD is a rare inherited metabolic disorder. It is considered the most prevalent among LSDs. It is characterized by an incidence rate ranging from 1:40000 to 1:60000 within the general population. In addition, certain ethnic communities exhibit an increased frequency of manifestation, such as the Jewish Ashkenazi population where the incidence range from 1:500- 1:2000.

The transmission of GD follows an autosomal recessive inheritance, arising from a deficiency in GCase activity attributed to loss-of-function mutations in the GBA gene. This results in the accumulation of uncatabolized GlcCer primarily within the lysosomes, affecting the reticulate endothelial system, nervous system, and skeletal apparatus. Consequently, GD is characterized by a spectrum of clinical phenotypes, with heterogeneous and multi-organ clinical manifestations.

Based on the rate of clinical progression and involvement of the nervous system, GD has been conventionally classified in 3 main types:

Type 1 GD is the most common non-neuronopathic form, which manifests early in childhood and is usually diagnosed between 10-20 years old; it is characterized by a high variability of symptoms including: hepatosplenomegaly, bone disease and hematopoietic system abnormalities such as anaemia and platelet deficiency. However, some variations in type I GD phenotype have been reported: compared to the general

population, patients with GD type I have a 20-fold increased risk of developing PD and some experience parkinsonism at various ages over the course of the illness [45].

Types 2 and 3 instead present neurological manifestations that progress rapidly.

Type 2 GD is the most severe, acute neuronopathic form; with a very early onset (in the first six month of age), it causes death in the first years of life; besides the symptoms of GD type 1, it shows also neurological impairment.

Type 3 GD is the subacute or chronic neuronopathic form; it shows the visceral manifestations of GD type 1 combined with progressively invalidating neurological symptoms. [46]

While the accumulation of GlcCer in affected tissues is a common characteristic across all three types of GD, the underlying causes of its phenotypic heterogeneity remain elusive. Significantly, there is a lack of clear correlation between the clinical phenotype, residual enzymatic activity, and specific mutations in the GBA gene. As a result, predicting the phenotype or prognosis based on these factors remains unreachable.

2.2.1.1.1 Diagnosis and therapy for GD

The diagnosis of GD can be either molecular or functional. To diagnose the condition, specific criteria must be taken into consideration, such as the detection of biallelic pathogenic variants in the GBA gene and the determination of GCase activity, which should register between 0-15% of the standard levels.

DNA analysis is utilized for molecular genetic tests, involving the characterization of gene mutations. However, when GD is suspected, the preferred diagnostic method is the enzymatic approach due to its immediacy and high reliability. This method employs a specific enzymatic assay to measure β-glucocerebrosidase activity, utilizing the fluorometric substrate 4-methylumbelliferyl-β-D-glucopyranoside. The assay can be easily conducted on various patient samples, including leukocytes, fibroblasts, and lymphoblasts and, for prenatal diagnosis, on chorionic villi and amniocytes.

The principal therapeutic approaches used to treat GD aim to restore the deficient GCase activity and include Enzyme Replacement Therapy (ERT) and Substrate Reduction Therapy (SRT).

ERT involves the daily intravenous administration of small quantities of recombinant β-glucocerebrosidase. Up to now, three available molecules are utilized: Vpriv (produced using human fibroblasts), Elelyso (produced using carrot cells), and Cerezyme. Cerezyme is generated in Chinese hamster ovary cells and incorporates two Man6P residues, which allow its recognition by Man6PR in the endolysosomal compartment. This strategy allows to increase the amount of GCase present at lysosomal level to catabolize the accumulated GlcCer. Despite these advancements, the inability of the enzyme to cross the blood-brain barrier restricts the application of these compounds for treating neurological symptoms in GD type 2 and 3.[47]

An alternative therapeutic approach is SRT, which focuses on reducing the accumulation of GlcCer in lysosomes. N-butyldeoxy-nojirimycin (NB-DNJ), known as Zavesca, inhibits glucosylceramide synthase—the enzyme responsible for GlcCer synthesis (Cox et al., 2000). Two FDA-approved drugs in the SRT category, Zavesca and Cerdelga, have demonstrated favourable safety and efficacy profiles.[47] In contrast to ERT, these drugs are orally administered and do not elicit immunogenic responses. Furthermore, SRT exhibits the ability to alleviate symptoms in GD type 2 and 3 patients by effectively crossing the blood-brain barrier (BBB). However, due to significant side effects impacting certain metabolic pathways, their prescription is limited to patients unsuitable for ERT therapy. [48]

Other possible therapies for GD consist in gene therapy (GT), allogeneic hematopoietic stem cell transplantation (allo-HSCT) and chaperone therapy. [47]

GT works replacing a disease-causing gene with a healthy copy of the gene using viral vectors. It can be *in vivo* GT when the vector is administered directly into the patient or *ex vivo* GT when the vector is administered in cultured cells taken from the patient that are subsequently transplanted back. Up to now, are ongoing some clinical trials using lentiviral vectors for *ex vivo* therapy of GD, while *in vivo* GT for GD manifests promising results in GD mice models, ameliorating the life span and the neuropathological phenotype by naturally crossing the BBB.

Allo-HSCT uses hematopoietic stem cell from healthy donor to restore GCase activity through “cross-correction”. Despite some advantages, allo-HSCT is usually replaced by ERT for a higher efficacy and lower toxicity.

Another approach is represented by chaperone therapy, which recovers GCase activity by correction of misfolding enzyme. A good candidate for GD therapy is represented by Ambroxol, a chaperone with promising effects on visceral manifestations of GD type I, however Ambroxol is a mutation-specific drug therapy.

2.2.1.2 GBA-dependent Parkinson’s Disease

Following AD, PD is the second most prevalent neurodegenerative disorder. Individuals with PD typically exhibit predominant motor symptoms, including tremors at rest, bradykinesia, muscle rigidity, postural instability, and akinesia. However, the pathology is not confined only to motor symptoms; it is also linked to a variety of non-motor manifestations such as cognitive decline, depression, anxiety, sleep disturbances, hyposmia and dysautonomia.

This neurodegenerative disorder is characterized by the selective loss of dopaminergic neurons in the *pars compacta* of the SN. These neurons play a crucial role in voluntary movements, and their regulatory pathway relies on the neurotransmitter dopamine, which is typically diminished in PD.

A prevalent neuropathological feature in PD involves the accumulation of misfolded α-synuclein protein, leading to the formation of Lewy Bodies within neurons in affected regions. Therefore, PD is categorized as a synucleinopathy. The precise mechanisms linking the aggregation of this small protein, essential for synaptic functioning, to the initiation of neurodegeneration in PD remain unclear. Current hypotheses propose the involvement of oxidative stress, inflammation, aberrant protein handling, and mitochondrial dysfunction in this process. [49]

From an epidemiological perspective, PD impacts 1-2 individuals per 1000 in the population, with its prevalence increasing with age. Specifically, PD affects 1% of individuals above 60 years and 4% of those above 85. Among cases of PD, 90-95% are sporadic or idiopathic, while only 5-10% have a genetic basis. According to a multicentre analysis conducted by Sidransky et al. (2009),[50] approximately 5-30% of PD patients present mutations in GBA, which are currently considered the most common genetic risk factor for PD development. Indeed, carriers of heterozygous GBA mutations exhibit a five-fold higher risk of developing PD compared to the general population. [50,51] In addition, individuals with type 1 GD, characterized by homozygous mutations in GBA, present a 20-fold increased risk of developing PD. Furthermore, GBA-dependent PD patients experience symptom onset 3-6 years earlier than idiopathic PD (iPD) patients, with a significant worsening of both motor and non-motor symptoms over the course of the disease. [52,53,54]

However, interestingly, individuals with the same GBA mutation may display different clinical presentations, and some may not develop PD at all. One possible explanation is the presence of genetic variants in other lysosomal enzymes that could modulate the penetrance of GBA mutations, influencing the development of PD. [55,56]

2.2.1.2.1 Diagnosis and therapy for PD

To date, there is no specific test for diagnosing PD. Diagnosis relies on assessing the patient's medical history and symptoms, coupled with a neurological and physical examination.

Current therapeutic approaches for PD are designed to address the deficit of dopamine in the striatum. However, these strategies primarily offer symptomatic relief and are not able to alter the course of the disease.

The preferred and established treatment for PD is Levodopa, a dopamine precursor known as the gold standard, able to cross the blood-brain barrier. When administered, it is combined with peripheral DOPA-decarboxylase inhibitors, which extend its half-life and increase the amount available to reach the central

nervous system. The co-administration of a catechol-O-methyltransferase (COMT) inhibitor further enhances drug absorption and prolongs its half-life, thus reducing motor complications associated with long-term Levodopa therapy. [57]

Alternatively, dopamine agonists offer another therapeutic approach. Unlike Levodopa, these drugs act directly on dopamine receptors without the need for metabolic conversion into an active compound. Although effective in controlling dopaminergic symptoms for a limited period, the drawback is the eventual development of pharmacological resistance over time. [57]

Another pharmacological treatment involves monoamine oxidase inhibitors (MAO), which act by reducing dopamine catabolism, increasing the dopaminergic tone. In addition, these compounds have been reported to potentially exert a neuroprotective effect, preventing the production of reactive oxygen species, and enhancing the levels of neurotrophic and anti-apoptotic factors in both neurons and glial cells. [58]

2.2.1.3 Correlation between GCase deficiency and α-synuclein accumulation

Until 2004, the GBA gene was primarily associated with GD. However, recent studies have revealed an elevated susceptibility to PD and different parkinsonian manifestations in individuals with GD type 1, especially those carrying the prevalent mutations p.N370S and p.L444P.[59] Additionally, a diminished GCase activity has been observed in the brains of PD patients, either carrying GBA mutations or sporadic.[60]

While the connection between GBA mutations and both GD and PD is well-established, the exact molecular mechanism that links GBA mutations with the onset of neurological impairment in GD and PD remains unclear. Two different theories have been proposed to try to explain the correlation between GCase deficiency and the onset of neuronal damage: one loss-of-function and the other gain-of-function.

The “loss of function” hypothesis suggests that a deficiency in GCase activity causes accumulation of GlcCer, impairing the autophagy-lysosomal system. As a result, the degradation of α-synuclein is only partially performed, leading to the accumulation of the protein and the formation of aggregates. When released into the extracellular space, these aggregates activate microglia, triggering neuroinflammation.[61]

In the existing literature, a proposed auto-propagation mechanism for the pathology has been suggested (**Figure 11**). Certain findings have shown in iPSCs-derived neurons obtained from GBA-PD patients that the accumulated GlcCer might act as a scaffold, facilitating the aggregation and stabilization of soluble oligomeric α-synuclein. This α-synuclein aggregation, in turn, results in GCase retention in ER, impairing intracellular trafficking and GCase activity. This creates a bidirectional pathogenetic loop, contributing to the self-

propagation of the disease. [62,63] Moreover, GCase deficiency and excessive α-synuclein impair the protein quality control system, exacerbating α-synuclein accumulation.

Furthermore, a malfunction in the autophagy-lysosomal system results in an impaired turnover of mitochondria, causing the accumulation of dysfunctional mitochondria, oxidative stress, and a decline in ATP production. [64]

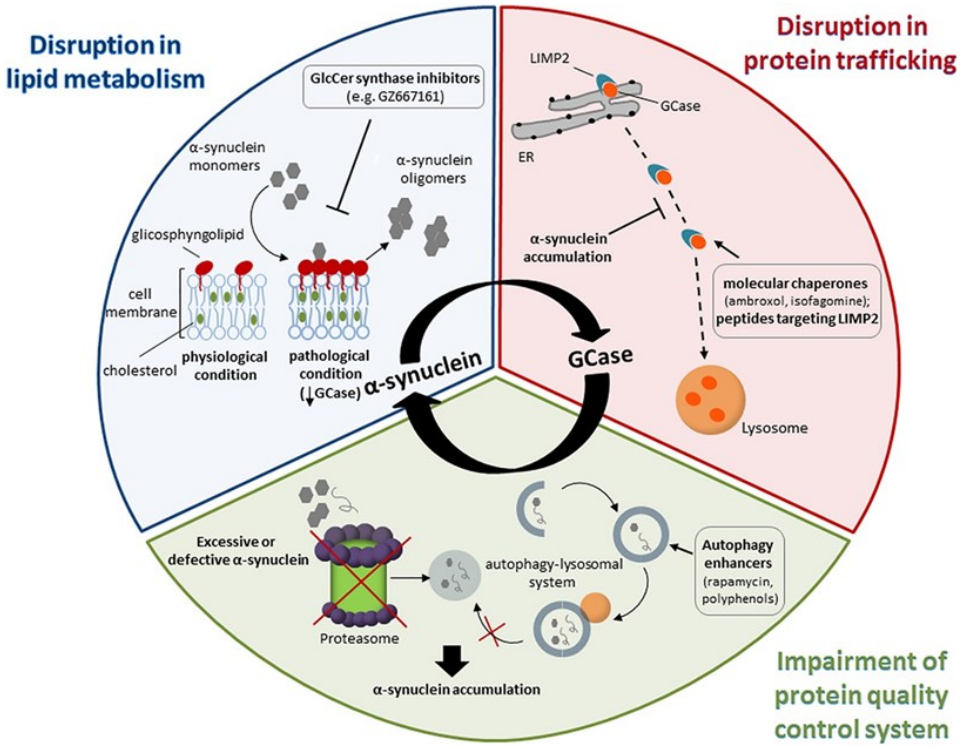

Figure 11. Bidirectional pathogenetic loop between α-synuclein and GCase – the loss-of- function hypothesis.

Blue, GCase-induced changes in membrane lipid composition promote toxic α-syn conversion; red, α-syn accumulation impairs GCase trafficking; green, excessive/defective α-syn and GCase deficiency impair quality control systems, exacerbating α-syn accumulation. Boxes, potential pharmacological strategies.

Conversely, the "gain of function" theory assesses that certain GBA mutations lead to the improper folding of GCase. This misfolded protein is transported back into the cytosol and eliminated by ubiquitin-proteasome system (UPS) through a process called Endoplasmic Reticulum Associated Degradation (ERAD). The constant effort necessary to process misfolded GCase was shown to increase ER stress, resulting in an impaired degradation of other misfolded proteins, including α-synuclein, thereby contributing to the process of neurodegeneration [61] (**Figure 12**).

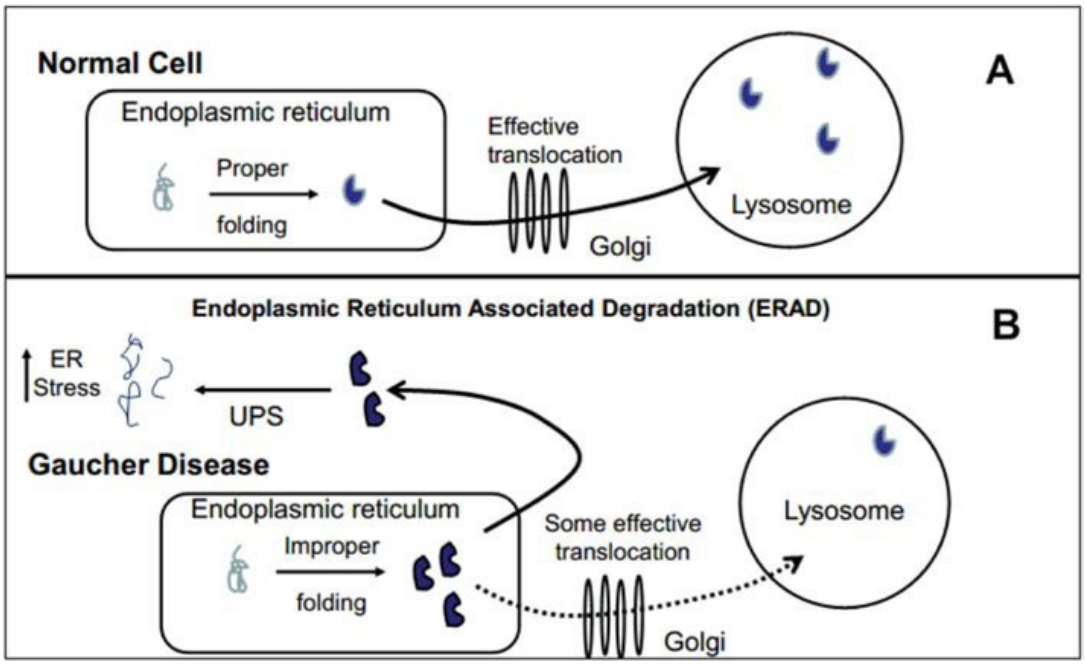

Figure 12. Role of GCase in α-synuclein pathology – the gain-of-function hypothesis.

A) In a wild-type cell, GCase is properly folded in the endoplasmic reticulum (ER) and successfully translocated through the Golgi into the lysosome. **B)** In the presence of a GBA1 mutation, the ER cannot consistently fold GCase correctly. GCase misfolded proteins are then exported into the cytosol and degraded via the ubiquitin-proteasome system (UPS). This process is called Endoplasmic Reticulum Associated Degradation (ERAD). The gain-of-function hypothesis states that GBA1 mutations increase utilization of ERAD, creating and sustaining ER and UPS stress and thus impairing degradation of α-synuclein oligomers.

2.2.1.4 In vitro models for PD and neuronopathic GD

Understanding the pathogenetic mechanisms involved in neurodegeneration in both GD and GBA-dependent PD is challenging due to the limited availability of suitable *in vitro* and *in vivo* models that accurately recapitulate the pathological features.

Indeed, the human brain *in vivo* is not directly accessible and work with post-mortem brain tissue from GD patients is complicated due to its low availability and rapid deterioration. For what concerns animal models, GBA knock-out mice, exhibiting complete enzyme deficiency, die within 24 hours after birth. Conversely, mice with partial GCase deficiency (where a single-allele is knocked-out) do not display nigrostriatal degeneration or behaviors associated with PD [65]. Furthermore, immortalized cells prove to be less reliable, as they carry intrinsic artifacts and undergo continuous mutations, resulting in an unstable genotype and, consequently, a variable phenotype. Commonly used models include differentiated neuroblastoma cell lines and fibroblasts derived from patient biopsies. However, primary cultures of patient-derived fibroblasts do not exhibit substrate accumulation [66] and neuroblastoma cell lines fail to recapitulate the same SL pattern observed in differentiated neurons.

Only recently, the development of new models exploiting human induced pluripotent stem cells (hiPSCs) has enabled the generation of human neurons with identical genetic features as those found in patients. Pluripotent stem cells, derived from fully committed adult cells, can be differentiated into various types of neurons, including dopaminergic, glutamatergic, GABAergic, or motoneurons [67]. Importantly, these neurons maintain the same pathogenic mutations as the patients from whom the hiPSCs were derived[68].

This provides a better understanding of the molecular processes not only responsible for the onset but also involved in the progression of the pathology. In the specific case of GBA-PD, hiPSCs can be derived from fibroblasts of PD patients and subsequently differentiated into dopaminergic neurons. This 2D model enhances our understanding of the molecular mechanisms implicated in the onset and progression of pathology. However, it lacks the capability to provide information about the surrounding environment which could influence the growth and development of neuronal populations, playing a crucial role in the pathogenesis.

Furthermore, research has demonstrated that utilizing a 3D matrix facilitates various biological functions, including differentiation, cellular signaling, lineage specification, and interactions between cells and their environment. Thus, in the last years the development of 3D cultures, called organoids, has been exploited to give better insights into the complexity and maturity of the studied organ or of its compartments.

A promising 3D in vitro model for GD and GBA-PD is represented by midbrain organoids, which are self-organized three-dimensional cultures of heterogeneous neuronal population, mainly composed by mature

dopaminergic neurons obtained from the patients-hiPSCs differentiation.

This new technique has opened a new research opportunity to better investigate the molecular mechanisms, the influence of surrounding cells and in general to better recapitulate the pathological features occurring in vivo.

2.2.1.5 ASM association with GBA

As reported above, individuals with GBA mutation may not develop PD, probably due to the presence of mutations in other lysosomal genes that could modulate the penetrance of GBA mutation in causing PD.

To this regard, our collaborators at Humanitas University conducted a comprehensive cohort study involving 207 asymptomatic carriers of the GBA mutation and 306 patients affected by GBA-PD. Using Next Generation Sequencing on a targeted panel of 50 LSD genes, the study revealed that the control group exhibited a higher prevalence of *SMPD1* mutations compared to the GBA-PD group, suggesting a potential protective role played by *SMPD1* mutations among GBA carriers.

A similar hypothesis has emerged from a recent study by Keatinge and colleagues, exploring the impact of ASM deficiency on a zebrafish model of GD. Their research revealed that inactivating ASM resulted in an improvement in the characteristic motor phenotype and enhanced survival in the zebrafish GD model. Additionally, the study demonstrated a restoration of neuronal health, as confirmed by RNAseq-based analyses, along with a rescue of mitochondrial respiratory chain function and a reduction in lipid peroxidation [69]. This unexpected rescue effect confirms ASM as a modifier of GBA deficiency *in vivo.*

In another study, Justice demonstrated that ASM inhibition significantly increases autophagy with preserved degradative potential. This finding is noteworthy, especially considering that GBA-dependent PD is characterized by lysosomal and autophagic impairment [70].

Furthermore, the lysosomal impairment characteristic of GBA-PD induces an enhanced fusion between lysosomes and the PM[71] resulting in an elevated presence of ASM at the cell surface. ASM, by hydrolysing SM molecules in the PM, generates an increased level of pro-apoptotic ceramide, which has been implicated in neurodegeneration [72]. Based on these considerations, the partial inhibition of ASM could reduce the production of pro-apoptotic ceramide and subsequently attenuate neurodegeneration.

On the other hand, however there are some contradictory results regarding the association between *SMPD*1 mutations and PD.

There are some other papers that show how specific *SMPD1* variants (R591C; L302P) could be identified as

risk factors for developing PD with an earlier age of onset of the disease. [73,74]

Moreover, in a recent work Alcalay and colleagues showed that *SMPD1* knock-down in cellular models results in decreased ASM levels, leading to α-synuclein accumulation, the protein closely linked to PD pathology [75].

2.2.1.6 Amitriptyline

Amitrptyline (AMI) was initially introduced in 1961 by Merck as a tricyclic antidepressant (TCA) primarily for major depressive disorder, which remains its only FDA (Food and Drug Administration) approved indication. Nevertheless, beyond its established use, AMI has demonstrated versatility in addressing a spectrum of additional symptoms.

Initially classified as a serotonin-norepinephrine reuptake inhibitor, this drug also presents antihistaminic and anticholinergic properties. It acts as a receptor antagonist for various histamine, muscarinic acetylcholine, and other receptors. Moreover, it has been reported to be able to block different sodium, calcium, and potassium channels. [72]

Furthermore, AMI assumes a significant role as a functional inhibitor of ASM. ASM resides in the inner leaflet of the lysosomal membrane attached by electrostatic forces. Upon ASM activating stimuli, occurs a translocation of the enzyme from the lysosome to the extracellular leaflet of the PM, where ASM generates ceramide from sphingomyelin. Several studies propose that the administration of functional inhibitors of ASM (FIASMAs), including AMI, results in the accumulation of the drugs within the acidic lysosomal compartments due to their weak basicity and high lipophilicity. Inside the lysosomes the drugs become protonated, avoiding the crossing of the membrane (acid trapping), and interfere with the binding of ASM to the membrane, resulting in its detachment and the consequent inactivation by proteolytic degradation[72] (**Figure 13**).

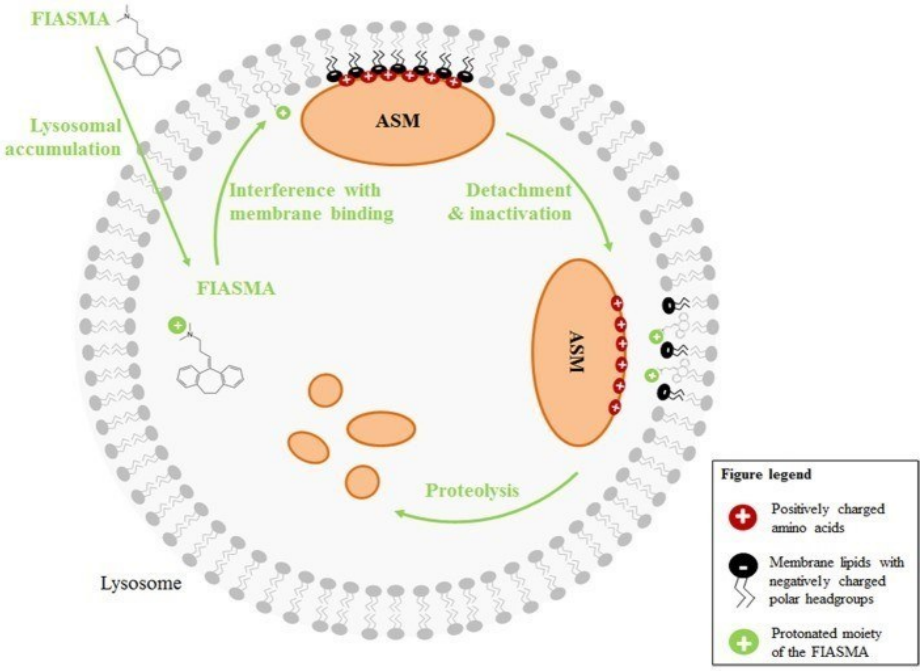

Figure 13. Mechanisms of action of functional inhibitors of ASM.

FIASMAs are weak bases and accumulate in acidic compartments like the lysosome because they become protonated at the acidic pH. Due to the positive charge, they can then no longer cross the membrane (acidic trapping). While the lipophilic moiety of the FIASMAs is anchored in the lysosomal membrane, the protonated, positively charged portion is exposed to the lumen, thus altering the electrostatic properties of the inner lysosomal membrane. As a result, the electrostatic adherence of ASM to the membrane is lost. Luminal ASM is inactive and targeted by intralysosomal proteases for proteolytic degradation.

AMI has demonstrated positive effects in various diseases, including cardiovascular, metabolic, cancer, and cystic fibrosis, as well as in neurodegenerative diseases [72]. In particular, in AD, the restoration of ASM levels has shown improvements in AD pathology, including reduced Aβ accumulation and enhanced learning and memory function.

Furthermore, studies involving ASM-overexpressing transgenic mice indicate that the administration of antidepressants, including AMI, can ameliorate depressive-like phenotypes. This treatment also increases neuronal proliferation, maturation, and survival in the hippocampus by reducing ceramide concentrations[76,77].

3 AIM

GBA gene encodes for GCase, a lysosomal enzyme involved in the catabolism of the glycosphingolipid GlcCer into glucose and ceramide. Biallelic mutations in *GBA* gene have been classically associated with GD, a systemic LSD with a variable degree of involvement of the central nervous system. Interestingly, it has been observed that monoallelic mutations in the same gene represent the major genetic risk factor for the development of PD with a 5-to-30-fold increased incidence of PD[64] .

However, subjects with the same *GBA* mutation show different clinical manifestations and may not develop PD. Emerging evidence addresses the reason to the possible existence of variants in other lysosomal genes that could modulate the penetrance of *GBA* mutations in causing PD [55,56] .

To this regard, in collaboration with Professor Duga of Humanitas Research Hospital, we conducted a study analysing a panel of 50 genes involved in LSD with Next Generation Sequencing in a cohort composed by 207 *GBA*-mutated asymptomatic carriers and 306 *GBA*-mutated PD patients. Second mutations in *GBA* and mutations in *SMPD1* were found to be the most frequent in this cohort. In particular, mutations in the *GBA* gene were present at a significantly higher frequency in symptomatic patients compared to controls, suggesting that a second variant in GBA represents the strongest modulator of the disease penetrance among GBA mutation carriers. Surprisingly, *SMPD1* was found more frequently mutated in asymptomatic carriers than in PD subjects, suggesting a possible protective effect of *SMPD1* in GBA carriers.

SMPD1 is a gene that encodes for another lysosomal hydrolase ASM that catabolizes the sphingomyelin into ceramide and phosphocholine. Even though in some papers heterozygous mutations in *SMPD1* were associated with increased risk of PD [73,74] , there is other experimental evidence that links ASM deficiency with an improvement in the phenotype and with a rescue of the mitochondrial respiratory chain function in a zebrafish GD model [69] .

Starting from this evidence and from the data obtained by Professor Duga, the aim of my PhD project was to verify whether ASM inhibition could have a beneficial role in GBA-dependent PD, exploiting the use of both pharmacological and patient-derived *in vitro* models.

The pharmacological model was constituted by WT iPSCs-derived dopaminergic neurons, treated with conduritol-B-epoxide to suppress GCase activity and mimic the pathological features of GD. The patient-derived model was represented by 3D midbrain organoids, derived from hiPSCs of a GD-PD patient carrying the biallelic mutation N370S/F213I in *GBA* gene.

For inducing the ASM inhibition, both models were treated with amitriptyline, a pharmacological inhibitor of ASM.

Both models were subjected to enzymatic, protein and lipid analyses to assess the effect of the ASM inhibition on neurodegeneration and GlcCer accumulation, the most important features of GD-PD pathology.

4 METHODS

4.1 Cell culture of human-induced pluripotent stem cells (hiPSCs)

Human induced pluripotent stem cells were obtained as follow:

- For the pharmacological model, hiPSCs were commercially purchased from Coriell Institute (AICS-0022-037) and derived from fibroblasts of healthy subjects reprogrammed using episomal vectors (OCT3/4, shp53, SOX2, KLF4, LMYC, and LIN28).

- For the patient derived model, hiPSCs were generated from fibroblasts of two subjects obtained from IRCSS Foundation Ca' Granda Ospedale Maggiore Policlinico. Specifically, fibroblasts were derived from a 2 mm diameter skin punch biopsy of a healthy donor and of a GD-PD patient, carrying the biallelic mutation N370S/F213I in *GBA1* gene. Fibroblasts were cultured in DMEM supplemented with 15% fetal bovine serum and 1% penicillin/streptomycin, in a humidified atmosphere at 37°C, 5% CO_2. Fibroblasts were reprogrammed to hiPSCs following the manufacturer's instruction of a commercial kit (CytoTune™-iPS 2.0 Sendai Reprogramming Kit, ThermoFisher Scientific, Waltham, MA, USA), through a non-integrative reprogramming strategy set by Yamanaka et al. *(2006)* [82] based on the transfection with a linear DNA fragment that leads the expression of Oct4, Sox2, Klf4, and c-Myc factors. The incubation with the virus lasted for 24 hours. After 3 weeks from the transfection, colonies were manually picked to isolate the different iPSCs clones, that were analyzed for the karyotype to be sure that don't present chromosomal rearrangements.

iPSCs were grown on Geltrex-coated (1% for 1h at 37 °C) 6-well plates and cultured in complete Essential 8™ Medium (ThermoFisher). At 80–90% confluence, cells were passaged using 0.5 mM PBS-EDTA (3 minutes, 37°C), and cultured in Essential 8™ Medium supplemented with 10 µM Rock inhibitor. After the first 24 hours RI was removed and replaced with fresh Essential 8™ Medium.

The pluripotency of the hiPSCs generated was confirmed by immunofluorescence technique using both nuclear (Sox2, Nanog) and cytoplasmatic (Tra-1-60, Tra-1-81) antibodies.

4.2 hiPSCs differentiation into dopaminergic neurons (DANs)

The hiPSCs were differentiated into DANs following the protocol described by Zhang et al. *(2014)* [67] (**fig.14**). Cells were cultured in proper media supplemented with specific factors at proper concentrations as follows:

- Day 0: KSR differentiation medium (81% DMEM, 15% KSR, 100x 1% non-essential amino acids, 100x 1 % 2-mercaptoethanol, 100 U/ ml penicillin, and 100 µg/ml streptomycin) supplemented with 10 µM SB431542 and 100 µM LDN-193189.
- Days 1 and 2: KSR differentiation medium supplemented with 10 µM SB431542, 100 nM LDN- 193189, 0.25 µM SAG, 2 µM purmorphamine, and 50 ng/ mL FGF8b.
- Days 3 and 4: KSR differentiation medium supplemented with 10 µM SB431542, 100 nM LDN-193189, 0.25 µM SAG, 2 µM purmorphamine, 50 ng/ mL FGF8b, and 3 µM CHIR99021.
- Days 5 and 6: 75% KSR differentiation medium and 25% N2 differentiation medium (97% DMEM, 100x 1% N2 supplement, 100 U/ ml penicillin, and 100 µg/ ml streptomycin) supplemented with 100 nM LDN-193189, 0.25 µM SAG, 2 µM purmorphamine, 50 ng/ mL FGF8b, and 3 µM CHIR99021.
- Days 7 and 8: 50% KSR differentiation medium and 50 % N2 differentiation medium supplemented with 100 nM LDN-193189 and 3 µM CHIR99021.
- Days 9 and 10: 25% KSR differentiation medium and 75% N2 differentiation medium supplemented with 100 nM LDN-193189 and 3 µM CHIR99021.
- Days 11 and 12: B27 differentiation medium (95% Neurobasal medium, 50x 2% B27 supplement, 1 % Glutamax, 100x, 100 U/ ml penicillin, and 100 µg/ ml streptomycin) supplemented with 3 µM CHIR99021, 10 ng/ mL BDNF, 10 ng/ mL GDNF, 1 ng/ mL TGF-β3, 0.2 mM ascorbic acid, and 0.1 mM cyclic AMP.
- From day 13 to the end of differentiation: B27 differentiation medium supplemented with 10 ng/ mL BDNF,10 ng/ mL GDNF, 1 ng/ mL TGF-β3, 0.2 mM ascorbic acid, and 0.1 mM cyclic AMP.

After 20 days of differentiation, cells were split using Accutase (3 min 37°C) on geltrex- coated plates at a density of 2×10^5 cells/cm^2. From D30 cells were treated with Conduritol-B-Epoxide (CBE) 500µM, a specific and irreversible inhibitor of β-glucocerebrosidase enzyme for 30 days. The medium was changed every day, and the cells were collected at day 60.

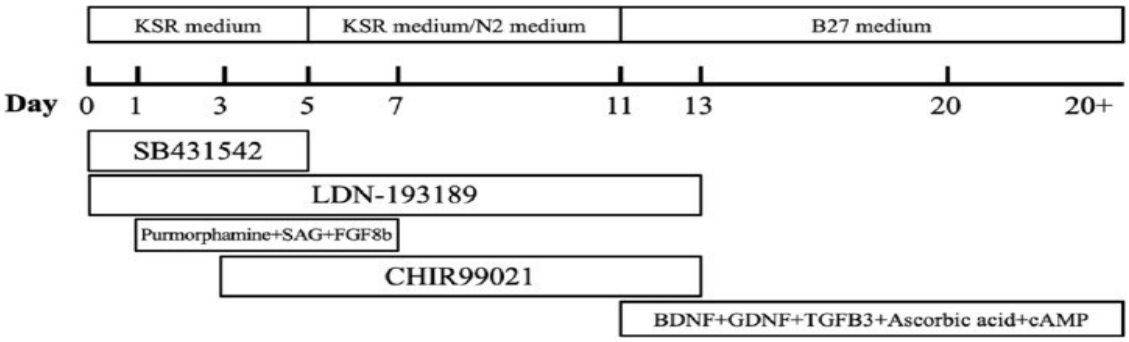

Figure 14. Schematic differentiation protocol of hiPSCs into dopaminergic neurons.

4.3 hiPSCs differentiation into human midbrain organoids (hMOs)

hMOs were generated readapting Lancaster et al. (*2014*) protocol [78], as reported in **figure 15** .

iPSCs were cultured in proper supports and media supplemented with specific factors at proper concentrations as follows:

- Days 0 - 5: generation of embryoid bodies (EB) in a low attachment 96-well U-bottom plate containing hES medium (75% DMEM-F12, 20% KSR, 3% ES-quality FBS, 1% 100X Glutamax supplement, 1% MEM-NEAA, 96 µM 2-Mercaptoethano) and supplemented by 4 ng/ml bFGF and 50 µM ROCK inhibitor until day 4. From day 4-6 the medium used was only hES medium without supplementation.
- Days 6-9: transfer of the EBs into a low attachment 24-well plate containing neural induction medium (97% DMEM-F12, 1% 100X N2 supplement, 1% 100X Glutamax supplement, 1% MEM-NEAA, and 1 µg/ml Heparin).
- Days 10-13: at D10 transfer of the EBs into matrigel droplets and culture in a 60 mm dish containing cerebral organoid differentiation medium (48% DMEM-F12, 48% Neurobasal, 0.5% 100X N2 supplement, 0.4 µM Insulin, 1% 100X Glutamax supplement, 0.5% MEM-NEAA, 1% 100X penicillin/streptomycin stock solution, 48 µM 2-Mercaptoethanol, and 1% 50X B27 supplement without vitamin A) until D13.
- Day 14: Transfer of the organoids into spinning bioreactors, which promote improved nutrient and oxygen exchange to support a better growth, avoiding the formation of a necrotic core. Starting of the differentiation into midbrain organoids following the dopaminergic differentiation protocol described by Zhang et al. as reported in the previous section.

From day 50, hMOs were transferred into Petri dish ϕ60 to be treated with amitriptyline and they were maintained in culture until day 120, harvesting them at different timepoints (D50, D80, D120) for lipid, protein, and enzymatic analysis.

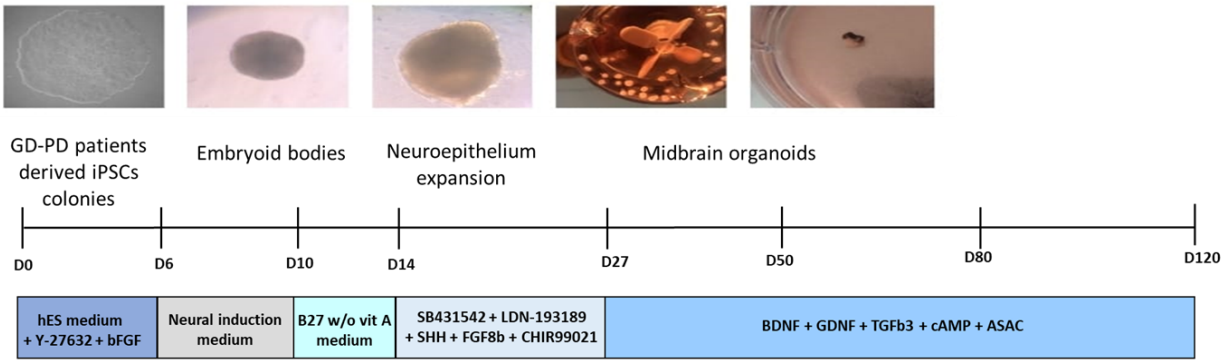

Figure 15. Schematic differentiation protocol of hiPSCs into midbrain organoids.

4.4 hiPSCs and DANs immunofluorescence staining

To evaluate the staminality of iPSCs generated and the correct differentiation into DANs, cells were stained by immunofluorescence technique.

iPSCs and DANs at day 60 of differentiation were plated at a density of $2x10^5$ cells/cm^2 on 24 mm cover glasses precoated with geltrex (1%, 1 h 37°C). Cells were fixed in 4% paraformaldehyde in PBS for 20 min at 23°C. Cells were then permeabilized in 0.2 % Triton X-100 in PBS for 10 min at 23°C and blocked in 1% BSA/ 2% Donkey serum in PBS for 1 h at 23°C. Cells were incubated 2 h at 23°C with primary antibodies diluted in 0.25% BSA/ 0.5% Donkey serum in PBS and 1 h at 23°C with secondary antibodies conjugated to Alexa Fluor, diluted in the same solution. Nuclei were stained by incubation with Hoechst solution (2 µg/ml in PBS) for 5 min at 23°C.

The following antibodies were used: monoclonal mouse anti-β3-tubulin (Cell Signalling, dilution: 1:200), monoclonal mouse anti-TH (Santa Cruz, dilution: 1:50), polyclonal rabbit anti-MAP2 (Cell Signalling, dilution: 1:50), monoclonal mouse anti-Nestin (Cell Signalling, dilution: 1:250), monoclonal mouse anti-Neurofilament H (Cell Signalling, dilution: 1:200), monoclonal rabbit anti-Sox2 (Cell Signalling, dilution 1:500), monoclonal rabbit anti-Nanog (Cell Signalling ,dilution 1:500), monoclonal mouse anti-TRA-1-81 (Cell Signalling ,dilution 1:500), monoclonal mouse anti-TRA-1-60 (Cell Signalling, dilution 1:500), polyclonal anti-mouse AlexaFluor568 (Abcam), polyclonal anti-rabbit AlexaFluor568 (Abcam), and polyclonal anti-rabbit

AlexaFluor488 (Abcam). Coverslips were mounted with Dako Fluorescent Mounting Medium (Agilent Technologies, Santa Cruz, CA, USA).

Images were taken using an Olympus BX50 Upright Fluorescence Microscope fluorescence with a fast-high resolution camera (Colorview 12).

4.5 Midbrain organoids immunofluorescence staining

Midbrain organoids for immunofluorescence experiments were fixed with 4% paraformaldehyde (PFA) for 30 minutes, followed by three washes with PBS at RT. The organoids were left overnight at 4°C in 15% sucrose solution in PBS 1X, which was substituted the day after with sucrose 30% solution in PBS 1X for a second overnight incubation at 4°C. The day after, organoids were embedded in an OCT matrix to be sectioned into 15 µm slices with the use of a cryostat. Slices were put on slides and washed in PBS for 10 minutes. After that, slides were incubated for 15 minutes with permeabilization buffer (500 ml PBS 1X, 2.5 ml Triton X-100), and then for 1 hour at room temperature with a blocking solution composed by PBS 1X, 10% goat serum and 0,1% Triton X-100. Primary antibodies were diluted in a solution containing PBS 1X, 3% goat serum and 0,1% Triton X-100 and the sections were incubated with the primary antibodies overnight at 4°C. The following day, organoids sections were washed three times with PBS 1X and subsequently incubated with secondary antibodies for 90 minutes at RT, in dark conditions. Secondary antibodies were diluted as the primary ones in a solution containing PBS 1X, 3% goat serum and 0,1% Triton X-100. The slices were washed twice in PBS 1X for 10 minutes each and consequently incubated 10 minutes at RT with DAPI (1:1000) for nuclear staining. After a last wash of 10 minutes, coverslips were mounted on glass slides using Fluoromount-G™ mounting medium.

The primary antibodies used were: anti-β3-tubulin (rabbit, Cell Signaling; 1:500), anti-TH (mouse, Santa Cruz; 1:100), anti-MAP2 (mouse, Sigma; 1:500), anti-SOX2 (rabbit, StemLightTM Pluripotency Antibody Kit; 1:50), the respective secondary antibody: anti-mouse AlexaFluor488 (Abcam, 1:2000) and anti-rabbit AlexaFluor568 (Abcam, 1:500).
Images were acquired using a Nikon Eclipse 90i Ni microscope at 200X magnification.

4.6 Samples collection

To obtain lysates for enzymatic assay, lipid, and protein analysis, iPSC-derived dopaminergic neurons and midbrain organoids were processed as described below:

iPSC-derived dopaminergic neurons were washed two times with PBS and cells were then harvested mechanically using disposable scrapers in water, with protease (Sigma Aldrich) and phosphatase inhibitors (sodium orthovanadate, Na3VO4) and transferred into 2 ml eppendorf tubes. The cell pellets were then sonicated using a tip immersion sonicator at 30mHz for 3 times 10 seconds each.

Midbrain organoids were collected into a 2ml Eppendorf, washed two times with PBS and sonicated into Milli-Q water supplemented with Protease Inhibitor Cocktail (SigmaAldrich) and phosphatases inhibitor NA_3VO_4 for 3 times at 30mHz 10 mins each.

4.7 Determination of protein content through DC protein assay

The protein concentration of the samples was determined through DC protein assay (Bio-Rad), which is based on Lowry's method.

The assay was performed in a 96-wells plate using: 5 µl of H_2O for the background, 5 µl of Bovine Serum Albumin (BSA) with increasing concentration (0.375 µg/µl, 0.75 µg/µl and 1.5 µg/µl) as standards and, for each sample, 5 µl of cell lysate properly diluted in Milli-Q water to be in assay's range of linearity. Blank, standards and samples were assayed in triplicate. After that, 25 µl of Reagent A (an alkaline copper tartrate solution) and 200 µl of Reagent B (a diluted Folin reagent) were added sequentially in each well and the plate was put on gently agitation for 15 minutes at room temperature (RT).

Finally, the absorbance was evaluated through a spectrophotometric reading at a wavelength of 750 nm using a microplate reader (Victor, Perkin-Elmer). Protein content was calculated interpolating the average absorbance value of each sample within the calibration curve obtained from the BSA standards' absorbance values.

The protein dosage is considered linear in a range between 0.2 and 2 mg proteins/ml.

4.8 Treatment with amitriptyline

To reproduce a partial ASM inhibition, hiPSCs-derived DANs and hMOs were treated with AMI, a functional inhibitor of acid sphingomyelinase enzyme.

10 µM AMI (Sigma Aldrich) was administered to DANs for the last 7 days or 24 hours of culture before the collection at day 60 of differentiation.

Midbrain organoids instead were treated with 20 µM AMI starting from DIC50 until DIC120. Organoids were collected at day 50, 80,120.
Cells under the same experimental conditions without AMI administration were used as control conditions.

4.9 Acid sphingomyelinase enzymatic activity evaluation

Acid sphingomyelinase enzymatic activity was evaluated in lysates of dopaminergic neurons and midbrain organoids with the use of radioactive sphingomyelin as a substrate.

Aliquotes of the sample's lysates corresponding to 50 µg of proteins were incubated with a reaction mixture composed of: buffer (2.5 M sodium acetate, 50 mM EDTA, 1% Triton X- 100), 5nM radioactive sphingomyelin and water to reach a final volume of 50 µl. Each reaction mixture has been incubated at 37 °C for 2 hours at 800 rpm agitation. Each sample has been assayed in triplicate.

Total lipid extraction was performed as entirely explained in section 4.12. Briefly, total lipids were extracted with the use of chloroform: methanol ($CHCl3$:CH_3OH, 2:1, v:v), evaporated under a nitrogen flow and partitioned adding chloroform:methanol ($CHCl_3$:CH_3OH 2:1, v:v). Then they were centrifuged at 13000 x g for 10 minutes at 4°C. The separation of the lipids was performed by HPTLC using the solvent system chloroform, methanol and water ($CHCl_3$:CH_3OH:H_2O, 110:40:6, v:v:v). To assess ASM activity, was quantified the amount of radioactive ceramide produced as a result of radioactive sphingomyelin hydrolysis. The radioactive ceramide was identified by co-migration with a purified standard and detected by digital autoradiography performed with a Beta-Imager ^{T}Racer instrument (BioSpace). The radioactivity associated with ceramide was quantified by M3 Vision software.
Specific activity of the enzyme was expressed as nanomoles of converted substrate/ hours/ mg of proteins.

4.10 Immunoblotting

Immunoblotting analysis of lysates obtained from hiPSCs-derived DA neurons and midbrain organoids was performed using standard protocols. Aliquots of the samples were mixed with 5X SDS-sample buffer (12% SDS, 0.375 M Tris-HCl pH 6.8, 60% glycerol, 0.06% bromophenol blue, 0.6 M DTT) and were heated at 95°C for 5 minutes to denature the proteins and bring them back to their primary structure.

Proteins were separated by SDS-PAGE on a 4-20% or 4-15% polyacrylamide gradient gel (Criterion PROTEAN® TGX™ Precast Gels (Bio-Rad)) and separated depending on their molecular weight by SDS-PAGE in a Mini-Protean-IV Cell electrophoretic cell. Electrophoretic run was performed in running buffer (Tris-HCl 25 mM, glycine 19 mM and 0.1% SDS) applying a 180V constant voltage. Separated proteins were transferred on Turbo Polyvinylidene difluoride (PVDF) Midi-membrane (Bio-Rad) using the Bio-Rad Trans-Blot® Turbo™ Blotting System for 7 minutes at a constant voltage of 25 V and current intensity of 1.3 A, a condition which allows the efficient transfer of the proteins contained within a very wide range of molecular weights. To verify the protein transfer, PVDF membranes were stained using Red Ponceau dye (Ponceau Red dye 0.1%, Acetic Acid 5% in H_2O) for 5 minutes under mild agitation at RT. Membranes were then rinsed three times in Milli-Q H_2O.

The PVDF membranes were then incubated with blocking solution (5% w/v non-fat dry milk in Tris-Buffered Saline (TBS: 10 mM Tris-HCl pH 8.0 and 0.15 M NaCl) containing Tween 0.1%)) for 1 hour at RT under gentle shaking, in order to block nonspecific binding sites, followed by an overnight incubation at 4°C in gentle agitation with primary antibodies, properly diluted.

Specifically, the following primary antibodies were used: polyclonal rabbit anti-MAP2 (Immunological Sciences, dilution: 1:1000), monoclonal mouse anti-TAU (Immunological Sciences, dilution: 1:1000), monoclonal mouse anti-LAMP1 (Developmental Studies Hybridoma Bank, dilution: 1:100), polyclonal mouse anti-GAPDH (Immunological Sciences, dilution: 1:10000), monoclonal mouse anti-β3-tubulin (Cell Signaling, dilution: 1:1000), monoclonal mouse anti-TH (Santa Cruz Biotechnology, dilution: 1:2500), polyclonal rabbit anti-p62 (Cell Signaling, dilution: 1:1000); polyclonal rabbit anti-LC3 (SigmaAldrich, dilution 1:1000). All the antibodies were previously diluted in blocking solution (5% non-fat dry milk in 0.1% Tween TBS-T). Whereas, anti-p62, anti-nestin and anti-β3-tubulin were diluted in in 5% w/v BSA in TBS-T 0.1%.

After overnight incubation, primary antibody was removed, and the membranes were washed three times for 5 minutes each in TBS-T 0.1%. Then membranes were incubated for 1 hour at RT with the appropriate secondary antibody diluted in 5% non-fat dry milk in TBS-T 0.1%. The following secondary antibodies were

used: goat anti-rabbit horseradish peroxidase (HRP)-conjugated (Immunological Sciences, dilution: 1:10000), goat-anti-mouse HRP conjugated (ThermoFisher: dilution: 1:2000 or 1:10000 for highly diluted primary antibodies i.e. anti- GAPDH). After removal of the secondary antibody solutions, membranes were subjected to three washes of 5 minutes each in TBS-T 0.1% and incubated 2 minutes in dark conditions with a commercial solution containing luminol (WESTAR ηC,Antares-Ultra-Supernova, Cyanagen) that reacts with HRP.

The resulting chemiluminescent signal was revealed through the Alliance Mini HD9 (UV TECH Cambridge) digital system and quantified by Image-J™ software. The chemiluminescent signal revealed was normalized on the signal of the housekeeping protein glyceraldehyde-3-phosphate dehydrogenase (GAPDH).

4.11 Evaluation of enzymatic activity through fluorigenic substrates

The enzymatic activity of glycohydrolases was determined in lysates of DA neurons and midbrain organoids using an already published method by Aureli et al. (*2011*).

The evaluated enzymes were the following: β-glucocerebrosidase (GCase, EC 3.2.1.45), non- lysosomal β-glucosylceramidase (NLGase, EC 3.2 .1.45), β-galactosidase (β-Gal, EC 3.2.1.23) and β-hexosaminidase (β-Hex, EC 3.2.1.52), α-mannosidase (α-Man, EC 3.2.1.24) and β- mannosidase (β-Man, EC 3.2.1.25).

The method exploits fluorigenic substrates (Glycosynth) specific for each glycohydrolase. The substrate is conjugated to methylumbelliferone, and the enzymatic activity determines its release. In this condition, methylumbelliferone at alkaline pH emits a fluorescent signal, which can be detected by a fluorimeter (Victor, Perkin-Elmer) (λex/λem=360 nm/450 nm).

Each sample has been assayed in triplicate and as background for each enzymatic assay, wells without cell lysate have been set up and processed under the same experimental conditions, in order to evaluate substrates autohydrolysis. Each reaction mixture has been put at 37 °C on gently agitation for at least 1.5 hours; after this incubation, 10 µl of the reaction mixture were transferred to a black 96-well plate (Black, 96-well, OptiPlate 96 F, Perkin Elmer) and 190 µl of 0.25 M glycine pH 10.7 was added to stop the reaction and reach the maximum fluorescence emission peak of the free MUB. Plates were subjected to fluorometric reading and analysed through a microplate reader (Victor, Perkin Elmer, λex/λem=360 nm/450 nm).

Considering the fluorescence associated with the free MUB standard at known concentrations, nanomoles of converted substrate in the different samples were calculated. Specific activity of the enzymes was expressed as nanomoles of converted substrate/ hours/ mg of proteins.

4.11.1 GCase and NLGase

Aliquots of the lysates corresponding to 20 µg of proteins were pre-incubated for 30 minutes at RT in a 96-well plate with a reaction mixture composed of: 25 µl of McIlvaine buffer 4X (0.4 M citric acid, 0.8 M Na_2HPO_4) pH 5.2 to assay GCase or pH 6 to assay NLGase, the specific inhibitor of the other enzyme to discriminate either GCase or NLGase activity and H_2O to a final volume of 75 µl. Specific inhibitor of GCase is CBE, used at the final concentration of 0.5 mM; while for NLGase inhibition, AMP-DNM (Adamantane-pentyl- dNM;N-(5-adamantane-1-yl-methoxy-pentyl)-Deoxynojirimycin) has been used at the final concentration of 5 nM. After 30 minutes, to start the enzymatic reaction, 25 µl of the specific fluorogenic substrate 4-Methylumbelliferyl-β-Dglucopyranoside (MUB-β-Glc) (Glycosynth) at a final concentration of 6

mM was added to the reaction mixture.

4.11.2 β -galactosidase, β-hexosaminidase, α-and β-mannosidase

Aliquotes of the lysates corresponding to 5 µg (for β-galactosidase and β-hexosaminidase) or 10 µg (for α-and β-mannosidase) of proteins were incubated with a reaction mixture composed of: 25 µl of McIlvaine buffer 4X pH 5.2, 50 µl of the specific fluorogenic substrate 4- Methylumbelliferyl-β-Dgalactopyranoside (MUB-β-Gal) for β-Gal, 4-Methylumbelliferyl-β- D-glucosaminide (MUG) for βHex, Methylumbelliferyl-α-D-mannopyranoside (MUB-α- Man) for α-Man and 4-Methylumbelliferyl-β-D-mannopyranoside (MUB-β-Man) for β-man at a final concentration of 500 µM and H_2O to a final volume of 100 µl

4.12 Evaluation of the lipid content

4.12.1 Cell sphingolipid labelling with [1-^{3}H]-sphingosine

Midbrain organoids were fed with [1-^{3}H]-sphingosine one week before the collection at different time points (D50, D80, D120), to label cell sphingolipids at the steady state. Radioactive sphingosine was solubilized in methanol and was therefore dried under nitrogen flow and solubilised in the complete culturing medium at the concentration 36 nM (specific radioactivity 1.06 Ci/ mmol). After 3 days, the medium was changed, an aliquot of the medium was counted by liquid scintillation to determine the radioactivity. At the end of the experimental plan, organoids were harvested to perform lipid analysis and therefore, pellets were lyophilized overnight.

4.12.2 Total lipid extraction

To perform lipid extraction, water was removed from the cell lysates by lyophilisation. Lyophilised pellets were then resuspended in 50 µl of Milli-Q H_2O, vortexed and sonicated for 5 minutes in a water bath. After, 500 µl of methanol (CH_3OH) was added and the samples were vortexed, sonicated for 5 minutes and then mixed at 1400 rpm for 10 minutes at room temperature using ThermoMixer® (Eppendorf). Finally, 1 ml of chloroform ($CHCl_3$) was added and, again, the samples were vortexed, sonicated for 5 minutes in a water bath and mixed at 1400 rpm for 10 minutes at RT using ThermoMixer® (Eppendorf). The samples were then centrifuged at 13000 x g for 10 minutes at 4 °C. The obtained supernatant, containing the total lipid extraction, was collected in Eppendorf of 2 ml, while the delipidised protein pellet was subjected to a second extraction with the addition of 250 µl chloroform, methanol ($CHCl_3$:CH_3OH, 2:1, v:v). The samples were vortexed, sonicated 5 minutes, agitated 10 minutes RT and centrifuged again at 13000 x g for 10 minutes at 4°C. The supernatant obtained from

the second extraction was added to the first one to form the total lipid extract (TLE), which was dried under nitrogen flow. For the samples previously subjected to sphingolipid labelling with [1^{-3}H]-sphingosine, the radioactivity associated with the total lipid extract (TLE) was determined by liquid scintillation counting by beta-counter (PerkinElmer).

4.12.3 Two-phase partitioning and alkaline methanolysis reaction

The partitioning is used to separate from the TLE gangliosides that are soluble in the aqueous phase (AP) and neutral sphingolipids that are contained in the organic phase (OP).

Aliquots of TLE were dried under nitrogen flow and partitioned according to Folch method:
1.5 ml of chloroform, methanol ($CHCl_3$:CH_3OH, 2:1, v:v) and 20% of Milli-Q H_2O were added to the dried samples, that were vortexed, sonicated in a water bath for 5 minutes and mixed at 1400 rpm for 10 minutes at RT using ThermoMixer® (Eppendorf).After, the samples were centrifuged at 13000 x g for 15 minutes at 4°C. The upper AP was collected, while the lower OP was subjected to a second partitioning adding a solvent system formed by chloroform:methanol:water ($CHCl_3$:CH_3OH:H_2O, 3:48:47, v:v:v) in a volume equivalent to the one of the obtained AP, vortexed, sonicated for 5 minutes in a water bath and then mixed at 1400 rpm for 10 minutes at RT using ThermoMixer® (Eppendorf). After being centrifuged at 13000 x g for 15 minutes at 4°C, the obtained acqueous phase was added to the first one. Both OP and AP were evaporated under nitrogen flow and resuspended in chloroform, methanol ($CHCl_3$:CH_3OH, 2:1, v:v).

OP was subjected to alkaline methanolysis to remove glycerophospholipids, breaking their ester bonds and preserving the amide bonds of sphingolipids. Aliquots of the OP were dried under nitrogen flow and resuspended in 800 µl chloroform ($CHCl_3$), vortexed and sonicated in a water bath for 1 minute. Then, 800 µl of KOH 0.5 M in methanol were added and samples vortexed. The reaction mixture was left overnight at 37°C. At the end of incubation, the reaction was blocked, and KOH was neutralized by the addition of 50 µl HCl 0.5 M in methanol. Samples were mixed, dried under nitrogen flow and further subjected to the two-phase partitioning in order to obtain the new alkali-stable organic phase, then resuspended in a known volume of chloroform, methanol ($CHCl_3$:CH_3OH, 2:1, v:v). For radioactive samples, aliquots of both AP and OP were analysed by liquid scintillation counting by beta-counter (PerkinElmer) to determine AP/OP-associated radioactivity.

4.12.4 Radioactive lipid analysis by High-Performance Thin Layer Chromatography (HPTLC)

The evaluation of the samples' lipid content was performed by high performance thin layer chromatography (HPTLC). This technique allows the separation of the different lipid species using a stationary phase represented by plates of silica gel (Merk Millipore) and a mobile phase consisting of different mixtures of organic solvents that vary according to the nature of the lipids that we want to separate.

The lipid species contained in the aqueous phase, that are mainly gangliosides, were separated using a solvent system composed by chloroform, methanol, calcium chloride 0.2% in water ($CHCl_3$:CH_3OH:$CaCl_2$, 50:42:11, v:v:v), while a mixture of chloroform, methanol and water ($CHCl_3$:CH_3OH:H_2O, 110:40:6, v:v:v) was used for the separation of the neutral sphingolipids contained in the alkali-stable organic phase.

To determine the amount of radioactivity associated to the organoids subjected to sphingolipid labelling with [1^{-3}H]-sphingosine, aliquots of TLE, OP and AP were counted by liquid scintillator. Their lipid content was then analysed by mono dimensional HPTLC, loading for each sample a volume corresponding to the same amount of radioactivity.
To segregate the different species and investigate glucosylceramide accumulation in OP samples, the solvent system was composed by chloroform, methanol and water ($CHCl_3$:CH_3OH:H_2O, 110:40:6, v:v:v).

Separated radioactive lipids were detected and quantified by digital autoradiography performed with a Beta-Imager™ TRacer instrument (BioSpace Lab, Paris, France). The identification of the different lipid species was determined by the co-migration with radioactive purified lipid standards. Samples were then analysed using M3 Vision Software™ (BioSpace Lab, Paris, France) and compared normalizing them on the samples' radioactivity associated with mg of protein.

4.12.5 Analysis of endogenous lipids by HPTLC

To analyze the endogenous lipid pattern of CBE-treated dopaminergic neurons, OP was seeded on silica plate loading volumes of samples equivalent to a predetermined protein content, the separation was performed in a chromatographic chamber. At the end of the run, after the separation, the HPTLC was dried and sprayed with different colorimetric reagents specific for the lipid species to be detected. The neutral sphingolipids contained in the organic phase were revealed by spraying the HPTLC with an anisaldehyde reagent (100 ml glacial acetic acid, 2 ml sulfuric acid, 1 ml anisic aldehyde).

The different species corresponding to each band were then identified by co-migration with the purified lipid

standards, quantified by densitometric analysis using ImageJ software and normalized on the mg of proteins seeded.

4.13 Immunoblot analysis of α-synuclein aggregates

Immunoblot analyses of α-synuclein aggregates obtained from the pellet of GD-PD midbrain organoids treated with AMI were performed with a protocol adapted from the one described by Tofaris et al. 2006. [79]

For soluble and detergent-insoluble a-syn collection, the sequential extraction was done in Tris-buffered saline $(TBS)^+$ (50 mM Tris–HCl, pH 7.4, 175 mM NaCl, 5 mM EDTA, 0.1 mM phenylmethylsulfonyl fluoride and 1 mM N-ethylmaleimide, plus complete proteasome inhibitor mixture; Roche Diagnostics, Mannheim, Germany)., Triton X-100, radioimmunoprecipitation (RIPA) buffer and 8 M urea/5% sodium dodecyl sulphate (SDS). Briefly MOs pellets were homogenized in TBS^+ solution plus 1% Triton X-100 and centrifuged for 30 min at 50 000 g at 4°C, with the resulting supernatants corresponding to TBS^+ soluble fraction. Supernatants were discarded and the resulting pellets were homogenized in RIPA buffer (50 mM Tris– HCl, pH 7.4, 175 mM NaCl, 5 mM EDTA, 1% NP-40 (Sigma-Aldrich) and 0.5% sodium deoxycholate) and 0.1% SDS followed by centrifugation at 1000 g. The detergent-insoluble pellets were then reconstituted in 8 M urea plus 5% SDS. For gel analysis, samples were run on 10% homemade polyacrylamide gel, blotted on nitrocellulose membranes, and probed with mouse monoclonal antibody syn-1 (BD-Bioscience, dilution 1:1000). After overnight incubation, primary antibody was removed, and the membrane was incubated for 1 hour at RT with the secondary antibody goat-anti-mouse HRP conjugated (ThermoFisher: dilution: 1:2000). The membrane was incubated with a commercial solution containing luminol (WESTAR ηC,Antares-Ultra-Supernova, Cyanagen) that reacts with HRP.

The resulting chemiluminescent signal was revealed through the Alliance Mini HD9 (UV TECH Cambridge) digital system and quantified by Image-J™ software. The chemiluminescent signal revealed was normalized on the signal of the housekeeping protein β-actin.

4.14 Statistics

All the experiments have been performed in triplicate and repeated. Data were tested for significance using GraphPad Prism 8 (GraphPad Software Inc., La Jolla, CA, USA). Data are expressed as mean value ± SEM. For normally distributed data, unpaired Student's t-test was used. For comparisons between multiple conditions was performed a one-way anova test. The level of significance was set at $p < 0.05$.

5 RESULTS

5.1 Biochemical characterization of an in vitro model of GCase deficiency exploiting CBE-treated dopaminergic neurons

GBA gene encodes for GCase, a lysosomal enzyme involved in the catabolism of GlcCer into glucose and ceramide. Biallelic mutations in GBA gene are responsible for GD. Monoallelic mutations in GBA instead are nowadays considered to be the major genetic recessive risk factor for the development of PD.

So far, the molecular mechanism linking GCase deficiency to the onset of neuronal degeneration in GD and GBA-PD is not entirely understood. The primary issue arises from the absence of suitable *in vitro* models that accurately replicate the pathology. Due to the limitations of studying the human brain *in vivo* and the complexities associated with post-mortem tissues, there is a critical need for the development of a new *in vitro* model. For this purpose, during my PhD I exploited as experimental model iPSCs -derived dopaminergic neurons treated with CBE in order to inhibit GCase activity.

WT iPSCs were commercially purchased from Coriell Institute and differentiated into dopaminergic neurons, according to the protocol published by Zhang P. (2014) [67] ,as described in the methods section, and I obtained neuronal populations enriched in A9 dopaminergic neurons (DANs), which are the first to degenerate in PD in the substantia nigra pars compacta of the brain.

The differentiation process was evaluated by indirect immunofluorescence technique by the use of antibodies against the neuronal markers MAP2, TUJ1, NFH, the marker of the dopaminergic commitment TH and the marker of the neuronal precursors Nestin. As shown in **fig.16**, at day 60 of differentiation, iPSCs-derived dopaminergic neurons highly expressed the neuronal markers MAP2, TUJ1 and NFH. (**Fig16 A,B,C**). They also expressed the dopaminergic marker TH (**Fig.16D**) and only a little percentage of Nestin (**Fig. 16E**), confirming the correct maturation of the neurons.

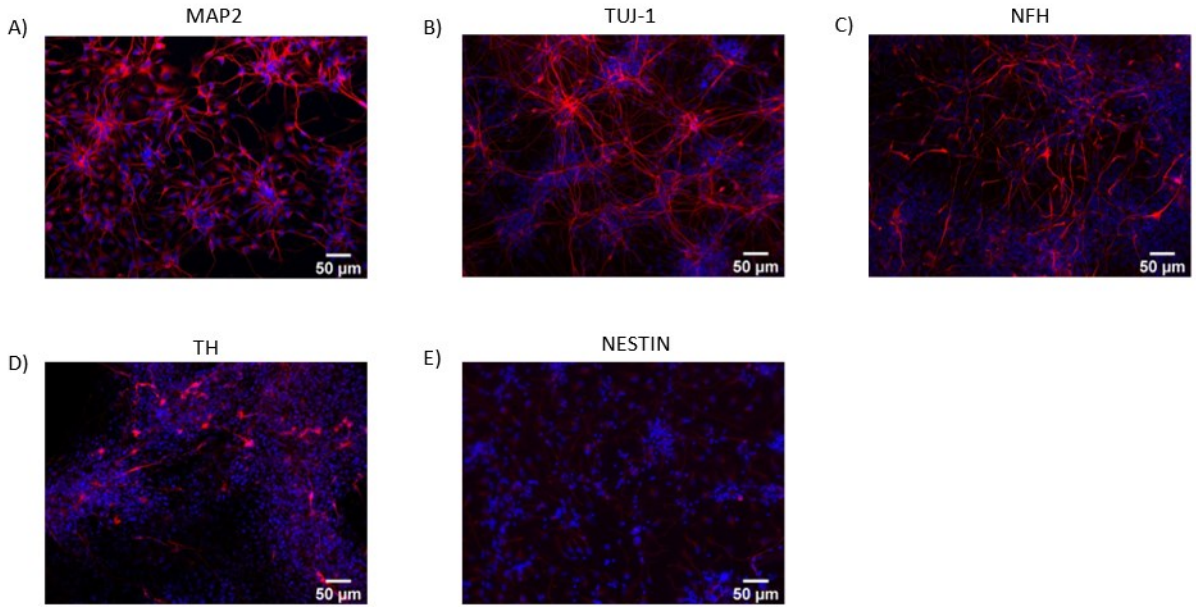

Figure 16. Characterization of iPSCs differentiated for 60 days into dopaminergic neurons.
Representative immunofluorescence images of human iPSC-derived dopaminergic neurons at day 60 of differentiation. Cells were stained (red) for the neuronal markers microtubule associated protein (MAP2), β-III-tubulin (TUJ-1), neurofilament H (NF-H), and tyrosine hydroxylase (TH), and for the neuronal precursor marker nestin. Cell nuclei were stained with Hoechst (blue). Images were acquired at 200× magnification.

To recapitulate the phenotype of GD-PD, I exploited a pharmacological model that has been developed in our laboratory that consist in the administration of 500 µM Conduritol-B-Epoxide (CBE), a specific and irreversible inhibitor of GCase, for 30 days before the collection at 60 days of differentiation (**Fig.17**). As reported by Dr. Lunghi and Carsana in a previous work[71] , CBE administration results in a strong GCase deficiency, neurodegenerative phenotype and GlcCer accumulation in iPSCs-derived neurons in comparison to the controls.

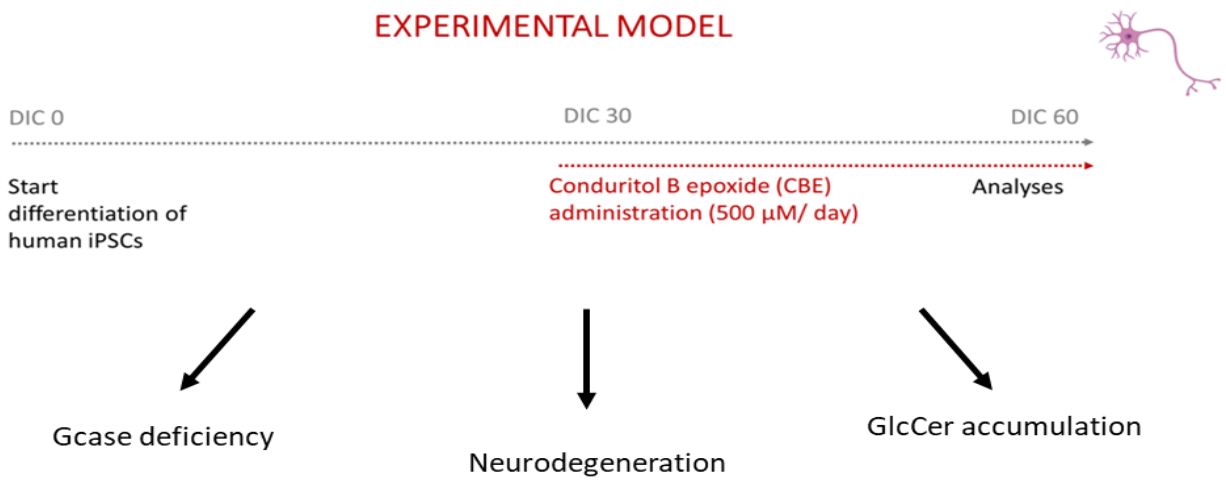

Figure 17. Generation of a neuronal *in vitro* model of GCase deficiency.

5.2 Evaluation of the effect of amitriptyline administration on CBE-treated dopaminergic neurons

As reported in the introduction, not all the GBA-mutated carriers develop PD, so it's possible to hypothesize the presence of variants in other lysosomal enzymes that could explain the difference in GBA mutation penetrance in causing PD.

In literature is reported that in a zebrafish GD model a deficiency in ASM, a lysosomal enzyme that catabolizes SM into ceramide and phosphocholine, could be protective against the development of PD.
Starting from this evidence, one of the aims of my PhD project was to verify whether ASM inhibition could have a beneficial effect also in GD-PD in vitro model.

For inducing ASM inhibition I administered to the CBE-treated neurons AMI, a tricyclic antidepressant known as a functional inhibitor of ASM.
Dopaminergic neurons were treated with 10 µM AMI for 7 days and 24 hours before the collection at day 60 of differentiation (**Fig.18**). Then they were subjected to protein, lipid, and enzymatic analyses.

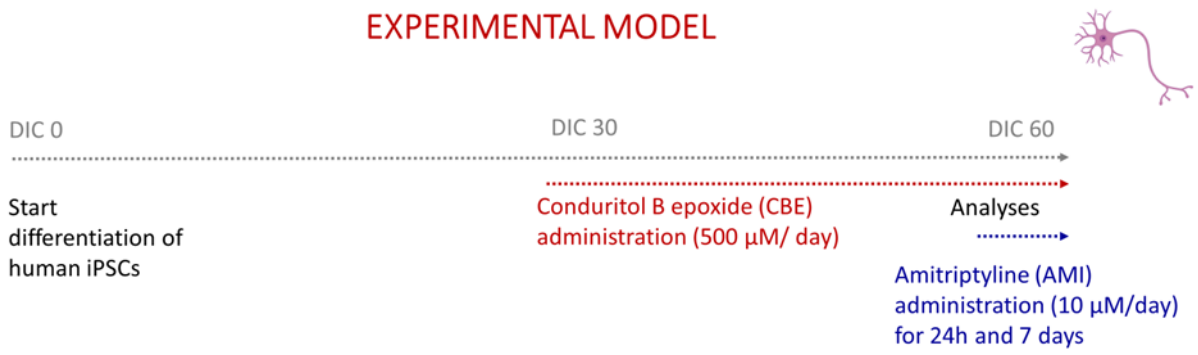

Figure 18. Generation of *in vitro* neuronal model of acid sphingomyelinase deficiency.
Schematic diagram of the experimental protocol to model in vitro a condition of ASM deficiency in CBE-treated dopaminergic neurons obtained from iPSCs. Cells were treated with 10 µM AMI to partially inhibit ASM 24h and 7 days before the collection. At day 60 of differentiation neurons were collected and analyzed for acid shingomyelinase activity, neuronal markers expression, glucosylceramide levels and glycohydrolases activity. DIC: days in culture.

At first, I have evaluated the effect of AMI as inhibitor of ASM in this model, performing an enzymatic assay with radioactive sphingomyelin as a substrate (**fig 19A**) and I have obtained a reduction of 20% of ASM activity in the cells treated with 24h AMI and a reduction of 50% after 7 days treatment (**fig 19B**).

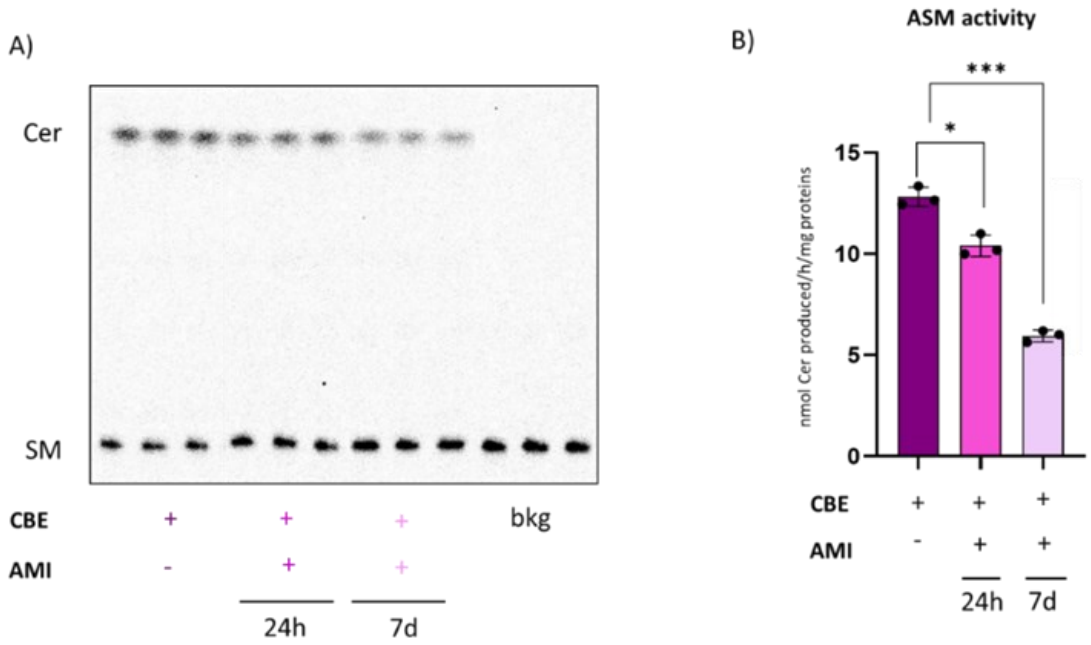

Figure 19. Evaluation of the enzymatic activity of ASM in CBE-treated DANs upon 10µM AMI administration. A) Representative HPTLC separation and B) quantification of the radioactive ceramide produced in CBE-treated dopaminergic neurons upon administration of 10 µM AMI for 24h and 7 days. Aliquots corresponding to 50 µg of cell lysate were incubated with 5nM of radioactive sphingomyelin for 2 hours at 37°C. Each reaction mixture was subjected to lipid extraction and partitioning using chloroform/methanol 2:1 (v:v). Ceramide content was evaluated by the separation of lipids by HPTLC using the solvent system 110:40:6 $CHCl_3$:CH_3OH:H_2O (v:v:v) and the radioactive lipid pattern was visualized by digital autoradiography performed with a Beta-Imager ^{T}Racer instrument (BioSpace). The radioactivity associated with ceramide was quantified by M3 Vision software. Specific activity of the enzymes was expressed as nanomoles of converted substrate/ hours/ mg of proteins. * $p<0.05$; *** $p<0.001$

To verify whether ASM inhibition was able to ameliorate the neurodegenerative phenotype, I evaluated the protein expression of neuronal-specific markers in CBE-treated DANs after 24 hours and 7 days of AMI treatment through immunoblot as described in the method section. As shown in **Fig.20**, the administration of CBE induced neurodegeneration that is partially improved after AMI treatment. Indeed, the protein expression of TH significantly increases in neurons treated with AMI with respect to the control. Specifically, the acute treatment of 24 hours generated a three-fold increase, while in neurons subjected to the chronic treatment the protein was almost 2 times more expressed than the untreated CBE-cells. Upon 7 days treatment also the neuronal marker TUJ1 displayed a four-time increase respect to the untreated one. In addition, I have evaluated the protein expression of MAP2 marker and TAU marker. The first one displayed an increased expression, in particular after 7 days treatment, while the second one showed a higher increase after 24h. All these results suggest that both the chronic and the acute amitriptyline treatment ameliorate the neurodegenerative phenotype of CBE-treated neurons.

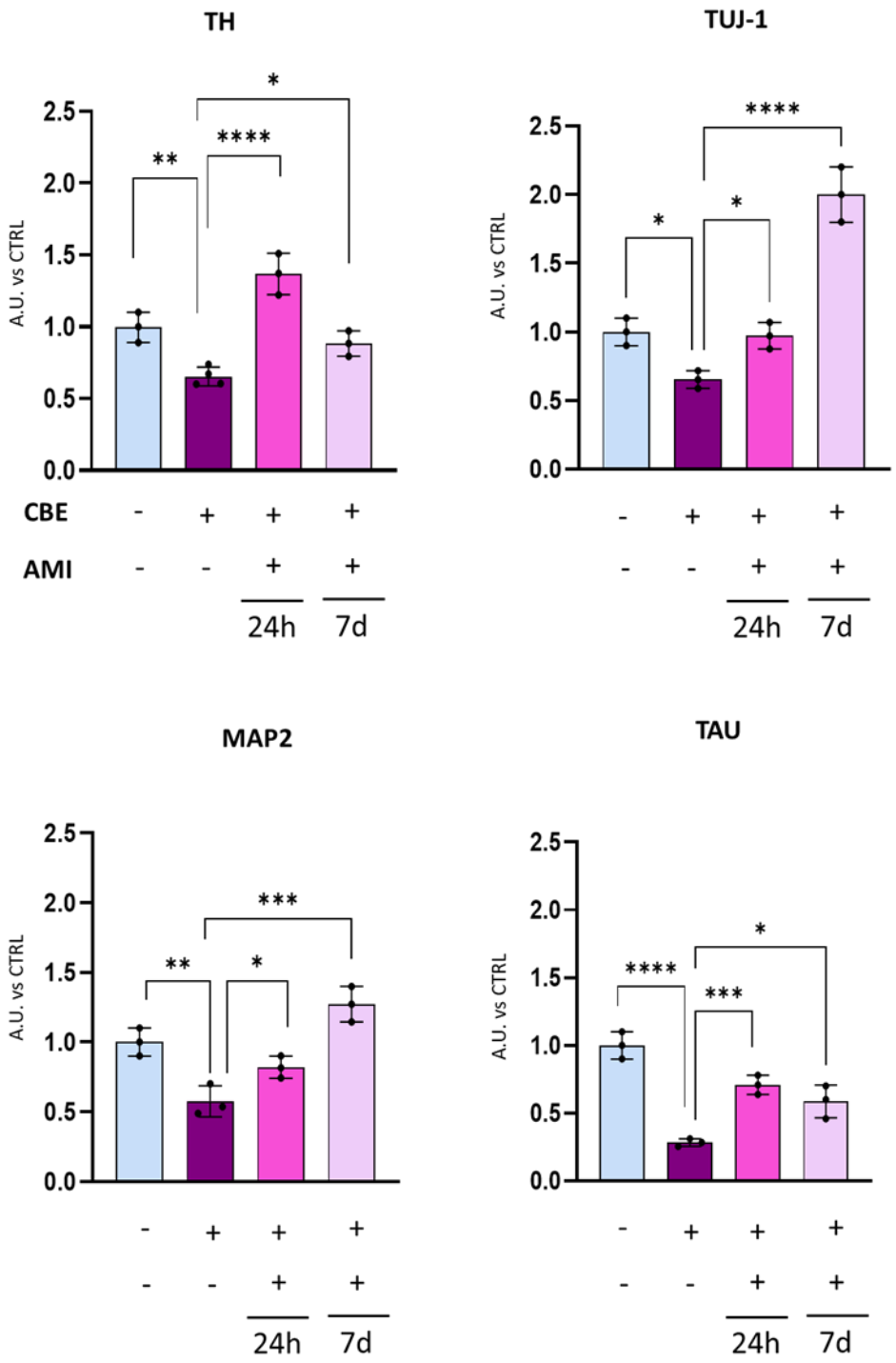

Figure 20. Evaluation of the protein expression of neuronal markers in CBE-treated DANs upon 10µM AMI administration.

Immunoblot analyses of TH, β-III-tubulin, MAP2, TAU protein levels. Same amount of cell lysate from CBE-treated dopaminergic neurons administered with 10 µM AMI for 24 hours or 7 days were separated by SDS-page. GAPDH was used as loading control. Optical densities of the individual bands were quantified using NIH ImageJ and normalized on GAPDH expression. Data are expressed as arbitrary units of antigen VS untreated and are the mean ± SEM of three different experiments. *p<0.05;**p<0.01; ***p<0.001; ****p<0.0001.

Since GD-PD is a pathology characterized by an accumulation of glucosylceramide, I have analysed the effect of ASM inhibition on glucosylceramide content in CBE-treated neurons. I performed a lipid extraction and a consequent HPTLC separation with the use of the solvent system chloroform:methanol:H2O 110:40:6 (v:v:v). As already demonstrated in our laboratory and reported in **fig.21A** the administration of CBE induced an accumulation of GlcCer in dopaminergic neurons ten-times higher in comparison with the control ones. This accumulation was found reduced both after the chronic and the acute treatment with AMI. (**Fig. 21B**)

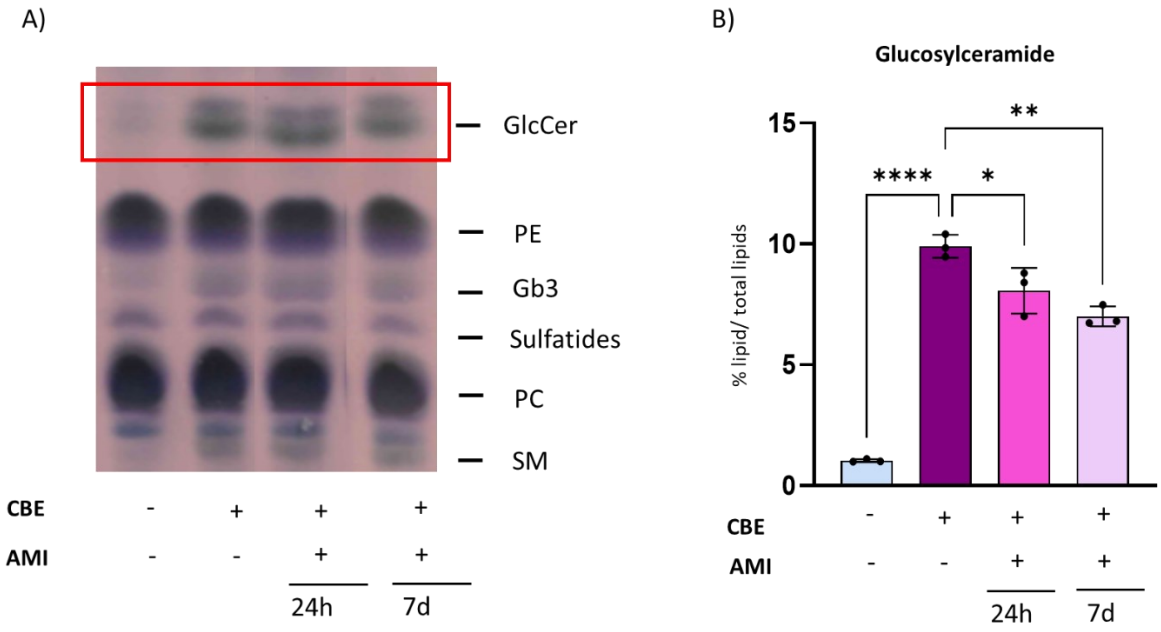

Fig. 21. Evaluation of the glucosylceramide level in CBE-treated dopaminergic neurons after AMI administration. A) representative HPTLC separation and B) quantification of GlcCer content in CBE-treated dopaminergic neurons after 24h and 7 days treatment with amitriptyline. Lipids were extracted and separated by HPTLC, loading the same amount of proteins for each sample, using the solvent system chloroform:methanol:H2O 110:40:6 (v:v:v). The relative amounts of lipid were determined by densitometry using ImageJ software and normalized on the mg of proteins seeded. *p<0.05;**p<0.01; ****p<0.0001.

Since I have observed a reduction in glucosylceramide in AMI treated neurons, I decided to analyse the enzymes involved in its catabolism: GCase and Non-Lysosomal Glucosylceramidase, shortly NLGase enzyme, mainly located at the cell surface. Performing a fluorimetric assay that allow the measurement of the enzymatic activity of the different enzymes, I have observed that, as expected, CBE has completely blocked GCase activity, and the activity hasn't changed after AMI treatment. (**Fig 22A**). Interestingly, I have found an increase of NLGase activity after the acute treatment with AMI of two-times and a three-time increase after the chronic administration (**Fig.22B**). This increase in NLGase activity could be considered responsible for the reduction in the GlcCer accumulation that I have observed.

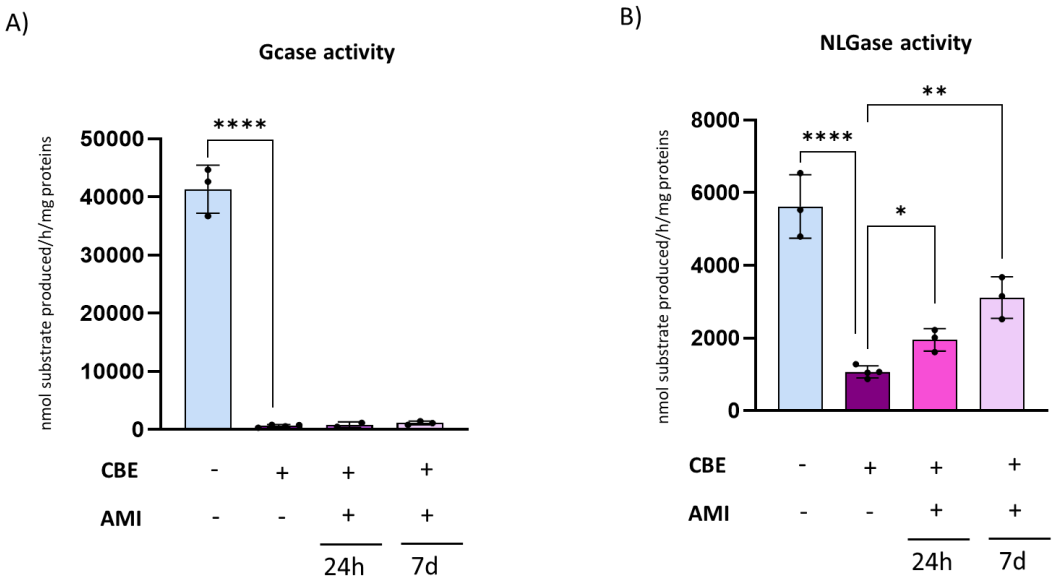

Figure 22. Evaluation of the total enzymatic activity of glycohydrolases in CBE-treated dopaminergic neurons administered with 10µM AMI.

Specific enzymatic activity of A) β-glucocerebrosidase (GCase) and B) non-lysosomal β- glucosylceramidase (NLGase) in CBE-treated dopaminergic neurons upon AMI administration. Aliquots corresponding to 20 µg of cell lysate were incubated in the presence of the fluorogenic substrate methylumbelliferyl β-D-glucopyranoside (MUB-Glc, 6mM). To discriminate between GCase and NLGase activity, lysates were preincubated with specific inhibitor AMP-DNM and CBE respectively. Data are expressed as nmols of product/mg proteins/hour and are the mean ± SEM of three experiments. *p<0.05; ** p<0.01; **** p<0.0001.

From the data obtained, it's possible to assume that in CBE-treated dopaminergic neurons, that already present neurodegeneration and glucosylceramide accumulation, both the acute and the chronic administration of amitriptyline exert a positive effect, ameliorating the neurodegenerative phenotype and reducing the glucosylceramide accumulation by increasing NLGase activity.

5.3 Biochemical characterization of an in vitro model of GCase deficiency exploiting human iPSCs-derived midbrain organoids

To further investigate the effect of the AMI treatment in a model that better recapitulate the complex structure of the brain, I generate a 3D *in vitro* model consisting in human midbrain organoids (hMO) derived from iPSCs of a GD-PD patient, carrying the biallelic mutation N370S/F213I in *GBA* gene, and a control subject. They were obtained following the protocol of Zhang and Lancaster[67,78] as described in the method section, growing them in spinning bioreactors to allow a correct maturation.

The hiPSCs were obtained from the reprogramming of fibroblasts, derived from the GD-PD patient and healthy subject skin biopsy.

The reprogramming was performed with the use of a Sendai virus-based kit (CytoTune™-iPS 2.0 Sendai Reprogramming Kit, ThermoFisher Scientific, Waltham, MA, USA), through a non-integrative reprogramming strategy set by Yamanaka et al. (2006)[82] based on the transfection with a linear DNA fragment that leads the expression of Oct4, Sox2, Klf4, and c-Myc factors.

I have performed an immunofluorescence staining to confirm the pluripotency of the hiPSCs generated. Different staminal markers, both nuclear (Sox2, Nanog) and cytoplasmic (Tra-1-60, Tra-1-81) were expressed in CTRL iPSCs (**fig. 23 A; B**) and GD-PD iPSCs (**fig 23 C;D**), confirming a correct reprogramming.

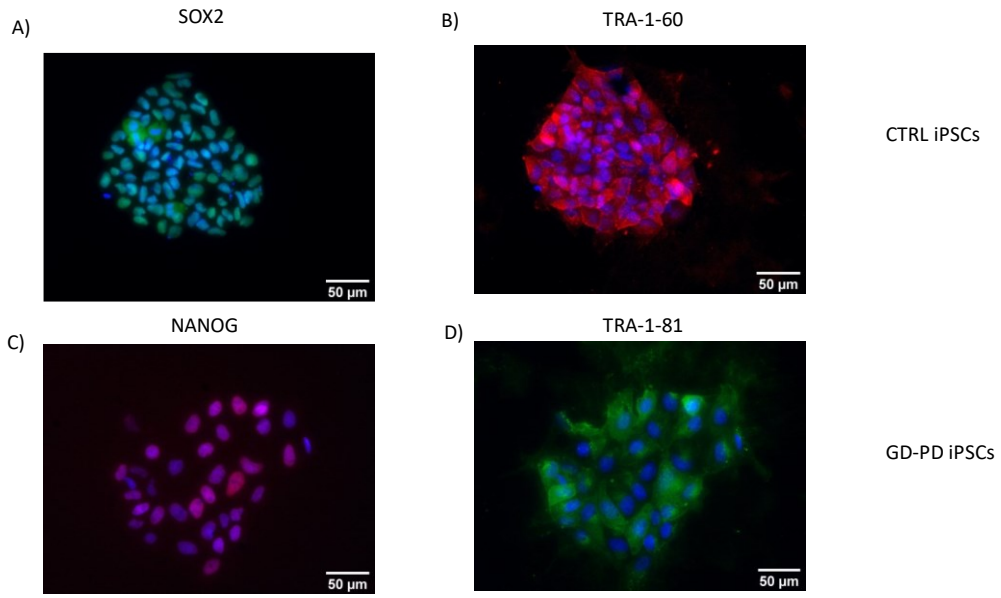

Figure 23. Characterisation of hiPSCs.
Representative immunofluorescence images of human iPSCs stained for the pluripotent nuclear markers Sox2 (A) and Nanog (C) and the cytoplasmic markers Tra-1-60 (B) and Tra-1-81 (D). Cell nuclei were stained with Hoechst (blue). Images were acquired at 400× magnification.

Midbrain organoids were obtained from hiPSCs of GD-PD patient and a healthy subject following the protocol of Zhang and Lancaster.[67,78]

The differentiation process was evaluated by indirect immunofluorescence technique using antibodies against the neuronal markers TUJ1 and MAP2, the marker of the dopaminergic commitment TH and the staminal marker Sox2. As shown in **figure 24,** at day 50 of differentiation, midbrain organoids highly express the neuronal markers TUJ1 (**Fig A and C**) and express only a little percentage of the staminal marker Sox2 (**fig B and D**), confirming the correct maturation of the organoids. Moreover, they also present high levels of TH (**fig E and G**) and MAP2 marker (**fig F and H**), suggesting a dopaminergic commitment and neuronal phenotype, which resulted reduced in GD-PD organoids (**fig. G and H**).

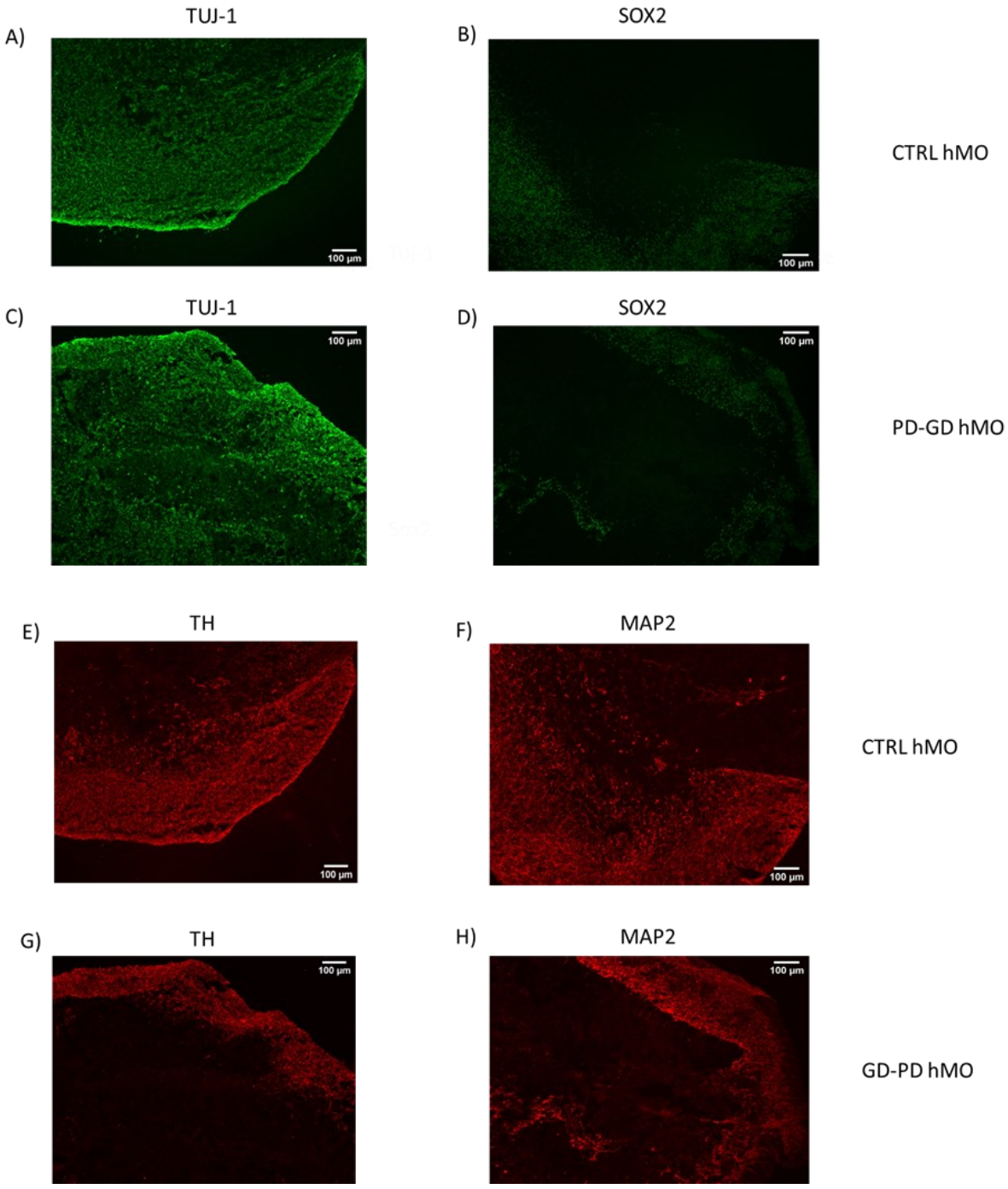

Figure 24. Characterization of hiPSCs-MO obtained from a healthy subject (CTRL) and one patient with N370S/F213I mutation in *GBA1* (GD-PD).

Representative immunofluorescence images of hiPSCs-derived midbrain organoids at 50 days of differentiation. Cells were stained (green) for the neuronal marker β-III-tubulin (TUJ-1) and the staminal marker Sox2 and were stained (red) for tyrosine hydroxylase (TH) and for microtubule associated protein (MAP2). Images were acquired at 200× magnification.

5.4 Phenotypical analysis of midbrain organoids derived from GD-PD hiPSCs

Thanks to the collaboration with my co-tutor Dr. Alessio di Fonzo from the Policlinico hospital of Milano I had the opportunity to generate midbrain organoids (hMOs) from a GD type 1 patient carrying the biallelic mutation N370S/F213I in GBA gene who also developed parkinsonism. The first step was to characterize this three-dimensional model and verify whether it recapitulates the pathological phenotype of the disease. I have investigated the activity of the main glycohydrolases, neuronal and autophagic markers, glucosylceramide content and α-synuclein aggregation of GD-PD midbrain organoids at various stages of differentiation, considering hMOs from a healthy subject as controls. To this end, as schematized in **figure 25** I had collected organoids at three different time points: 50, 80 and 120 days after the beginning of differentiation.

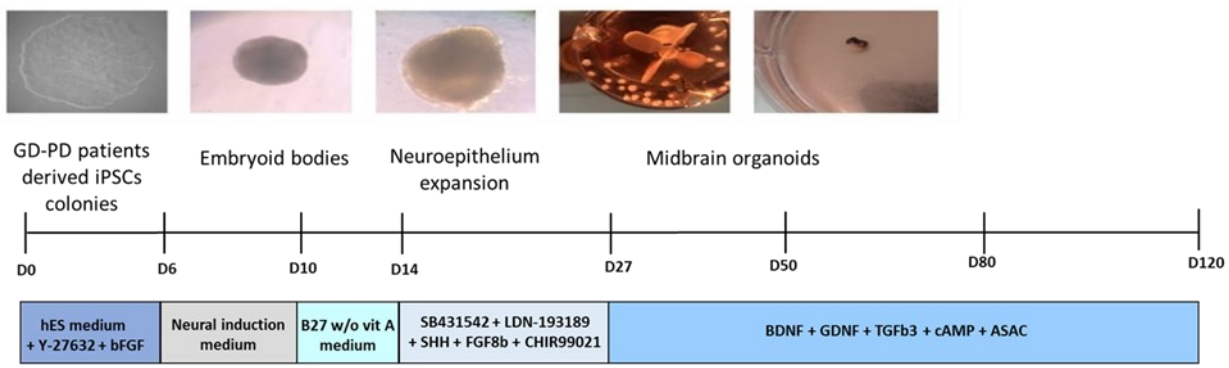

Figure 25. Generation of *in vitro* three-dimensional model of β-glucocerebrosidase deficiency.

Schematic diagram of the experimental protocol to generate human midbrain organoids: human-induced pluripotent stem cells (iPSCs) from one healthy subject (CTRL) and a GD-PD patient (N370S/F213I) were differentiated in midbrain organoids. After different time points (50, 80, 120 days of differentiation), organoids were harvested and analysed for β-glucocerebrosidase activity, neuronal and autophagic markers expression, glucosylceramide content and α-synuclein aggregation.

First, I evaluated GCase activity, performing an enzymatic assay employing the fluorogenic substrate MUB-β-Glc, as explained in the method chapter, and measuring the activity on organoids lysates at the three considered stages of differentiation. To evaluate only β- glucocerebrosidase activity (GCase), the non-lysosomal β-glucosilceramidase (NLGase) was inhibited.

As showed in **figure 26**, GD-PD midbrain organoids presented a reduced GCase activity compared to healthy subject at all the considered time points. In particular, the reduction was about 97% at day 50, 79% at day 80 and 75% at day 120.

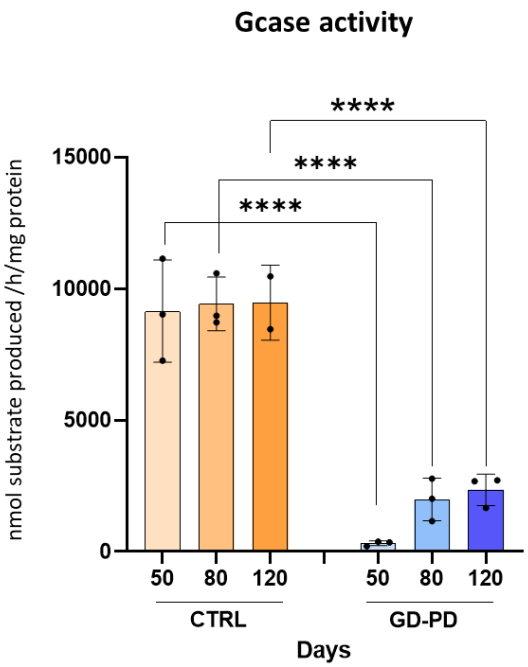

Figure 26. Evaluation of GCase enzymatic activity in lysates of hiPSCs-MO from a healthy subject (CTRL) and one patient with the N370S/F213I mutation on *GBA* (GD-PD).

Specific enzymatic activity of β-glucocerebrosidase (GCase) was measured after 50, 80, 120 days of differentiation, on aliquots corresponding to 20 µg of cell lysate proteins, incubated in the presence of the specific inhibitor of the NLGase enzyme AMP-DNM (50 nM) and using the specific fluorogenic substrate methylumbelliferyl β-D- glucosylpyranoside (MUB-Glc, 6mM). Data are expressed as nmols of product/ mg proteins/ hour and are the mean ± SEM of three experiments. One-way Anova test: ****p<0.0001.

I evaluated the effect of GCase deficiency on the neuronal homeostasis studying the differential expression levels of neuronal markers between pathological and healthy organoids. I considered day 50 of differentiation as a starting condition, in which neurons are already matured and they haven't presented neurodegeneration yet, and normalized on that day the value obtained from day 80 and 120.

As shown in the immunoblotting analysis reported in **figure 27**, CTRL organoids presented an increase over time of TH and TAU protein, especially at day 120, when they resulted respectively 25 times (for TH) and 4 times (in case of TAU) more expressed than at day 50. This time-dependent increase was not observed in TUJ1 and MAP2 levels, that remain almost constant.

GD-PD organoids instead express low TH protein levels at all the different timepoint, in particular at D120 they presented a reduction of almost 8 times in comparison to the control. At the same time point also TAU, TUJ1 and MAP2 expression result diminished in GD-PD organoids compared to the controls, respectively of four, two and three times. These data highlight the strong reduction in TH expression in GD-PD organoids as expected in a Parkinson's *in vitro* model and suggest a neurodegenerative phenotype in GD-PD organoids respect to the CTRL ones at D120.

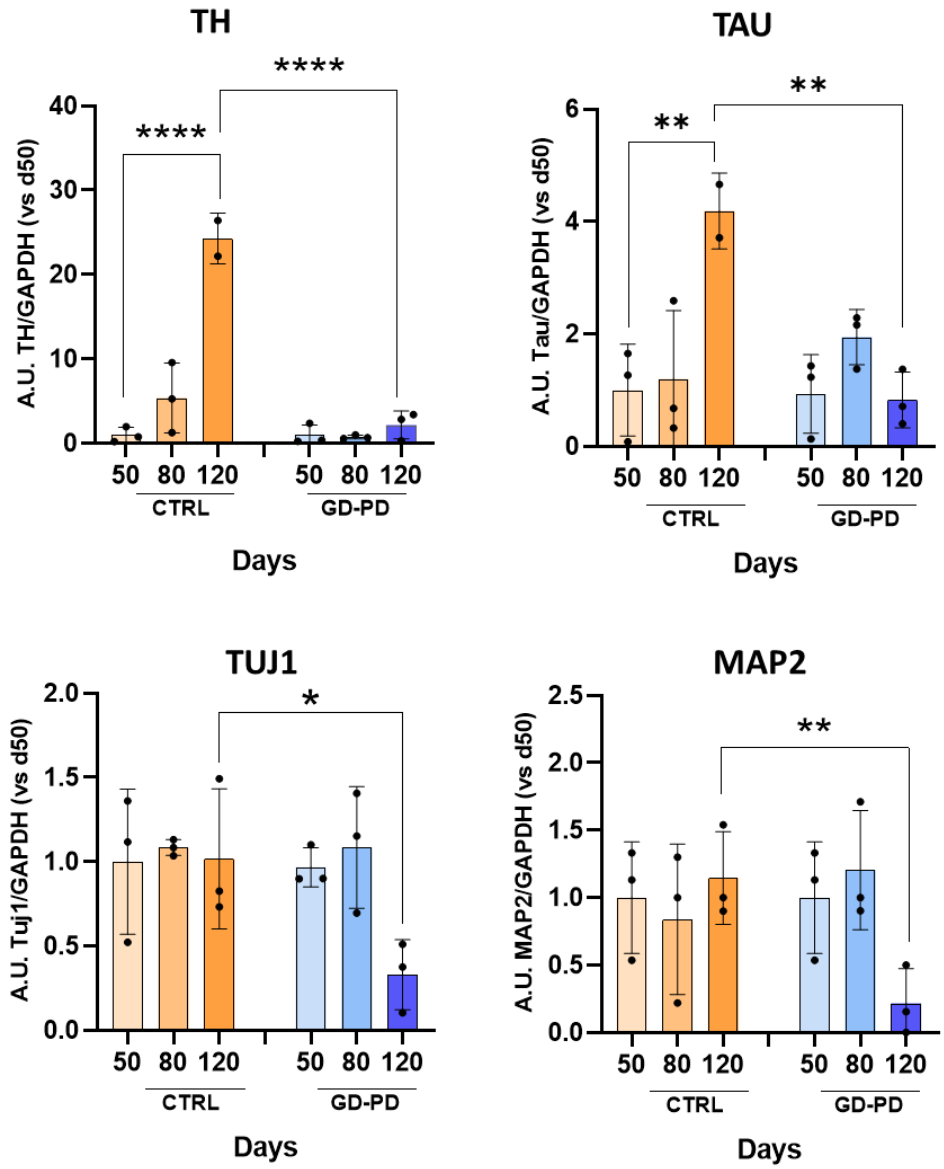

Figure 27: Evaluation of the protein expression of neuronal markers in hiPSCs-MO from a healthy subject (CTRL) and one patient with the N370S/F213I mutation on *GBA* (GD-PD).
Semiquantitative analysis of TH, TAU, TUJ1 and MAP2 protein levels. Same amount of cell lysate of midbrain organoids from one healthy subject (CTRL) and a GD-PD patient with the N370S/F213I mutation on *GBA1* collected at day 50, 80 and 120 of differentiation were separated by SDS-page. Protein content was analysed through immunoblot using primary antibodies anti-MAP2, anti TUJ1, anti-TAU and anti-TH. GAPDH was used as loading control. Optical densities of the individual bands were quantified using NIH ImageJ and normalized on GAPDH expression. Data are expressed as arbitrary units of antigen VS day50.

Since Gaucher Disease is lysosomal storage disorder, a typical feature of this pathology is the presence of lysosomal and consequent autophagy impairment due to the accumulation of uncatabolized materials. Therefore, I decided to investigate the lysosomal and autophagic compartment by evaluating the expression of LC3-II, an autophagosomal marker, p62, a ubiquitin-binding scaffold protein, and LAMP1, a lysosomal marker.

As shown in **figure 28**, in GD-PD organoids the expression of LC3II resulted increase of almost 2.5 and 2 times respectively at D80 and D120 in comparison to the controls. P62 and LAMP1 remained constant in CTRL organoid at the different time points, while increase of almost three times at D120 in GD-PD organoids. These data suggest a lysosomal impairment in GD-PD organoids in comparison to the control one.

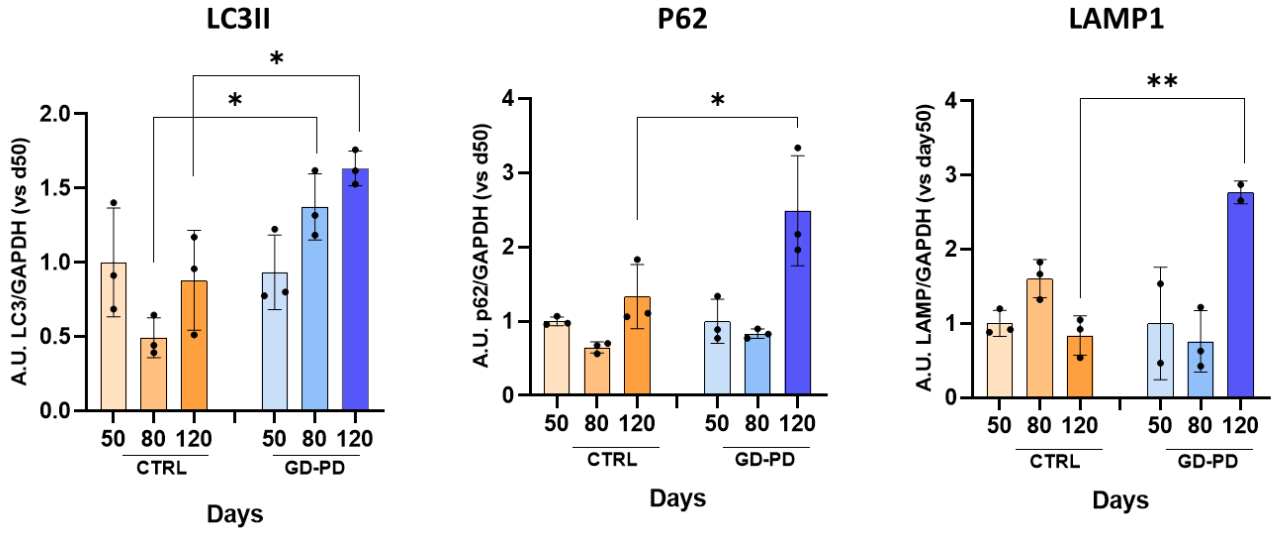

Figure 28: Evaluation of the protein expression of lysosomal and autophagic markers in hiPSCs-MO from a healthy subject (CTRL) and one patient with the N370S/F213I mutation on *GBA* (GD-PD).
Semiquantitative analysis of LC3-II, p62, LAMP-1 protein levels. Same amount of cell lysate from midbrain organoids from one healthy subject (CTRL) and a GD-PD patient with the N370S/F213I mutation on *GBA* collected at day 50, 80 and 120 of differentiation were separated by SDS-page. Protein content was analyzed through immunoblot using primary antibodies anti-LC3-II, anti-p62 and anti-LAMP-1. GAPDH was used as loading control. Optical densities of the individual bands were quantified using NIH ImageJ and normalized on GAPDH expression. Data are expressed as arbitrary units of antigen VS day50.

Based on the already described findings about endolysosomal markers in response to lysosomal impairment, I decided to investigate the effect of *GBA* mutation also on lysosomal enzymes other than GCase, in order to assess a possible lysosomal involvement in the onset on neurodegeneration in my GD-PD *in vitro* model. I performed an enzymatic assay that allow to measure the activity of non-lysosomal β-glucocerebrosidase (NLGase), β-galactosidase (β-gal), β-hexosaminidase (β-hex), α- mannosidase (α-man) and β-mannosidase (β-man).

As shown in **figure 29A**, NLGase presents an opposite trend over the time in pathological and healthy samples: in CTRL gradually decreased during differentiation, while in GD-PD organoids NLGase levels increased, especially from day 50 to 80. In particular, at D50 the residual NLGase activity of pathological hMO was 94% lower than the control, while after 120 days of differentiation NLGase activity in GD-PD organoids was 2 times higher than in CTRL.

The other glycohydrolases (**fig. 29B**) such as β-gal, β-hex, α-man and β-man did not show significant

changes in the activity of between CTRL and GD-PD organoids at the different time points.

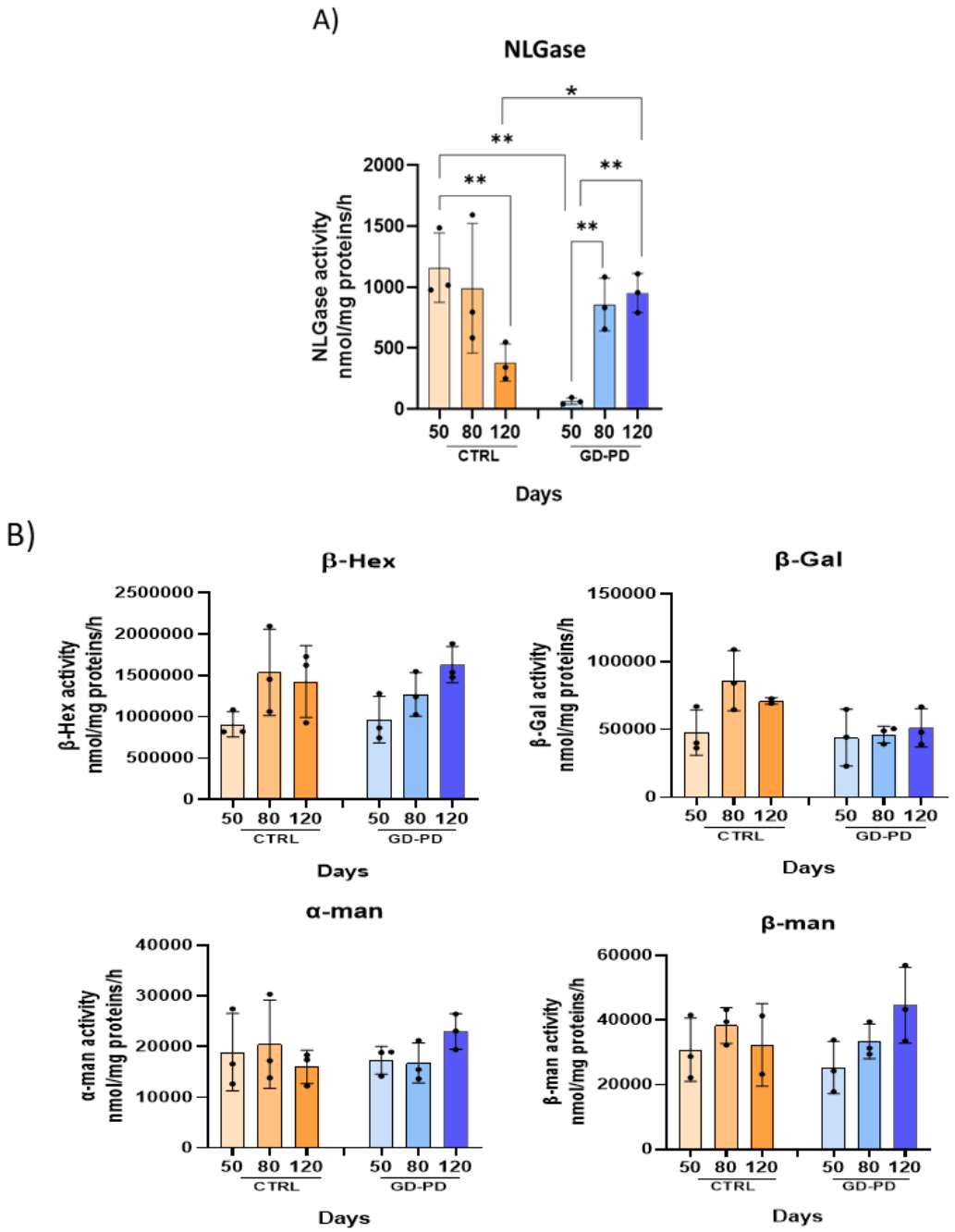

Figure 29. Evaluation of the total enzymatic activity of lysosomal glycohydrolases in lysates of hiPSCs-MO from a healthy subject (CTRL) and one patient with the N370S/F213I mutation on *GBA* (GD-PD).

Specific enzymatic activity of non-lysosomal β-glucocerebrosidase (NLGase), β-galactosidase (β-gal) and β- hexosaminidase (β-hex), α-mannodìsidase (α-man) and β-mannosidase (β-man) was measured after 50, 80 and 120 days of differentiation. Aliquots corresponding to 20 µg of cell lysate proteins for NLGase, 5µg for β-Gal and β-Hex, 10 µg of proteins α-man and β-man were incubated in the presence of the respective florigenic substrates methylumbelliferyl β-D-glucosylpyranoside (MUB-Glc, 6mM) for NLGase, methylumbelliferyl β-D- galactosylpyranoside (MUB-Gal, 500µM) for β-gal, methylumbelliferyl-Nacetyl β-D-glucosamide (MUG, 500µM) for (β-hex), Methylumbelliferyl-α-D-mannopyranoside (MUB-α-Man) for α-Man and 4- Methylumbelliferyl-β-D-mannopyranoside (MUB-β-Man) for β-man. To discriminate between β- glucocerebrosidase and NL-β-glucosylceramidase activity, lysates were preincubated with specific inhibitor AMP-DNM and CBE respectively. Data are expressed as nmols of product/mg proteins/hour and are the mean ± SEM of three experiments. Two-way Anova test: *p<0.05, ** p<0.01.

Moreover, I evaluate ASM activity, performing an enzymatic assay with radioactive SM as substrate, and I found an increased ASM activity in GD-PD patients in respect to healthy subjects at day 50 and 120. (**figure 30**).

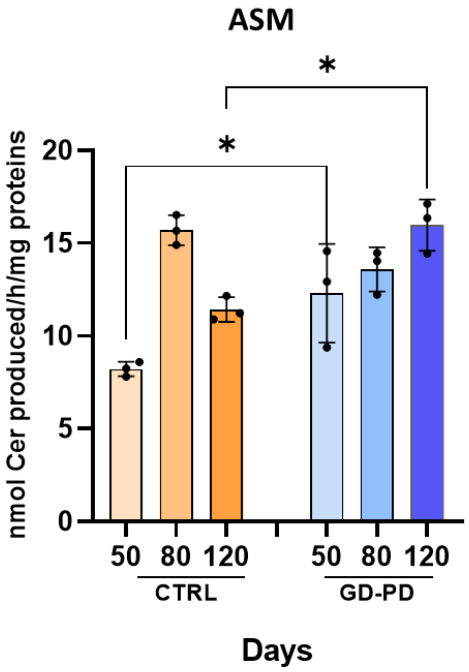

Figure 30. Evaluation of the enzymatic activity of ASM in lysates of hiPSCs-MO from a healthy subject (CTRL) and one patient with the N370S/F213I mutation on *GBA* (GD-PD).

Aliquots corresponding to 50 µg of cell lysate proteins derived from hiPSCs-MO at 50, 80, and 120 days in culture were incubated with 5nM radioactive sphingomyelin for 2 hours at 37°C. Each reaction mixture was subjected to lipid extraction and partitioning using chloroform/methanol 2:1 (v:v), The separation of the lipids was performed by HPTLC using the solvent system 110:40:6 $CHCl_3$:CH_3OH:H_20 (v:v:v). The radioactive ceramide was detected by digital autoradiography performed with a Beta-Imager TRacer instrument (BioSpace). The radioactivity associated with ceramide was quantified by M3 Vision software. Specific activity of the enzymes was expressed as nanomoles of converted substrate/ hours/ mg of proteins. *$p<0.05$.

One of the main features of GD-PD is the presence of glucosylceramide accumulation due to a defective activity of GCase. Therefore, I analysed the GlcCer level in midbrain organoids, extracting the lipids and separating them by HPTLC, after the metabolic labelling at the steady state with radioactive sphingosine.

As reported in **figure 31**, GD-PD midbrain organoids showed a more than double increase of GlcCer level in comparison to the CTRL one at all the considered time points.

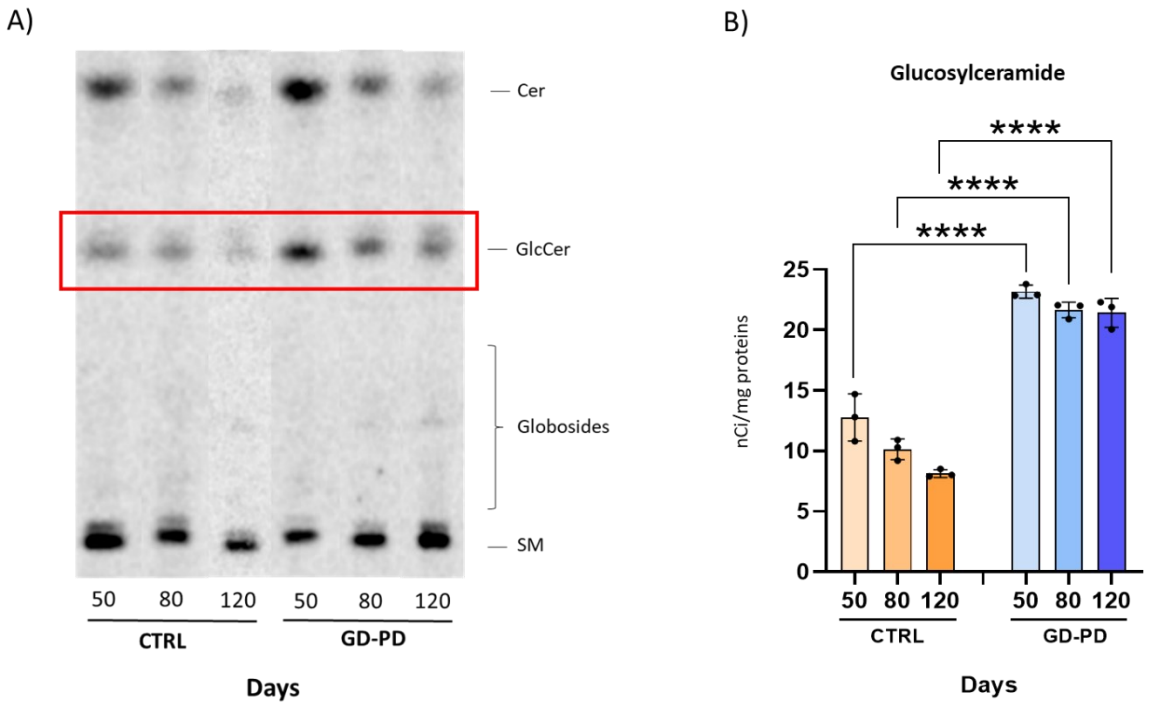

Figure 31. Glucosylceramide content in midbrain organoids at different time points.

A) Representative HPTLC separation and B) quantification of GlcCer level in midbrain organoids derived from healthy subject (CTRL) and GD-PD patient. Sphingolipid pattern was evaluated at different time points from D50 to D120 by the metabolic labelling at the steady state using radioactive sphingosine. Radioactive lipids were separated by HPTLC using the solvent system chloroform: methanol: H_2O 110:40:6 (v:v:v). And identified by co-migration with authentic standards (Ceramide, Cer; Glucosylceramide, GlcCer, Globosides, Gb, Sphyngomyelin, SM;). Radioactive sphingolipids were quantified using M3 vision software and expressed as nCi/mg of proteins. **** $p<0.0001$.

Parkinson's disease is characterized by the accumulation of misfolded α-synuclein, a protein involved in synaptic transmission, leading to the formation of Lewy Bodies within neurons in SN pars compacta of the brain. Since it is an important feature of this pathology, in collaboration with Bellucci's group of Brescia university, I analysed my GD-PD in vitro model to evaluate if it also presents this trait, considering only D80 and D120 as time points because previously data indicate that hMOs start to accumulate α-synuclein after 80 days of differentiation.

As reported in **figure 32**, in GD-PD organoids we found an increase over time of insoluble α-synuclein, that became more than double. Moreover, patient-derived organoids also presented an increase of insoluble α-synuclein at all the considered time points respect to the controls, in particular the aggregation is higher at D120.

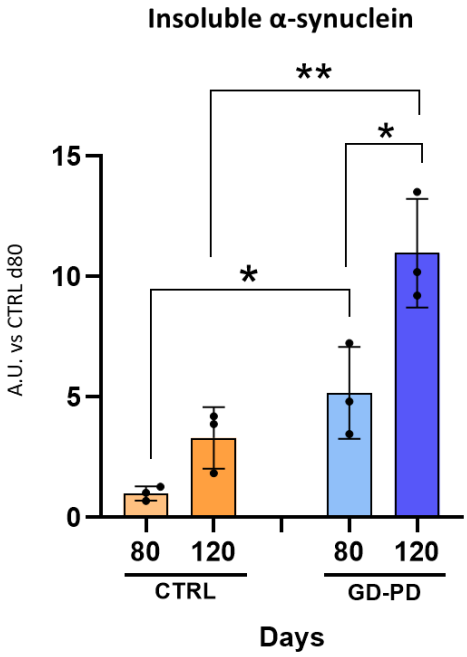

Figure 32. Evaluation of α-synuclein aggregation in CTRL and GD-PD midbrain organoids over time.

Immunoblot analyses of α-synuclein aggregates after protein extraction with urea 8M plus 5% SDS. Same amount of cell lysate from GD-PD MO and CTRL MO were separated by SDS-page. β-actin was used as loading control. Optical densities of the individual bands were quantified using NIH ImageJ and normalized on β-actin expression. Data are expressed as arbitrary units of antigen VS CTRL at day80 and are the mean ± SEM of three different experiments. * $p>0.05$; ** $p<0.01$.

5.5 Evaluation of the effect of amitriptyline treatment on midbrain organoids from a GD-PD patient

Another aim of my PhD project was to validate in a 3D model, that better resemble the physiology of the brain, the previous findings obtained in CBE-treated neurons. In this model upon AMI administration, as described in the first part of the results section, I observed a partial amelioration of the neurodegenerative phenotype and a reduction in GlcCer accumulation, probably due to an increase in NLGase activity.

As reported in **figure 33**, I have differentiated hiPSCs into midbrain organoids, carrying on the differentiation until D120 and collecting them at two different time points: D80 and D120. From D50 I have treated the organoids with two different ASM inhibitors: either amitriptyline at two different concentrations: 20 µM AMI or 40 µM AMI or ARC, a competitive inhibitor of ASM acting on the catalytic site.

AMI 40 µM and ARC have resulted cytotoxic because they have totally inhibited ASM activity and they have induced cell death, so I have focused the analyses only on AMI 20 µM, considering not treated hMO (NT) as controls.

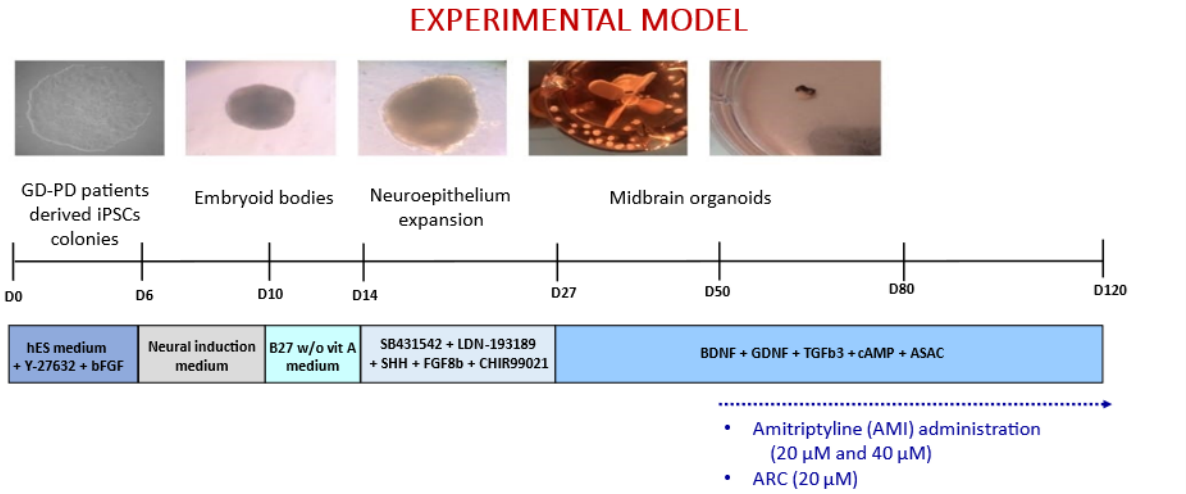

Figure 33. Generation of in vitro three-dimensional model of acid sphingomyelinase deficiency.
Schematic diagram of the experimental protocol to generate human midbrain organoids from one healthy subject (CTRL) and a GD-PD patient (N370S/F213I). From D50 of differentiation, organoids were treated with either 20 µM AMI or 40 µM AMI or ARC, a competitive inhibitor of ASM. At D80 and D120 organoids were harvested and analysed for acid sphingomyelinase activity, neuronal and autophagic markers expression, glucosylceramide content, glucocerebrosidases activity and α-synuclein aggregation.

To test the efficacy of AMI as an inhibitor in this model as well, I have measured the change in ASM activity on hiPSCs-derived midbrain organoids treated with 20µM AMI for 30 and 70 days and then harvested respectively at day 80 and 120.

In GD-PD organoids AMI treatment induce a significant reduction in ASM activity respect to the untreated, that increases over time, as showed in **figure 34**. In particular, upon 20 µM AMI administration I found a 40% reduction in ASM activity at D80, and 70% reduction at D120 (**Figure 34B**).

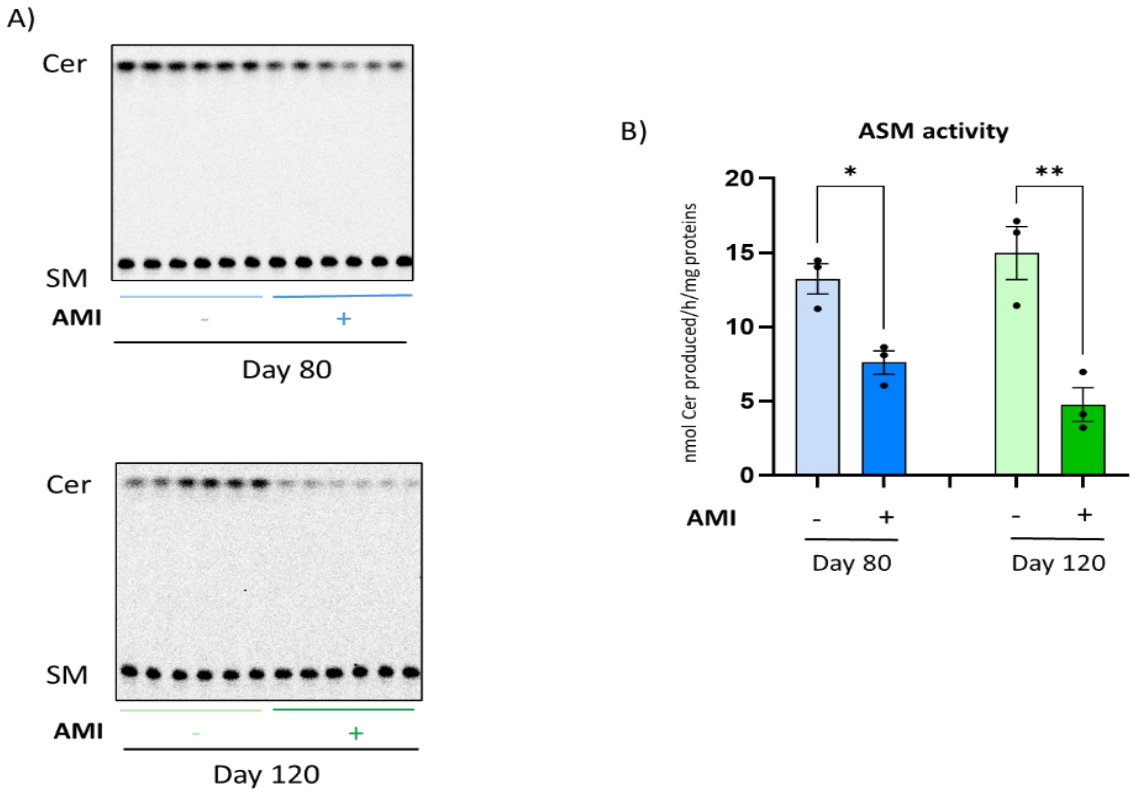

Figure 34. Evaluation of ASM enzymatic activity in GD-PD midbrain organoids after 20 µM AMI administration. A) Representative HPTLC separation and B) quantification of the radioactive ceramide produced in GD-PD midbrain organoids upon administration of 20 µM AMI for 30 and 70 days. Aliquots corresponding to 50 µg of cell lysate were incubated with 5nM of radioactive sphingomyelin for 2 hours at 37°C. Each reaction mixture was subjected to lipid extraction and partitioning using chloroform/methanol 2:1 (v:v). Ceramide content was evaluated by the separation of lipids by HPTLC using the solvent system 110:40:6 $CHCl_3$:CH_3OH:H_2O (v:v:v) and the radioactive lipid pattern was visualized by digital autoradiography performed with a Beta-Imager ^{T}Racer instrument (BioSpace). The radioactivity associated with ceramide was quantified by M3 Vision software. Specific activity of the enzymes was expressed as nanomoles of converted substrate/ hours/ mg of proteins. * $p<0.05$; ** $p<0.001$

To investigate the effect of ASM inhibition on neuronal homeostasis, I performed immunoblot analysis to detect the expression of the neuronal markers: TUJ1, MAP2 and TAU and of the marker of dopaminergic commitment TH.

I have found that at D80, amitriptyline-treated organoids did not show the expected ameliorative effect that I previously found in CBE-treated dopaminergic neurons, since the neuronal markers show a tendency to decrease after amitriptyline treatment (**Fig.35A**). Moreover, at D120 the reduction of TH, TUJ-1 and TAU expression upon amitriptyline administration has become more pronounced, suggesting an exacerbation of the neurodegenerative phenotype (**Fig.35B**).

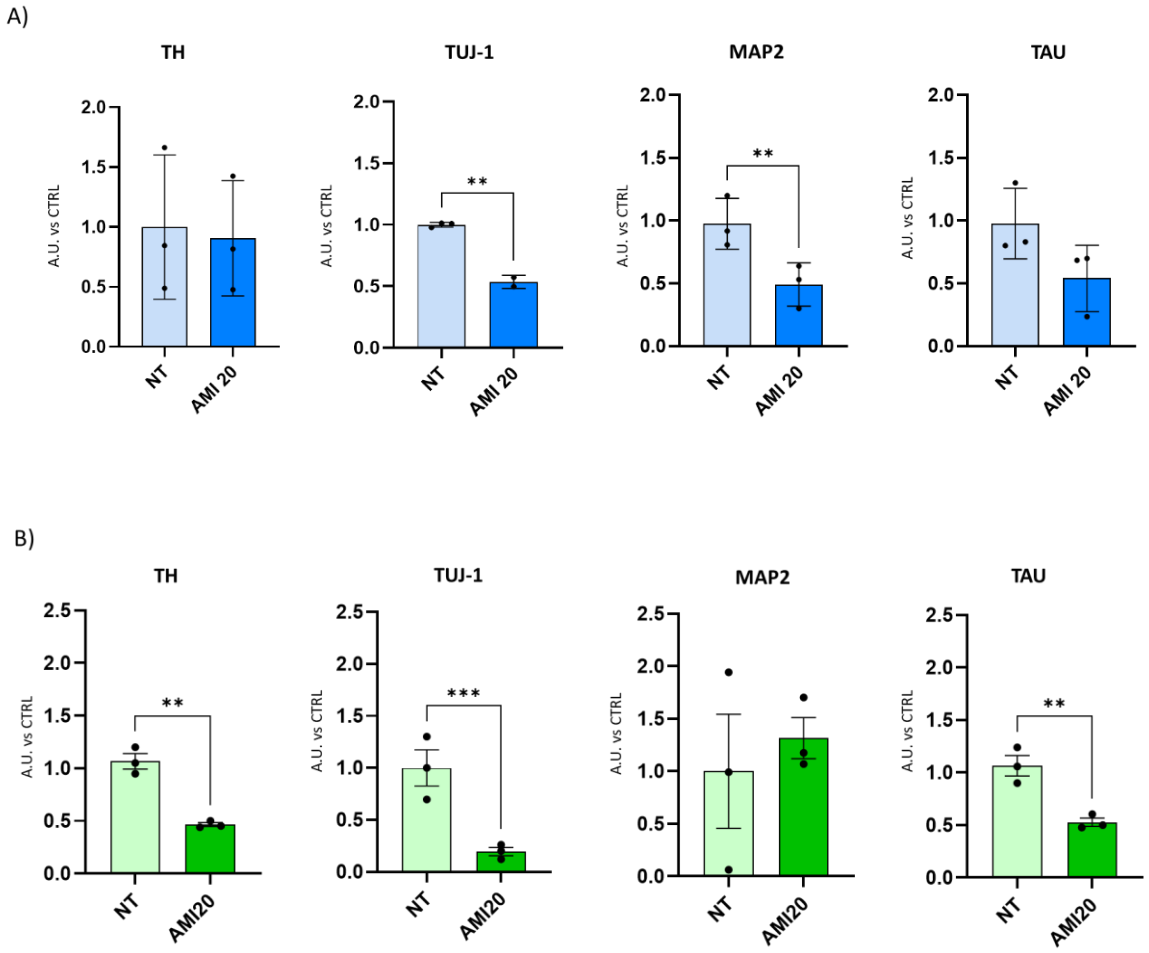

Figure 35. Evaluation of the protein expression of neuronal markers in GD-PD midbrain organoids upon 20µM AMI administration.

Immunoblot analyses of TH, β-III-tubulin, MAP2, TAU protein levels. Same amount of cell lysate from GD-PD MO administered with 20 µM AMI for 30days (Fig A) or 70 days (Fig B) were separated by SDS-page. GAPDH was used as loading control. Optical densities of the individual bands were quantified using NIH ImageJ and normalized on GAPDH expression. Data are expressed as arbitrary units of antigen VS untreated and are the mean ± SEM of three different experiments. **p<0.01; ***p<0.001.

Since I observed in pathological organoids an alteration of the autophagy and of the endolysosomal compartment, I investigated the possible effect of AMI treatment on these cellular processes.

I studied the autophagic compartment by evaluating the expression of LAMP1, a lysosomal marker, LC3-II, an autophagosomal marker, and p62, a ubiquitin-binding scaffold protein. Since p62 accumulates when autophagy is inhibited, and decreases when autophagy is induced, it may be used as a marker to study autophagic flux. As showed in **figure 36,** I have observed an increase in the autophagic markers expression after 30 days treatment with amitriptyline (**Fig.36A**), that were further increased over time upon a prolonged exposition to amitriptyline, suggesting a worsening of the autophagic impairment (**Fig.36B**). In particular, after 70 days treatment, there was an increase in P62 level more than double respect to the untreated one.

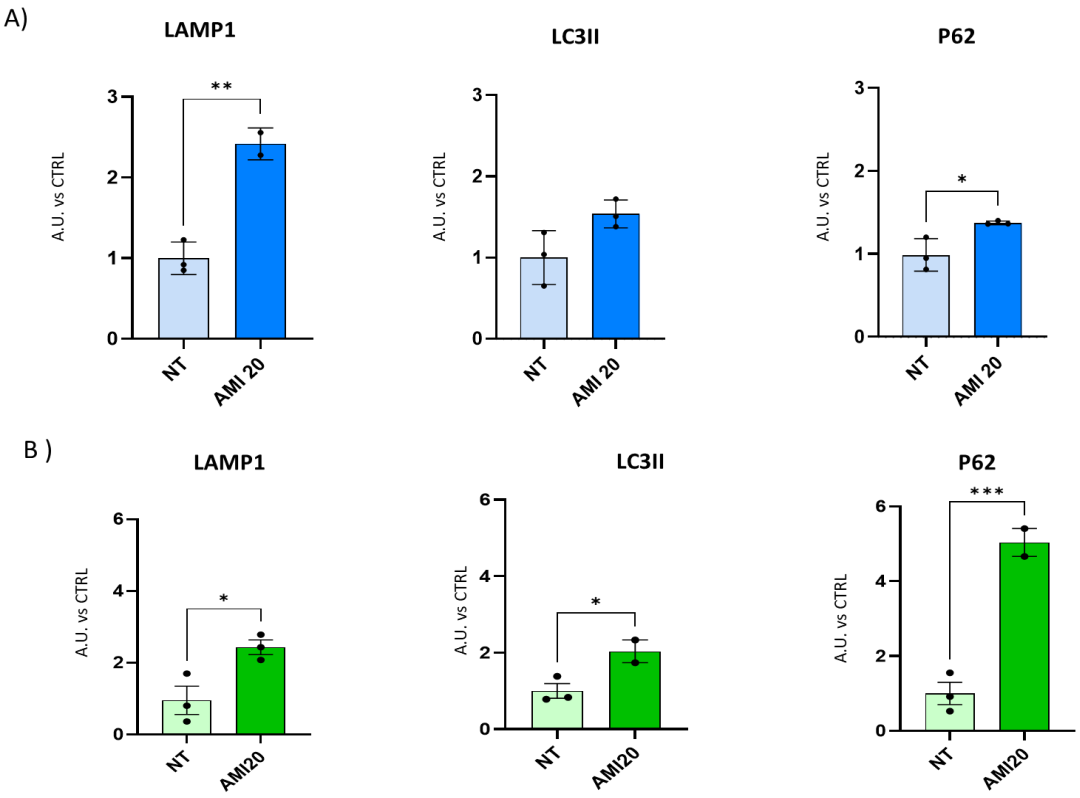

Figure 36. Evaluation of the protein expression of lysosomal and autophagic markers in GD-PD MO after AMI administration

Immunoblot analyses of LAMP-1, LC3-II and P62 protein levels. Same amount of cell lysate from midbrain organoids after 30 days treatment with AMI (Fig A) or 70 days treatment (Fig B). were separated by SDS-page. GAPDH was used as loading control. Optical densities of the individual bands were quantified using NIH ImageJ and normalized on GAPDH expression. Data are expressed as arbitrary units of antigen VS untreated one. *P<0.05; **p<0.01; *** p<0.001.

Since I found a differential expression of lysosomal markers upon ASM inhibition, I also analyze the activity of lysosomal glycohydrolases in treated and untreated midbrain organoids at D80 and D120 of differentiation. I focused on a GCase and NLGase activity, since the other glycohydrolases in GD-PD organoids didn't present changes respect to the control one.

As displayed in **figure 37**, I found no difference in GCase and NLGase activity after 30 days of treatment with AMI, however I found a tendency to increase of GCase (**Fig.37A**) and NLGase activity (**Fig. 37B**) after 70 days administration.

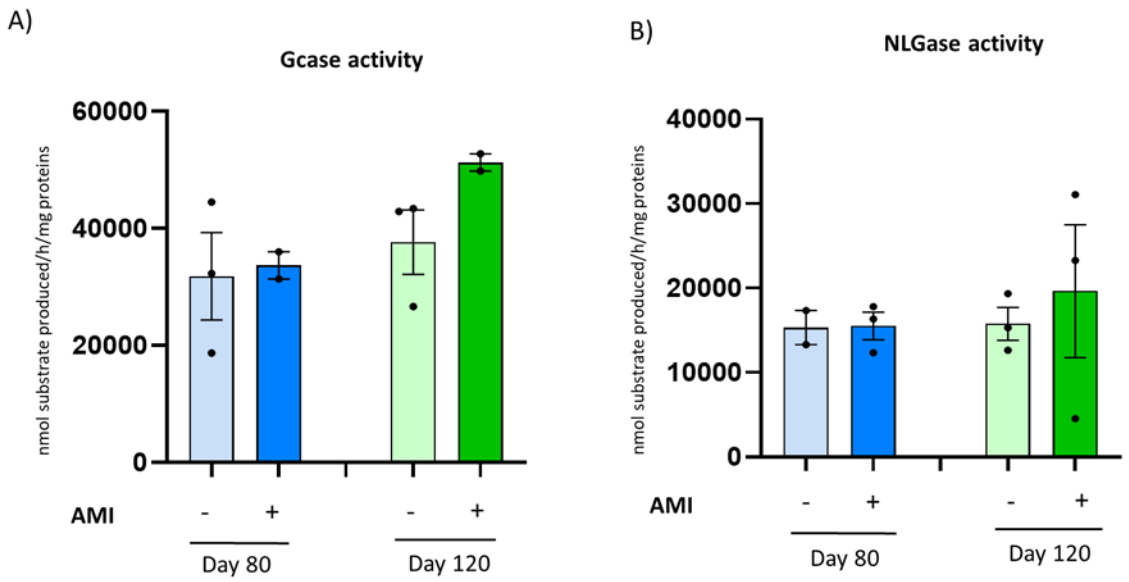

Figure 37. Evaluation of the enzymatic activity of glucocerebrosidases in GD-PD MO administered with 20µM AMI.

Specific enzymatic activity of A) β-glucocerebrosidase (GCase) and B) non-lysosomal β- glucosylceramidase (NLGase) in GD-PD midbrain organoids upon AMI administration. Aliquots corresponding to 20 µg of cell lysate were incubated in the presence of the fluorogenic substrate methylumbelliferyl β-D-glucopyranoside (MUB-Glc, 6mM). To discriminate between GCase and NLGase activity, lysates were preincubated with specific inhibitor AMP-DNM and CBE respectively. Data are expressed as nmols of product/mg proteins/hour and are the mean ± SEM of three experiments.

Considering that I have observed an increase in GlcCer accumulation in GD-PD midbrain organoids compared to the controls, I decided to also evaluate the effect of ASM inhibition on GlcCer content.

I have found that the amitriptyline-treated organoids showed a tendency to increase glucosylceramide accumulation respect to the untreated one after 30 days of treatment (**Fig. 38**). At day 120, I have found no difference in GlcCer level between treated and untreated, probably due to the tendency of increase GCase and NLGase activity in AMI-treated GD-PD organoids observed at day 120.

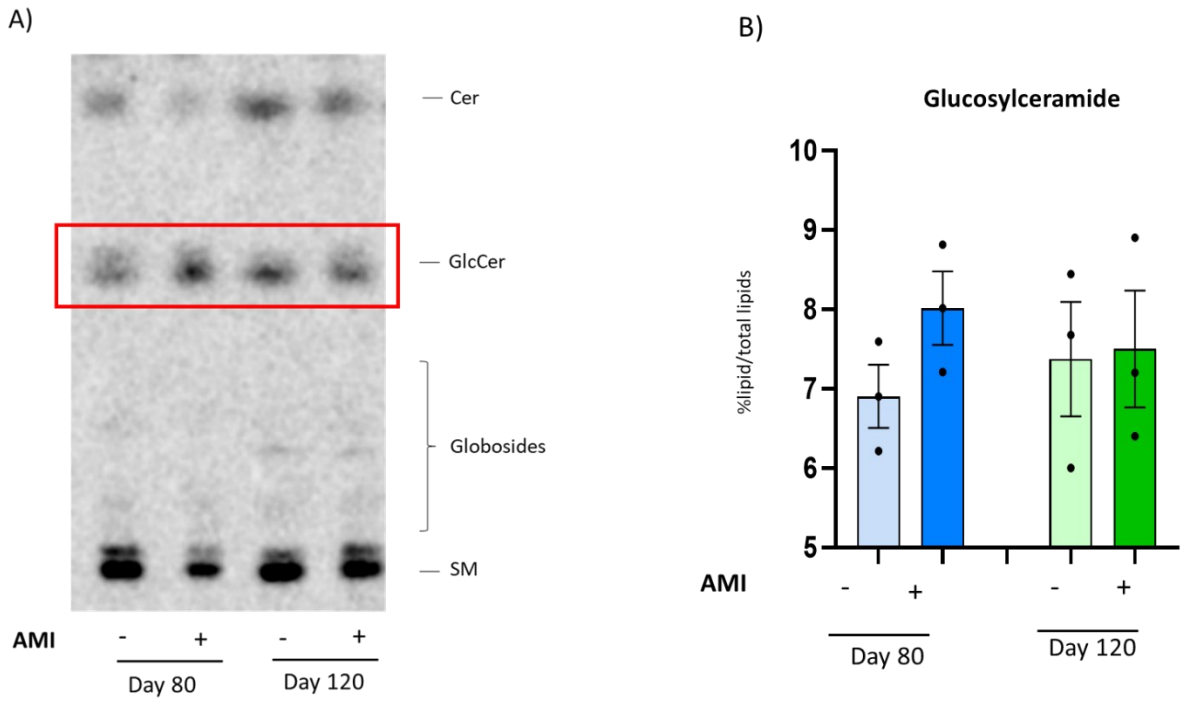

Fig. 38. Evaluation of the glucosylceramide level in GD-PD MO after AMI administration.
Quantification of GlcCer content in GD-PD midbrain organoids after 30 and 70 days treatment with amitriptyline. Lipids were extracted and separated by HPTLC, loading the same amount of proteins for each sample, using the solvent system chloroform:methanol:H_2O 110:40:6 (v:v:v). The relative amounts of lipid were determined by densitometry using ImageJ software and normalized on the mg of proteins seeded.

Since α-synuclein aggregation is one of the main features of PD, I evaluate the impact of ASM inhibition on its aggregation.

As showed above, GD-PD midbrain organoids presented α-synuclein aggregation over time in comparison to the CTRL one. Here, I found an increase in α-synuclein aggregation after 30 days treatment with AMI and a tendency to aggregate also after 70 days administration (**Fig.39**).

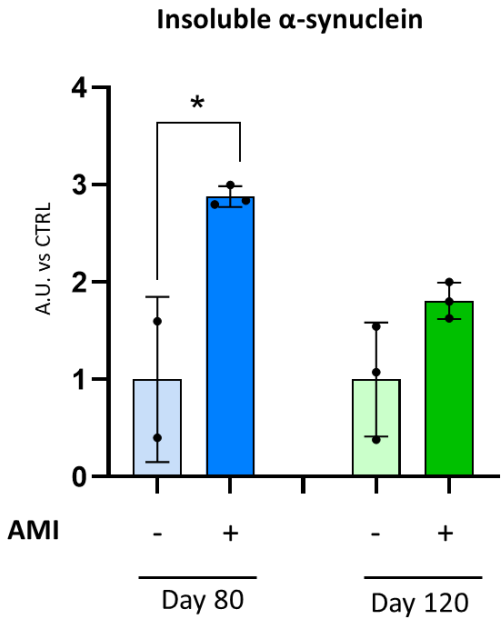

Figure 39. Evaluation of α-synuclein aggregation in GD-PD MO after AMI administration.

Immunoblot analyses of α-synuclein aggregates after protein extraction with urea 8M plus 5% SDS. Same amount of cell lysate from GD-PD MO, treated and untreated with 20 µM AMI for 30 days and 70 days. β-actin was used as loading control. Optical densities of the individual bands were quantified using NIH ImageJ and normalized on β-actin expression. Data are expressed as arbitrary units of antigen VS CTRL at day80 and are the mean ± SEM of three different experiments. * $p<0.05$.

From the data obtained, it's possible to assume that the ASM inhibition, given by the prolonged AMI administration, was detrimental in GD-PD midbrain organoids, exacerbating the neurodegeneration, increasing the autophagic impairment, and promoting α-synuclein aggregation without changes in GlcCer accumulation.

Interestingly these results are in contrast with the data obtained in CBE-treated dopaminergic neurons, in which AMI administration ameliorated the pathological phenotype and reduced the GlcCer accumulation.

6 DISCUSSION

Lysosomal storage disorders (LSDs) are a group of inherited metabolic disorders caused by a defective activity of lysosomal enzymes resulting in the accumulation of undegraded substrates. Among the various genes involved in the onset of LSD, *GBA* emerges for its important role in neuronal physiology. Loss of function mutations in *GBA* lead to GCase deficiency, and a diminished activity of this enzyme is associated with the onset of neuronal damage in several neurodegenerative disorders. [50,54,80]

Homozygous mutations in the *GBA* gene result in Gaucher Disease (GD), while monoallelic mutations are considered the most prevalent genetic risk factor for the onset of Parkinson's disease (PD), carrying a 7-fold higher risk of developing PD that manifests 3-6 years earlier compared to the idiopathic form [50]. Furthermore, recent observations reveal that individuals with GD type I, traditionally seen as the visceral form without neurological impairment, have a 20-fold higher risk of developing a neuronopathic syndrome with parkinsonism during aging. [45]

The observation that several individuals with GD also experience parkinsonism, and conversely, some PD patients exhibit characteristic features of GD, such as reduced GCase activity[60], enhances the association between *GBA* mutations and the degeneration of dopaminergic neurons in the substantia nigra pars compacta, which are specifically affected in Parkinson's Disease. However, the contribution of mutated *GBA* to the pathogenesis of PD is still unclear.

The main problem of studying the link between GCase deficiency and neuronal damage is the lack of suitable *in vitro* or *in vivo* models. The conventional model frequently employed involved primary cultures of fibroblasts obtained from patients' skin biopsies. However, these cells do not accurately recapitulate neuronal physiology. A significant drawback of this model is that fibroblasts, despite being derived from patients, are not the primary cell type affected in the LSD, and they do not exhibit substrate accumulation. [81] Animal models with partial enzymatic inhibition often display phenotypes differing from those observed in human diseases, or they develop compensatory mechanisms that enable them to overcome the deficiency of a specific enzyme. Studying post-mortem human brain tissue is challenging due to its limited availability and rapid deterioration. Additionally, as it represents the endpoint situation, cells derived from such tissues do not allow for analyses of the molecular pathways involved in the onset of the pathology. Therefore, they do not provide insights into the association between the decrease in lysosomal enzymatic activity and neurodegeneration.

Starting from 2006 with the discovery of Yamanaka and Takahashi [82], the advent of induced-pluripotent stem cells (iPSCs) has revolutionized the scientific research field, in particular regarding neurodegenerative disorders. Induced pluripotent stem cells (iPSCs) can be derived from the reprogramming of fully committed adult cells into a broad kind of neuronal populations—such as dopaminergic, glutamatergic, GABAergic, or motoneurons[67] that share the same genetic background of the patient from whom they originated. This

approach allows for a more comprehensive understanding of both the molecular processes responsible for the onset of the pathology and those involved in its progression.

However, since iPSCs-derived dopaminergic neurons (DANs) is a 2D model, it doesn't provide information regarding the cellular environment, that might have an impact on the pathogenesis of the disease. For this reason, in the last years 3D cell cultures, called organoids, have been developed. This *in vitro* model conserves the same genetic features of the patient from which it derived, but it is also characterized by a defined spatial organization that allows differentiation in different cell types and favours their communication. So, it's possible to create a network of heterogeneous cellular populations that mimic the brain *in vivo*.

Based on these considerations, in my PhD project I generated two *in vitro* models able to recapitulate the phenotype of neurons affected by GD-PD.
I exploited the use of a pharmacological model that consists in DANs, treated with conduritol-B-epoxide (CBE), a specific inhibitor of GCase, to suppress its activity and mimic the pathological features of GD. However, since DANs is a 2D model, to have a better insight into neurodegeneration at a more complex level, in collaboration with my co-tutor Dr. Alessio di Fonzo of Policlinico Hospital of Milano, I also generated a 3D *in vitro* model represented by human midbrain organoids (hMOs) differentiated from iPSCs of a GD-PD patient carrying the biallelic mutation N370S/F213I in GBA gene. These three-dimensional cultures are thought to generate a model that better recapitulate the brain physiology.

Starting from the 2D model, I used the CBE model since it's an experimental model that we have developed in our laboratory, and we have already demonstrated to recapitulate the phenotype of GD-PD. As reported by Dr. Lunghi and Carsana in a previous work[71], CBE administration results in a strong GCase deficiency, neurodegenerative phenotype and GlcCer accumulation in iPSCs-derived neurons in comparison to the controls.

For what concern the midbrain organoid model, I characterized it during my PhD, confirming the neuropathological features observed in the bidimensional DANs. I analysed patient midbrain organoids at day 50, 80 and 120, and they presented a reduction in GCase activity compared to the healthy subject at all the considered time-points. GD-PD hMOs also showed significant decrease expression of neuronal markers and an increase in the autophagic markers, suggesting neurodegeneration and lysosomal impairment. Moreover, they also exhibited GlcCer accumulation and α-synuclein aggregation, typical features of GD-PD.

Taken together these results, it becomes evident that both DANs and hMOs partially reproduce the observed GD-PD phenotypes *in vivo*. Thus, they serve as valuable models for studying the molecular mechanisms underlying the diseases and assessing the feasibility of specific therapeutic strategies to rescue or, at least, improve the pathological phenotype.

Regarding this last aspect, during my PhD I exploited both models to verify whether the inhibition of acid sphingomyelinase (ASM), codified by *SMPD1* gene, has a protective role in GBA-dependent PD.

I started from an experimental finding of some collaborators at Humanitas University that, besides *GBA* mutation, have studied the possible existence of gene variants in other lysosomal enzymes that can contribute to cause PD. They analyzed a panel of 50 LSD genes in a cohort composed by *GBA* asymptomatic carriers and *GBA*-mutated PD patients. They found that *SMPD1* gene was more frequently mutated in controls than in GBA-PD, suggesting a possible protective effect of *SMPD1* mutation in *GBA* carriers.

In addition, a recent study seems to confirm the role of ASM as a modifier of *GBA* deficiency *in vivo.* Keatinge and colleagues demonstrate that in a zebrafish GD model the inactivation of ASM showed a marked ameliorating effect on behavior and disease duration, with a rescue of the characteristic motor phenotype and an improved survival. Furthermore, they also found a restoration of neuronal health confirmed by RNAseq-based analyses and a rescue of the mitochondrial respiratory chain function, followed by a reduction in lipid peroxidation [69].

Based on the available evidence, I conducted experiments in both *in vitro* models with the administration of amitriptyline (AMI), a functional inhibitor of ASM. This is a tricyclic antidepressant drug already approved for the clinical use, that exerts some positive effects in different neurodegenerative and neuropsychiatric diseases. Indeed, in Alzheimer disease it was reported that the restoration of ASM levels had shown improvements in the pathology, including reduced Aβ accumulation and enhanced learning and memory function.[72] Furthermore, studies involving ASM-overexpressing transgenic mice indicated that the administration of AMI could ameliorate depressive-like phenotypes and increase neuronal proliferation, maturation, and survival in the hippocampus by reducing ceramide concentrations. [76,77]

CBE-treated dopaminergic neurons were treated with 10 µM of AMI for 24 hours and 7 days before the collection at 60 days of differentiation. In midbrain organoids instead I tried three different treatments: 20 µM AMI, 40 µM AMI and 20 µM ARC39, a specific inhibitor of ASM, for 30 days and 70 days. I found that the complete inhibition of the enzyme obtained administering ARC and AMI 40 µM doesn't lead to an amelioration of the phenotype. On the contrary, worsens the phenotype and exacerbates the already present condition of neurodegeneration and lysosomal stress. The partial inhibition given by AMI treatment, instead, generates an opposite effect in the two models.

Indeed, in CBE-treated dopaminergic neurons I found that both the acute (24h) and the chronic (7 days) treatment with AMI ameliorate the neurodegenerative phenotype and reduce glucosylceramide accumulation. Upon the administration of the drug, I have also observed an increase in NLGase activity, which could be seen as the possible counteracting mechanism against glucosylceramide accumulation.

These data are in line with the above-mentioned findings that sustain a positive effect of ASM inhibition in GBA-PD.

However, in the 3D model I obtained opposite results, since in the treated hMOs the neuronal markers TUJ1 and MAP2 were found reduced already after 30 days of amitriptyline administration. A prolonged treatment of 70 days resulted even more detrimental for GD-PD organoids, reducing all the neuronal markers and the marker of the dopaminergic commitment TH. Thus, the prolonged treatment with AMI exacerbated the neurodegeneration in this model. Moreover, I have also observed an increase in the autophagic markers expression after 30 days treatment with amitriptyline, that were further increased over time upon a prolonged exposition to the drug, suggesting a worsening of the autophagic impairment.
Afterwards, I have also evaluated the effect of the drug on GlcCer content and on GCase and NLGase activity. I found no difference in GCase and NLGase activity after 30 days of treatment with AMI, however I found a tendency to increase of GCase and NLGase activity after the prolonged administration with the drug, even if not enough to induce some changes in GlcCer content.
In addition, since patient hMOs present α-synuclein aggregation in comparison to the control one, in collaboration with Arianna Bellucci's group at University of Brescia, I also analysed the effect of the treatment on this pathological feature. I have observed an increase in α-synuclein aggregation after 30 days treatment with AMI and a tendency to aggregate also after 70 days administration.

The impact of ASM inhibition on GD-PD hMOs appears to contradict the beneficial effect observed in DANs and the initial hypothesis of *SMPD1* mutations as a protective factor against PD development. However, existing literature presents conflicting evidence as well. Some authors assert that specific rare variants in *SMPD1* (R591C; L302P) are linked to an increased risk of PD and an earlier onset of the disease, while other *SMPD1* mutations were not associated with PD. [73,74]

In support of the negative effect of ASM inhibition observed in midbrain organoids, in particular regarding α-synuclein aggregation, there are also other experimental demonstrations.
A recent study has revealed that *SMPD1* knock-down in cellular models results in reduced ASM levels, leading to the accumulation of α-synuclein. [75]

Kim and colleagues reported in *in-vitro* models of GCase deficiency that a reduction in ceramide leads to α-synuclein accumulation due to impaired secretory autophagy. Consequently, the restoration of ceramide level by the administration of carmofur, an inhibitor of acid ceramidase, reduced the accumulation of oxidized α-synuclein. [83] Thus, in my AMI-treated GCase-deficient hMO model, the ceramide level is further reduced due to the defective catabolism of SM, explaining the aggregation of α-synuclein that I have observed upon the treatment.

Moreover*, in-vivo* and *in-vitro* studies on PD showed that the reduction of ASM impaired autophagy, reduced neurogenesis, and lead to an excessive accumulation of SM into cell membrane lipid microdomains that promote α-synuclein aggregation. Thus, is crucial for brain physiology to maintain a correct SM/Cer balance. [84]

In addition, a possible speculation that could allow to interpret the different outcome that I have observed in dopaminergic neurons and midbrain organoids upon amitriptyline administration is reported in **fig 40**.

Cells employ lysosomal exocytosis as a mechanism to mitigate lysosomal impairment, releasing uncatabolized material extracellularly. Inhibition of ASM activity may intensify lysosomal impairment due to the accumulation of uncatabolized SM. This accumulation, in addition to the accumulation of GlcCer, could, in turn, trigger increased lysosomal exocytosis. In the context of organoids, which are 3D models consisting in different cell types such as astrocytes and other neurons, the uncatabolized material might be taken up by other cells, activating them and inducing inflammation. This process could contribute to the self-propagation of the disease, potentially neutralizing the observed positive effects of amitriptyline administration in dopaminergic neurons (**Fig. 40A**).

Conversely, in neurons treated with CBE, the aberrant material released via lysosomal exocytosis might get diluted in the cell culture medium, avoiding the negative effects observed in organoids following amitriptyline administration (**Fig.40B**). Consequently, in these neurons, the overall outcome of ASM inhibition could be positive, potentially exerting a protective effect.

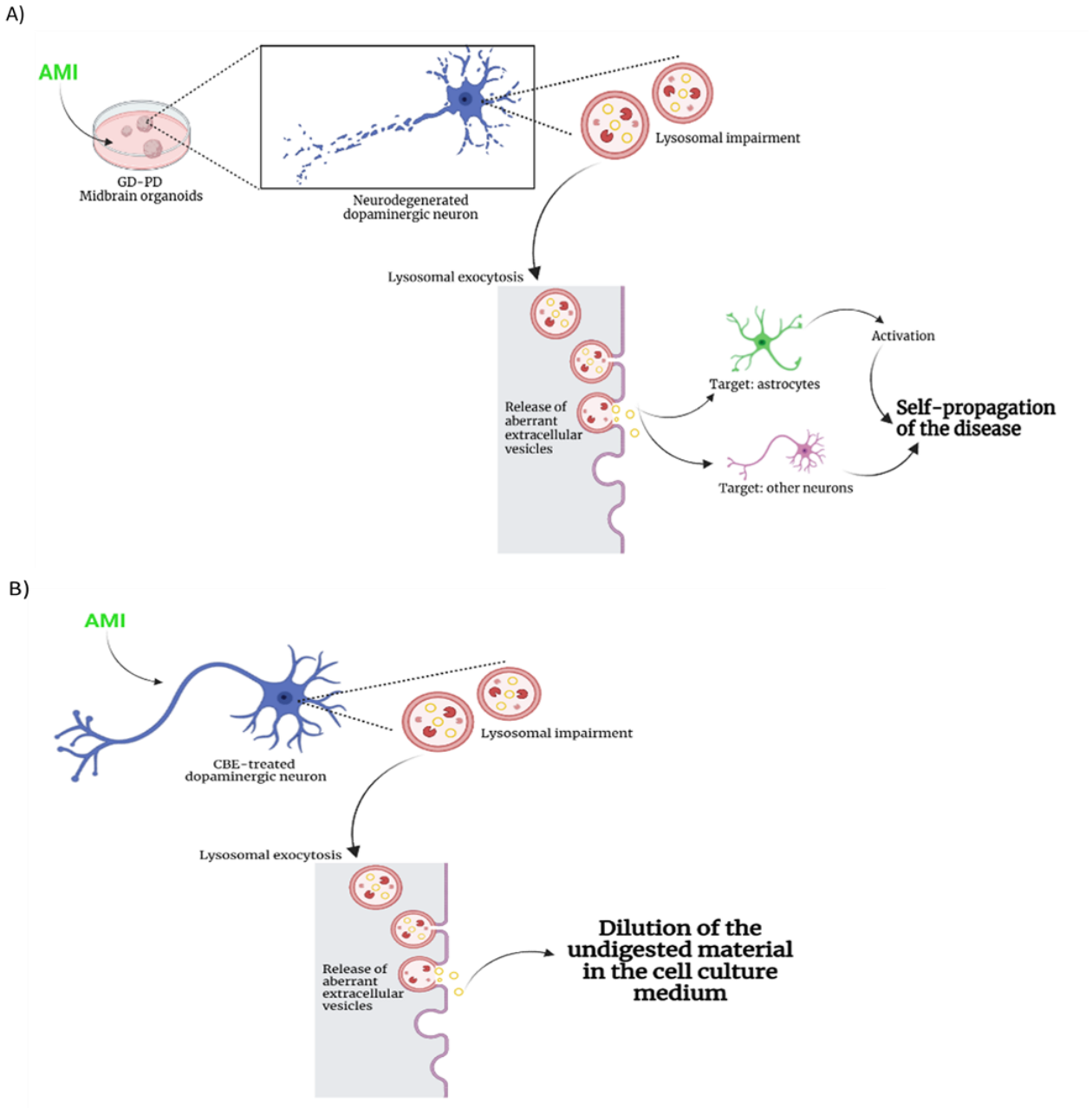

Figure 40. A) Representative image of the effect of amitriptyline treatment in GD-PD hMOs; B) Representative image of the effect of amitriptyline administration in CBE-treated DANs.

This work presents two reliable *in vitro* models to study the impact of GCase deficiency in neurons and opens a new scenario for the study of GCase-related neurodegenerative disorders. However, when considering the distinctions between the two models, midbrain organoids emerge as the more suitable option for studying the impact of ASM inhibition, given their closer resemblance to brain physiology. And according to the results obtained, it's possible to speculate that ASM inhibition has a damaging effect on GBA-dependent Parkinson's disease *in vitro* models.

7 BIBLIOGRAPHY

1. Simons, K. and Toomre, D. (2000). Lipid rafts and signal transduction. Nat Rev Mol Cell Biol 1, 31-9.

2. Quinville, B.M., Deschenes, N.M., Ryckman, A.E. and Walia, J.S. (2021). A Comprehensive Review: Sphingolipid Metabolism and Implications of Disruption in Sphingolipid Homeostasis. Int J Mol Sci 22

3. Merrill, A. H. Sphingolipid and glycosphingolipid metabolic pathways in the era of sphingolipidomics. *Chemical Reviews* vol. 111 6387–6422 (2011).

4. Ayub, M.; Jin, H.-K.; Bae, J. Novelty of Sphingolipids in the Central Nervous System Physiology and Disease: Focusing on the Sphingolipid Hypothesis of Neuroinflammation and Neurodegeneration. *Int. J. Mol. Sci.* 2021, *22*, 7353, doi:10.3390/ijms22147353

5. Svennerholm, L., Boström, K., Jungbjer, B. & Olsson, L. Membrane lipids of adult human brain: lipid composition of frontal and temporal lobe in subjects of age 20 to 100 years. *J. Neurochem.* 63, 1802–1811 (1994).
6. Suchański, J. & Ugorski, M. [The biological role of sulfatides]. *Postepy Hig. Med. Dosw. (Online)* 70, 489–504 (2016).
7. Tettamanti, G., Bassi, R., Viani, P. & Riboni, L. Salvage pathways in glycosphingolipid metabolism. *Biochimie* 85, 423–437 (2003).
8. Perry, R. J. & Ridgway, N. D. Molecular mechanisms and regulation of ceramide transport. *Biochimica et Biophysica Acta - Molecular and Cell Biology of Lipids* vol. 1734 220–234 (2005)
9. Lannert, H., Gorgas, K., Meißner, I., Wieland, F. T. & Jeckel, D. Functional organization of the Golgi apparatus in glycosphingolipid biosynthesis. Lactosylceramide and subsequent glycosphingolipids are formed in the lumen of the late Golgi. *J. Biol. Chem.* 273, 2939–2946 (1998).

10. Sundberg, E. L., Deng, Y. & Burd, C. G. Monitoring Sphingolipid Trafficking in Cells using Fluorescence Microscopy. *Curr. Protoc. cell Biol.* 82, (2019).

11. Kolter, T., Doering, T., Wilkening, G., Werth, N. & Sandhoff, K. Recent advances in the biochemistry of glycosphingolipid metabolism. *Biochem. Soc. Trans.* 27, 409–415 (1999).

12. Kolter, T. & Sandhoff, K. Principles of lysosomal membrane digestion: stimulation of sphingolipid degradation by sphingolipid activator proteins and anionic lysosomal lipids. *Annu. Rev. Cell Dev. Biol.* 21, 81–103 (2005).

13. Inui, K. *et al.* The gene coding for a sphingolipid activator protein, SAP-1, is on human chromosome 10. *Hum. Genet.* 69, 197–200 (1985).

14. Li YT, Li SC, Enzymatic hydrolysis of glycosphingolipids, *Anal Biochem*, 1999

15. Yamamoto, Y. *et al.* Isolation, characterization, and mapping of a human acid beta- galactosidase cDNA. *DNA Cell Biol.* 9, 119–127 (1990).

16. Huang, M., Gu, G., Ferguson, E. *et al.* A stomatin-like protein necessary for mechanosensation in *C. elegans*. *Nature* 378, 292–295 (1995).

17. Aureli, Loberto, Chigorno, Prinetti & Sonnino, Remodeling of sphingolipids by plasma membrane-associated glycosyltransferases, *J Biol Chem*, 2011a.

18. Aureli, Bassi, Loberto, Regis, Prinetti, Chigorno, Aerts, Boot, Filocamo & Sonnino, Cell surface associated glycohydrolases in normal and Gaucher disease fibroblasts, J Inherit Met Dis, 2012.

19. Beccari, T., Stinchi, S. & Orlacchio, a. Lysosomal alpha-D-mannosidase. *Biosci. Rep.* 19, 157–62 (1999).

20. Percheron, F., Foglietti, M. J., Bernard, M. & Ricard, B. Mammalian beta-D-mannosidase and beta-mannosidosis. *Biochimie* 74, 5–11 (1992).

21. Korchen, Yildiz, Raju, Schonauer, Bonigk, Jansen, Kremmer, Kaupp & Wachten, The non- lysosomal beta-glucosidase *GBA*2 is a non-integral membrane-associated protein at the endoplasmic reticulum (ER) and Golgi, *J Biol Chem*, 2012.

22. Hammer, M. B. *et al.* Mutations in GBA2 cause autosomal-recessive cerebellar ataxia with spasticity. *Am. J. Hum. Genet.* 92, 245–251 (2013).

23. Vitner, E.B., Platt, F.M. and Futerman, A.H. (2010). Common and uncommon pathogenic cascades in lysosomal storage diseases. J Biol Chem 285, 20423-7.

24. Henrissat, B. *et al.* Conserved catalytic machinery and the prediction of a common fold for several families of glycosyl hydrolases. *Proc. Natl. Acad. Sci. U. S. A.* 92, 7090–7094 (1995).

25. Aureli, Masilamani, Illuzzi, Loberto, Scandroglio, Prinetti, Chigorno & Sonnino, Activity of plasma membrane beta-galactosidase and beta-glucosidase, *FEBS Letter*, 2009.

26. Boot, R.G., Verhoek, M., Donker-Koopman, W., Strijland, A., van Marle, J., Overkleeft, H.S., Wennekes, T. and Aerts, J.M. (2007). Identification of the non-lysosomal glucosylceramidase as beta-glucosidase 2. J Biol Chem 282, 1305-12.

27. Yildiz, Y. *et al.* Mutation of beta-glucosidase 2 causes glycolipid storage disease and impaired male fertility. *J. Clin. Invest.* 116, 2985–2994 (2006).

28. Matern, H., Boermans, H., Lottspeich, F. & Matern, S. Molecular cloning and expression of human bile acid beta-glucosidase. *J. Biol. Chem.* 276, 37929–37933 (2001).

29. Zampieri S, Filocamo M, Pianta A, et al. SMPD1 Mutation Update: Database and Comprehensive Analysis of Published and Novel Variants. Human Mutation. 2016 Feb;37(2):139-147. DOI: 10.1002/humu.22923. PMID: 26499107

30. Wasserstein MP, Aron A, Brodie SE, Simonaro C, Desnick RJ, McGovern MM. Acid sphingomyelinase deficiency: prevalence and characterization of an intermediate phenotype of Niemann-Pick disease. J Pediatr. 2006;149(4):554–559. 10.1016/j.jpeds.2006.06.034.

31. Rodriguez-Pascau L, Gort L, Schuchman EH, Vilageliu L, Grinberg D, Chabas A. Identification and characterization of SMPD1 mutations causing Niemann-Pick types A and B in Spanish patients. Hum Mutat 2009; 30(7):1117-22. doi: 10.1002/humu.21018.

32. Palmano, K., Rowan, A., Guillermo, R., Guan, J. & McJarrow, P. The role of gangliosides in neurodevelopment. *Nutrients* 7, 3891–3913 (2015).

33. Yu, R. K., Nakatani, Y. & Yanagisawa, M. The role of glycosphingolipid metabolism in the developing brain. *J. Lipid Res.* 50 Suppl, (2009).

34. Bruel-Jungerman, E., Davis, S. and Laroche, S. (2007). Brain plasticity mechanisms and memory: a party of four. Neuroscientist 13, 492-505.

35. Ngamukote, S., Yanagisawa, M., Ariga, T., Ando, S. & Yu, R. K. Developmental changes of glycosphingolipids and expression of glycogenes in mouse brains. J. Neurochem. 103, 2327– 2341 (2007).

36. Ledeen, R.; Wu, G. Gangliosides of the Nervous System. In *Gangliosides: Methods and Protocols*; Sonnino, S., Prinetti, A., Eds.; Springer New York: New York, NY, 2018; pp. 19– 55 ISBN 978-1-4939-8552-4.

37. Ledeen, R.W.; Wu, G. Gangliosides, α-Synuclein, and Parkinson's Disease. *Prog. Mol. Biol. Transl. Sci.* 2018, *156*, 435–454, doi:10.1016/bs.pmbts.2017.12.009.

38. Schneider, J.S. Altered Expression of Genes Involved in Ganglioside Biosynthesis in Substantia Nigra Neurons in Parkinson's Disease. *PloS One* 2018, *13*, e0199189, doi:10.1371/journal.pone.0199189.

39. Rajkumar V, Dumpa V. Lysosomal Storage Disease. In: StatPearls. StatPearls Publishing, Treasure Island (FL); 2022. PMID: 33085417.

40. Jiang, P. *et al.* The HOPS complex mediates autophagosome-lysosome fusion through interaction with syntaxin 17. *Mol. Biol. Cell* 25, 1327–1337 (2014).

41. Peng, C. *et al.* Vps18 deficiency inhibits dendritogenesis in Purkinje cells by blocking the lysosomal degradation of Lysyl Oxidase. *Biochem. Biophys. Res. Commun.* 423, 715–720 (2012).

42. Lerche S, Wurster I, Roeben B, et al. Parkinson's Disease: Glucocerebrosidase 1 Mutation Severity Is Associated with CSF Alpha-Synuclein Profiles. Movement Disorders : Official Journal of the Movement Disorder Society. 2020 Mar;35(3):495-499. DOI: 10.1002/mds.27884. PMID: 31670439.

43. Gaubert S, Hourregue C, Mounton-Liger F, Millot P, Franco M, Amar-Bouaziz E, Aarsland D, Hugon J, Paquet C. Exploring the link between GBA1 mutations and Dementia with Lewy bodies, A mini-review. Neurosci Biobehav Rev 2022 Oct:141:104856.

44. Sidransky, E. & Lopez, G. The link between the GBA gene and parkinsonism. *Lancet Neurol.*11, 986–998 (2012).

45. Westbroek, W., Gustafson, A. M. & Sidransky, E. Exploring the link between glucocerebrosidase mutations and parkinsonism. *Trends Mol. Med.* 17, 485–493 (2011).

46. Sidransky, E. Gaucher Disease and Parkinsonism. Mol. Genet. Metab. 2005, 84, 302–304, doi:10.1016/j.ymgme.2004.11.007.

47. Kong, W., Lu, C., Ding, Y. and Meng, Y. (2022). Update of treatment for Gaucher disease. Eur J Pharmacol 926, 175023.

48. Futerman, A. H., Sussman, J. L., Horowitz, M., Silman, I. & Zimran, A. New directions in the treatment of Gaucher disease. *Trends Pharmacol. Sci.* 25, 147–151 (2004).

49. Hayes, M.T. (2019). Parkinson's Disease and Parkinsonism. Am J Med 132, 802-807.

50. Sidransky, E.; Nalls, M.A.; Aasly, J.O.; Aharon-Peretz, J.; Annesi, G.; Barbosa, E.R.; Bar- Shira, A.; Berg, D.; Bras, J.; Brice, A.; et al. Multicenter Analysis of Glucocerebrosidase Mutations in Parkinson's Disease. *N. Engl. J. Med.* 2009, *361*, 1651–1661, doi:10.1056/NEJMoa0901281.

51. McNeill, A., Duran, R., Hughes, D. A., Mehta, A. & Schapira, A. H. V. A clinical and family history study of Parkinson's disease in heterozygous glucocerebrosidase mutation carriers. *J. Neurol. Neurosurg. Psychiatry* 83, 853–854 (2012).

52. Gan-Or, Z.; Giladi, N.; Rozovski, U.; Shifrin, C.; Rosner, S.; Gurevich, T.; Bar-Shira, A.; Orr- Urtreger, A. Genotype-Phenotype Correlations between GBA Mutations and Parkinson Disease Risk and Onset. *Neurology* 2008, *70*, 2277–2283, doi:10.1212/01.wnl.0000304039.11891.29.

53. Lopez, G.; Kim, J.; Wiggs, E.; Cintron, D.; Groden, C.; Tayebi, N.; Mistry, P.K.; Pastores, G.M.; Zimran, A.; Goker-Alpan, O.; et al. Clinical Course and Prognosis in Patients with Gaucher Disease and Parkinsonism. *Neurol. Genet.* 2016, *2*, e57, doi:10.1212/NXG.0000000000000057.

54. Cilia, R. *et al.* Survival and dementia in GBA-associated Parkinson's disease: The mutation matters. *Ann. Neurol.* 80, 662–673 (2016).

55. Do CB., Tung JY., Dorfman E., Kiefer A.K., Drabant EM., Francke U., Mountain JL., Goldman SM., Tanner CM., Langston JW., Wojcicki A., Eriksson N. (2011) Web-based genome-wide association study identifies two novel loci and a substantial genetic component for Parkinson's disease, PLoS Genetics, 7(6)

56. Chang D., Nalls MA., Hallgrímsdóttir IB., Hunkapiller J., Van der Brug M., Cai F., Kerchner GA., Ayalon G., Bingol B., Sheng M., Hinds D., Behrens TW., Singleton AB., Bhangale TR., Graham RR. (2017) A meta-analysis of genome-wide association studies identifies 17 new Parkinson's disease risk loci, Nature Genetics, 49(10) pp1511-1516.

57. Connolly, B.S. and Lang, A.E. (2014). Pharmacological treatment of Parkinson disease: a review. JAMA 311, 1670-83.

58. Robakis, D. and Fahn, S. (2015). Defining the Role of the Monoamine Oxidase-B Inhibitors for Parkinson's Disease. CNS Drugs 29, 433-41.

59. Asselta, R. et al. (2014). Glucocerebrosidase mutations in primary parkinsonism. Parkinsonism Relat Disord 20, 1215-20.

60. Gegg, M. E. *et al.* Glucocerebrosidase deficiency in substantia nigra of parkinson disease brains. *Ann. Neurol.* 72, 455–463 (2012).

61. Johnson, P.H.; Weinreb, N.J.; Cloyd, J.C.; Tuite, P.J.; Kartha, R.V. GBA1 Mutations: Prospects for Exosomal Biomarkers in α-Synuclein Pathologies. *Mol. Genet. Metab.* 2020, *129*, 35–46, doi:10.1016/j.ymgme.2019.10.006.

62. Mazzulli, J. R. *et al.* Gaucher disease glucocerebrosidase and α-synuclein form a bidirectional pathogenic loop in synucleinopathies. *Cell* 146, 37–52 (2011).

63. Blandini F., Cilia R., Cerri S., Pezzoli G., Shapira A.H.V., Mullin S., Lanciego J.L. (2019) Glucocerebrosidase Mutations and Synucleinopathies: Toward a Model of Precision Medicine, Movement Disorders, 34,1.

64. Smith L, Schapira A. H.V. GBA Variants and Parkinson Disease: Mechanisms and Treatments. Cells. 2022 Apr; 11(8): 1261.

65. Enquist, I.B.; Bianco, C.L.; Ooka, A.; Nilsson, E.; Månsson, J.-E.; Ehinger, M.; Richter, J.; Brady, R.O.; Kirik, D.; Karlsson, S. Murine Models of Acute Neuronopathic Gaucher Disease. *Proc. Natl. Acad. Sci.* 2007, *104*, 17483–17488, doi:10.1073/pnas.0708086104.

66. Sillence, D.J.; Puri, V.; Marks, D.L.; Butters, T.D.; Dwek, R.A.; Pagano, R.E.; Platt, F.M. Glucosylceramide Modulates Membrane Traffic along the Endocytic Pathway. *J. Lipid Res.* 2002, *43*, 1837–1845, doi:10.1194/jlr.M200232-JLR200.

67. Zhang P., Xia N., Reijo Pera A. Directed dopaminergic neuron differentiation from human pluripotent stem cells. *J Vis Exp* 2014, 51737

68. Soldner, F.; Hockemeyer, D.; Beard, C.; Gao, Q.; Bell, G.W.; Cook, E.G.; Hargus, G.; Blak, A.; Cooper, O.; Mitalipova, M.; et al. Parkinson's Disease Patient-Derived Induced Pluripotent Stem Cells Free of Viral Reprogramming Factors. *Cell* 2009, *136*, 964–977, doi:10.1016/j.cell.2009.02.013.

69. Keatinge M, Gegg ME, Watson L, Mortiboys H, Li N, Dunning M, Ailani D, Bui H, Van Rens A, Lefeber D.J, Shapira A.H.V, MacDonald R.B, Bandmann O. (2023) Unexpected phenotypic and molecular changes of combined glucocerebrosidase and acid sphingomyelinase deficiency, Dis Model Mech;16(6):dmm049954.

70. Justice MJ, Bronova I, Schweitzer KS, et al. (2018) Inhibition of acid sphingomyelinase disrupts LYNUS signaling and triggers autophagy. J Lipid Res. 59(4): pp596-606.

71. Lunghi G, Carsana EV, Loberto N, Cioccarelli L, Prioni S, Laura Mauri et al. β-Glucocerebrosidase Deficiency Activates an Aberrant Lysosome-Plasma Membrane Axis Responsible for the Onset of Neurodegeneration. Cells. 2022 Aug; 11(15): 2343.

72. Beckmann N, Sharma D, Gulbins E, Becker KA, Edelmann B (2014) Inhibition of acid sphingomyelinase by tricyclic antidepressants and analogons. Front Physiol; 5:331.

73. Foo JN, Liany H, Bei JX, Yu XQ, Liu J, Au WL, Prakash KM, Tan LC, Tan EK (2013) Rare lysosomal enzyme gene SMPD1 variant (p.R591C) associates with Parkinson's disease. Neurobiol Aging. 34(12):2890.

74. Gan-Or Z, Ozelius LJ, Bar-Shira A, Saunders-Pullman R, Mirelman A, Kornreich R, Gana-Weisz M, Raymond D, Rozenkrantz L, Deik A, Gurevich T, Gross SJ, Schreiber-Agus N, Giladi N, Bressman SB, Orr-Urtreger A (2013) The p. L302P mutation in the lysosomal enzyme gene SMPD1 is a risk factor for Parkinson disease. Neurology 80(17): pp1606-1610.

75. Alcalay RN, Mallett V, Vanderperre B, et al. (2019) SMPD1 mutations, activity, and α-synuclein accumulation in Parkinson's disease. Mov Disord.34(4): pp526-535.

76. Park M.H, Jin H.K, Bae J.S (2020). Potential therapeutic target for aging and age-related neurodegenerative diseases: the role of acid sphingomyelinase. Experimental and Molecular Medicine, 52, pp380-389.

77. Gulbins, E., Palmada, M., Reichel, M. *et al.* Acid sphingomyelinase–ceramide system mediates effects of antidepressant drugs. *Nat Med* 19, 934–938 (2013). https://doi.org/10.1038/nm.3214

78. Lancaster MA., Knoblich JA., (2014) Generation of cerebral organoids from human pluripotent stem cells, Nature Protocols, Vol.9 N.10

79. Tofaris GK, Garcia Reitböck P, Humby T, Lambourne SL, O'Connell M, Ghetti B, Gossage H, Emson PC, Wilkinson LS, Goedert M, Spillantini MG. Pathological changes in dopaminergic nerve cells of the substantia nigra and olfactory bulb in mice transgenic for truncated human alpha-synuclein(1-120): implications for Lewy body disorders. J Neurosci. 2006 Apr 12;26(15):3942-50. doi: 10.1523/JNEUROSCI.4965-05.2006. PMID: 16611810; PMCID: PMC6673887

80. Stirnemann J, Belmatoug N, Camou F, Serratrice C, Froissart R, Caillaud C, Levade T, Astudillo L, Serratrice J, Brassier A, Rose C, Billette de Villemeur T, Berger MG. A Review of Gaucher Disease Pathophysiology, Clinical Presentation and Treatments. Int J Mol Sci. 2017 Feb 17;18(2):441. doi: 10.3390/ijms18020441. PMID: 28218669; PMCID: PMC5343975.

81. Sasagasako N, et al., 1994. Glucosylceramide and glucosylsphingosine metabolism in cultured fibroblasts deficient in acid beta-glucosidase activity. *J Biochem*. 115, 113–9.

82. Takahashi, K. & Yamanaka, S. Induction of pluripotent stem cells from mouse embryonic and adult fibroblast cultures by defined factors. Cell 126, 663–676 (2006)

83. Kim MJ, Jeon S, Burbulla LF, Krainc D. Acid ceramidase inhibition ameliorates α-synuclein accumulation upon loss of GBA1 function. Hum Mol Genet. 2018 Jun 1;27(11):1972-1988. doi: 10.1093/hmg/ddy105. PMID: 29579237; PMCID: PMC6251682.

84. Signorelli, P.; Conte, C.; Albi, E. The Multiple Roles of Sphingomyelin in Parkinson's Disease. *Biomolecules* 2021, *11*, 1311. https://doi.org/10.3390/biom11091311

RINGRAZIAMENTI

Vorrei esprimere i miei più sentiti ringraziamenti:

- Al Professor Massimo Aureli per avermi permesso di fare questa esperienza di dottorato nel suo laboratorio, luogo che mi ha permesso di imparare moltissimo e di diventare indipendente nel gestire i miei esperimenti. Grazie per avermi concesso la possibilità di andare a moltissimi congressi per ampliare i miei orizzonti scientifici. Grazie di aver sostenuto la mia decisione di andare a NY per poter vivere una parte della mia esperienza lavorativa anche all'estero.
- Al dottor Alessio di Fonzo, Emanuele e Manuela per aver collaborato nel portare avanti il mio progetto di dottorato, insegnandomi la tecnica degli organoidi che è stata punto cruciale del progetto, e per aver fatto sì che la mia esperienza lavorativa all'estero avesse luogo.
- A Emma, grazie per avermi insegnato moltissimo, per essere stata sempre disponibile ad aiutarmi e per aver condiviso con me infinite frustrazioni e risate. La mia esperienza in lab non sarebbe stata la stessa senza di te.
- A Loredana, grazie per la compagnia, le risate e l'appoggio ricevuto durante i miei anni trascorsi al LITA, li ho vissuti decisamente meglio grazie alla tua presenza.
- A Chiara, per avermi sopportato come tutor e per avermi aiutato a portare avanti questo progetto, analizzando i 2 milioni di campioni che avevamo, senza il tuo aiuto sarei diventata matta.
- A Dorina, grazie per i bei momenti passati insieme ai vari congressi, per tuttora condividere la vita quotidiana in laboratorio caratterizzata da attimi spensierati, ma anche grandi sbattimenti.
- A Giulia, Maria, Nicoletta ed Elena grazie per essere colleghe che non pensano solo al lavoro, con cui si può parlare di tutto e che creano un ambiente lavorativo sereno e rilassato. In particolare, grazie Giulia per l'aiuto nel portare avanti i vari esperimenti.
- A Louisa e ad Eva, per aver condiviso con me l'esperienza newyorkese, regalandomi infinite risate, momenti indimenticabili e per avermi fatto sentire sempre a casa. Non potrei mai essere stata più fortunata.
- Ad Alba, per tutto l'aiuto in laboratorio e gli infiniti suggerimenti su cosa fare al di fuori del lab. La mia esperienza a NY non sarebbe stata la stessa senza di te.
- A tutte le belle persone conosciute a NY che hanno reso la mia esperienza ricca di significato e indimenticabile.
- Alla mia famiglia per avermi permesso di studiare e avermi sempre sostenuto e supportato nelle scelte fatte.
- Agli amici e a mia cugina Roberta che mi stanno accanto da quando sono piccola, rendendo la mia vita più gioiosa e spensierata.
- A Lorenzo, che mi ha accompagnato durante tutto questo percorso di dottorato, supportandomi sempre, soprattutto nei momenti di sconforto. Non so come avrei fatto senza di te al mio fianco.

I would like to express my warmest thanks:

- To Professor Massimo Aureli for allowing me to perform this doctoral experience in his laboratory, a place that has allowed me to learn a lot and become independent in managing my experiments. Thank you for granting me the opportunity to attend many conferences to broaden my scientific horizons. Thank you for supporting my decision to go to NY to experience a part of my work abroad.
- To Dr. Alessio di Fonzo, Emanuele, and Manuela for collaborating in advancing my doctoral project, teaching me the technique of organoids which was a crucial point of the project, and making my work experience abroad possible.
- To Emma, thank you for teaching me so much, for always being willing to help me, and for sharing endless frustrations and laughter with me. My lab experience wouldn't have been the same without you.
- To Loredana, thank you for the friendship, laughter, and support during my years at LITA; I lived them much better thanks to your presence.
- To Chiara, for tolerating me as a tutor and helping me carry out this project, analyzing the 2 million samples we had, I would have gone crazy without your help.
- To Dorina, thank you for the great moments spent together at various conferences, for still sharing everyday life in the lab characterized by carefree moments but also great problems.
- To Giulia, Maria, Nicoletta, and Elena, thank you for being colleagues who not only think about work, with whom you can talk about everything and who create a serene and relaxed working environment. In particular, thank you Giulia for helping me carry out various experiments.
- To Louisa and Eva, for sharing the New York experience with me, giving me endless laughter, unforgettable moments, and always making me feel at home. I could never have been luckier.
- To Alba, for all the help in the laboratory and endless suggestions on what to do outside the lab. My experience in NY wouldn't have been the same without you.
- To all the wonderful people I met in NY who made my experience meaningful and unforgettable.
- To my family for allowing me to study and always supporting me in my choices.
- To friends and my cousin Roberta who have been with me since I was little, making life more joyful and light-hearted.
- To Lorenzo, who accompanied me throughout this doctoral journey, always supporting me, especially in moments of discouragement. I don't know how I would have done it without you by my side.